From the Institute for Cardiogenetics
of the University of Lübeck
Director: Prof. Dr. Jeanette Erdmann

Functional Analysis of the CAD-Risk Gene *Zc3hc1*

Dissertation
for Fulfillment of
Requirements
for the Doctoral Degree
at the University of Lübeck

from the Department of Natural Sciences

submitted by

Jaafar Al-Hasani
from Hamburg

Lübeck, May 2017

First Referee:	Prof. Dr. Jeanette Erdmann
Second Referee:	Prof. Dr. Henrik Oster
Date of oral examination:	17.10.2017
Approved for printing:	24.10.2017

Many thanks go to...

Prof. Jeanette Erdmann for giving me the opportunity to carry out my thesis at the Institute for Cardiogenetics (formerly known as Institute for Integrative und Experimental Genomics, formerly known as Molecular Genetics Lab 1 of the Medical Clinic 2), for her warmness and kindness, and for all the possibilities she opened up for us students

Dr. Zouhair Aherrahrou for his supervision, for his support with the experiments, and for suggesting the trip to the KongWei-Lab in Beijing

Maria for being not only a great colleague, but also a friend, and for her helpful comments

Krishan for being the kind of friend that makes people question certain things...

Annett, Maren, Petra, Sabine und Sandra for a warm and nice atmosphere, for their infinite knowledge, for countless genotypings and their support in carrying out the experiments: for a myriad of dissections and a beautiful aortic heart; for countless, beautiful stainings; for being the coolest (ex-)pirate i ever met; for being always cheerful and never giving up on the aortas; for knowing everything about cells and nucleic acids, and XKCD and Fefe

all other colleagues in the institute for such a nice and productive atmosphere, and for a great time

the CVRC in Leicester for a nice and fruitful collaboration, for being great hosts and for an unforgettable soccer-match-in-a-pub-watching-experience

the Institute for Human Genetics, especially Juliane und Frank, for their knowledge and help with the Two-Hybrids

the KongWei-Lab in Beijing, and Gabriele Huhn (and the DZHK), the first for showing me the art of smooth muscle cell isolation and for a very nice time in Beijing, and the latter for her support with the trip to China

the Leducq Consortium CADgenomics for a great, collaborative experience, for being such a great family; and a special thanks to Heri and Jake for bringing so many people from different backgrounds together

my family for their unconditional support through all my life, and who made me who I am

Sogol for her love

Abstract

Cardiovascular Diseases (CVDs), such as stroke, cardiomyopathy, Coronary Artery Disease (CAD) or Myocardial Infarction (MI), are the major cause of death worldwide. They are mainly caused by atherosclerosis, an inflammatory thickening of the vessel wall. Atherosclerosis can develop early in life, and many risk factors are known to promote atherosclerosis, like smoking, alcohol consumption, unhealthy diet, physical inactivity, high blood pressure, diabetes, high blood cholesterol, and obesity, but also age, gender, stress, and familial predisposition. Genomewide Association Studies (GWAS) have identified many genomic regions, or loci, marked by Single Nucleotide Polymorphisms (SNPs), a form of genetic variation, that contribute to the risk of CAD and MI; however, the underlying causalities are still unclear. Functional follow-up studies are needed to find the causal genetic variation or gene, in order to understand the association between the identified loci and the disease.

In this thesis, the CAD-risk gene *Zc3hc1* was investigated. The locus containing the gene *Zc3hc1* is marked by only one SNP, rs11556924, which causes a missense mutation in NIPA, the protein encoded by *Zc3hc1*, and is hence considered a good candidate for functional analyses. NIPA is involved in cell-cycle control, binding Cyclin B1, a promoter of mitosis, and tagging it for degradation during the interphase.

To analyse the impact of the aminoacid exchange caused by the SNP on the binding of NIPA and Cyclin B1, the two proteins were expressed in a mammalian-two-hybrid system. Furthermore, the role of the gene *Zc3hc1* in atherosclerosis was analysed. For this, the *Zc3hc1*-knockout (KO) mouse line was established, confirmed, phenotyped, and backcrossed to the proatherogenic Apolipoprotein E (ApoE)-KO background. Then, an *in-vivo* atherosclerosis study was conducted, analysing many parameters, such as lesion size or plaque composition, to assess the impact of the gene *Zc3hc1* on the development of the disease.

No results were obtained from the binding experiment; the used mammalian-two-hybrid assay seems not to be the appropriate model to assess the influence of the SNP on the binding between the proteins NIPA and Cyclin B1.

The *in-vivo* atherosclerosis study revealed no influence of NIPA on lipid parameters or plaque size, but showed a significant decrease in collagen content, and a trend towards less Smooth Muscle Cell (SMC)-content, in plaques from *Zc3hc1*-deficient animals. Further experiments showed that primary aortic SMCs from these animals had significantly lower proliferation, but higher migration capabilities compared to control cells.

Zusammenfassung

Erkrankungen des Herz-Kreislaufsystems, wie Schlaganfall, Kardiomyopathie, Koronare Herzkrankheit (KHK) oder Herzinfarkt (HI), stellen die Haupttodesursache weltweit dar. Sie werden hauptsächlich durch Atherosklerose, einer entzündlichen Verdickung der Gefäßwand, verursacht. Atherosklerose kann sich schon in jungen Jahren ausbilden, und wird durch viele Faktoren in der Entstehung begünstigt: Rauchen, Alkoholkonsum, ungesunde Ernährung, Bewegungsmangel, hoher Blutdruck, Diabetes, hohe Blutfettwerte und Übergewicht, aber auch Alter, Geschlecht, Stress sowie familiäre Prädisposition. In genomweiten Assoziationsstudien wurden viele genomische Regionen, oder loci, markiert durch sogenannte Single-Nucleotide-Polymorphismen (SNPs), einer Form genetischer Variation, identifiziert, die zum Risiko für KHK und HI beitragen. Die zugrundeliegenden Mechanismen jedoch sind bisher nicht aufgeklärt. Funktionelle Studien werden benötigt, um die jeweils ursächliche genetische Variation bzw. das verantwortliche Gen herauszufinden, um die Assoziation zwischen den identifizierten loci und der Krankheit zu verstehen.

In dieser Dissertation wurde das KHK-Risikogen *Zc3hc1* untersucht. Der locus, der das Gen *Zc3hc1* enthält, ist durch nur einen einzigen SNP, rs11556924, markiert, welcher einen Aminosäuren-Austausch in NIPA verursacht, dem Protein, das durch das Gen *Zc3hc1* kodiert wird; der locus gilt daher als vielversprechender Kandidat für funktionelle Analysen. NIPA ist involviert in die Zellzyklus-Kontrolle, indem es während der Interphase Cyclin B1, ein Mitose-einleitendes Protein, bindet und zum Abbau markiert. Um den Einfluß des Aminosäuren-Austauschs, der durch den SNP verursacht wird, auf die Bindung zwischen den Proteinen NIPA und Cyclin B1 herauszufinden, wurden beide Proteine in einem Mammalian-Two-Hybrid exprimiert. Weiterhin wurde die Rolle des Gens *Zc3hc1* in der Entstehung von Atherosklerose analysiert. Dafür wurde die *Zc3hc1*-knockout (KO) Mauslinie etabliert, bestätigt, phänotypisch untersucht, sowie auf den proatherogenen genetischen Hintergrund der Apolipoprotein E (ApoE)-KO Mauslinie zurückgekreuzt, und anschließend eine *in-vivo* Atherosklerose-Studie durchgeführt, in der verschiedene Parameter, wie zum Beispiel Plaque-Größe oder -Zusammensetzung,

analysiert wurden, um so den Einfluß des Gens *Zc3hc1* auf die Entwicklung der Krankheit zu messen.
Die Bindungsstudie erbrachte keine Ergebnisse, das hierfür genutzte Versuchsmodell des Mammalian-Two-Hybrid scheint nicht das geeignete Mittel darzustellen, um den Einfluß der Mutation auf die Bindung der Proteine NIPA sowie Cyclin B1 zu untersuchen.
In der *in-vivo* Atherosklerose-Studie zeigte sich zunächst, daß das Protein NIPA keinen Einfluß auf Blutfettwerte oder die Größe atherosklerotischer Plaques besaß; es konnte jedoch eine signifikante Verringerung des Kollagen-Gehalts, sowie eine niedrigere, aber nicht signifikant reduzierte, Anzahl glatter Muskelzellen in Plaques von *Zc3hc1*-defizienten Mäusen gemessen werden.
Weiterführende Experimente zeigten, daß bei primären glatten Muskelzellen aus Aorten dieser Tiere die Proliferationsrate im Vergleich zu Zellen aus Kontroll-Tieren signifikant verringert, die Migrationsfähigkeit jedoch signifikant höher war.

Contents

List of Tables

List of Figures

1. Introduction

1.1. Cardiovascular Disease

Cardiovascular Diseases (CVDs) account for the majority of deaths and years of lost life worldwide (GBD 2013 Mortality and Causes of Death Collaborators, 2015). They include diseases like stroke, cardiomyopathy, Coronary Artery Disease (CAD) or Myocardial Infarction (MI). CVDs are mainly caused by atherosclerosis, an inflammatory process that involves the deposition of lipids in the endothelial layer of vessel walls. Such deposits are called plaques, and they lead to a narrowing of the blood vessel, resulting in disturbed or reduced blood flow. Plaques also may rupture, causing a thrombus to form, which can occlude the vessel and entirely interrupt the blood flow and hence cut off the downstream tissue from oxygen supply. This results in severe tissue death, which is called gangrenes in the extremities, stroke in the brain, or MI in the heart.

1.2. Atherosclerosis

Atherosclerosis is a progressive disease characterised by the deposition of lipids in the intima, the inner vessel wall of arteries (Lusis, 2000). The development can be divided into different stages (see figure 1.1). The first stage, the accumulation of lipid-laden macrophages, or Foam Cells, which can occur early in life (McGill et al., 2008; Tuzcu et al., 2001), eventually leading to so called 'fatty streaks' (Stary et al., 1994), the second stage. Monocytes are recruited to the early depositions of lipids in the intima, where they differentiate into macrophages (Aqel et al., 1984) and try to clear up the lipid deposits by phagocytosis (Moore & Tabas, 2011). Enrichment of lipid droplets in the cytoplasm of the macrophages gave rise to the name Foam Cells. Though clinically not significant, and to this point a reversible process (Björkegren et al., 2014), fatty streaks are the

precursor of advanced lesions, or plaques, the third stage of atherosclerosis. Advanced lesions develop later in life, as an inflammatory response (Libby, 2002), which mediates vascular remodeling (Libby & Theroux, 2005; Schoenhagen et al., 2000). If more and more lipids accumulate, macrophages eventually become overstressed and die (Witztum, 1994), releasing their cellular content. This builds up the so called lipid-rich, or necrotic, core (Wilcox et al., 1989), which is covered by a layer of Smooth Muscle Cells (SMCs) and Collagen. SMCs are recruited from the media, most likely by signals released from macrophages (Ross et al., 1990). They undergo a change in their phenotype, from contractile to synthetic SMCs (G. R. Campbell & J. H. Campbell, 1985; Doran et al., 2008; Rensen et al., 2007), and migrate towards the intima, where they proliferate and synthesise collagen (Jaeger et al., 1991; O'Callaghan & Williams, 2000), to form the so called fibrous cap (Newby & Zaltsman, 1999). The fibrous cap stabilises a plaque and preserves residual functionality of the vessel (Loree et al., 1992).

By time, plaques even may calcify (Demer et al., 1994), either by a passive or by an active mechanism. In the passive calcification model, dying SMCs in the cap release their intracellular calcium, which then crystallises (Reynolds et al., 2004). The active model involves osteoblast-like cells (Doherty et al., 2003; Watson et al., 1994), similar to those found in bone formation, which secrete a scaffold for calcium phosphate deposition. Anyhow, calcification contributes to an increased stiffening of the vessel (Lee et al., 1991).

Advanced lesions grow larger, mainly towards the lumen of the vessel, leading to stenosis (narrowing; see figure 1.1, IV). Two processes contribute to plaque growth: continued lipid deposition, or slow growth (Guyton & Klemp, 1994), and rupture and healing of vulnerable plaques, or rapid growth (Bruschke et al., 1989; Falk, 1983). The latter can also happen repeatedly.

Vulnerability is defined by a thin fibrous cap (Davies, 1996; Falk, 1992), and, but not necessarily, low or medium levels of calcification (Wexler et al., 1996). Mechanical stress can cause an injury of the fibrous cap (Demer et al., 1994), leading to a release of thrombotic material into the blood stream (Falk, 1983). This leads either to a small, containable thrombotic reaction with subsequent 'healing' of the plaque surface (Burke et al., 2001; Nemoto et al., 2013), mediated by SMC growth and collagen secretion (Galis et al., 1994), or to a larger thrombus. Depending on the degree of stenosis (Falk, 1983), this thrombus may then block the vessel at the site of its origin, or detach and, as an embolus, obstruct blood flow in a distant, smaller vessel (Fuster et al., 1988).

Interruption of the blood flow, or ischemia, results in insufficient oxygen supply, and subsequent damage, of the downstream tissue. Blockage of coronary arteries, which supply the heart itself with oxygen, leads to death of heart tissue, also called Myocardial Infarction.

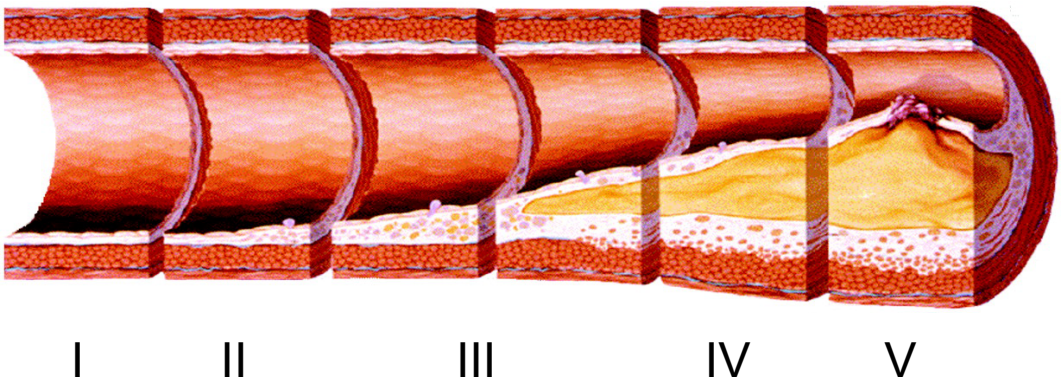

Figure 1.1.: Progression of atherosclerosis. Stages of the development of an atherosclerotic plaque are shown: (I) early accumulation of Foam Cells, (II) Fatty Streaks, (III) growing lesion, (IV) advanced plaque, (V) complicated plaque. In stage V, stenosis, calcification, and repeated rupture and healing, may occur. Image modified from (Koenig & Khuseyinova, 2007)

1.3. Risk factors for atherosclerosis

Atherosclerosis develops early in life, with fatty streaks occurring in the first decade (McGill et al., 2008; Tuzcu et al., 2001). Several risk factors are known to promote atherosclerosis, and they can be used to calculate a score, assessing a person's individual risk for CAD/ MI (Assmann et al., 2007; D'Agostino et al., 2008). Historically grown, risk factors are classified as traditional and non-traditional (see table 1.1).

A more comprehensible approach, particularly with regard to possible therapeutical interventions, divides risk factors into controllable and non-controllable (Mendis et al., 2011). Factors that, to a certain extent, can be controlled, so called behavioural or lifestyle factors, are smoking, drinking alcohol, unhealthy diet, lack of physical activity, high blood pressure, diabetes, high blood cholesterol, and obesity. A change in behaviour, or application of lipid-lowering medication can lead to a beneficial lowering of risk. Non-controllable conditions, and hence insurmountable for therapy, are advancing age, male gender, stress, and familial, or inherited, predisposition.

Table 1.1.: Traditional and non-traditional risk factors for CAD. The first column represents mainly physical features, whereas the second column contains more physiological parameters. Newer, non-traditional, risk factors comprise of metabolic parameters. TC: total cholesterol; LDL: low-density lipid cholesterol; HDL: high-density lipid cholesterol; ApoB/ApoA-I: Apolipoprotein B/A-I; oxLDL: oxidised LDL; CRP: C-reactive protein. Modified from Fruchart et al. (2004).

traditional		non-traditional
Gender (male > female)	Metabolic Syndrome	ApoB, ApoA-I
Age	Diabetes Mellitus	Triglycerides
Family History	TC, LDL, HDL (protective)	oxLDL
Smoking		Lipoprotein(a)
Overweight/ Obesity		Homocysteine
Hypertension		CRP

1.4. Studying the genetic risk of atherosclerosis

Family burden is an indicator for the heritability of atherosclerosis (Mayer et al., 2007). Members of families with an enriched occurrence of MIs are known to be at higher risk for atherosclerosis or MI, respectively (Hawe et al., 2003; Boer et al., 1999; Andresdottir et al., 2002). This risk increase was seen even more in identical twins (Marenberg et al., 1994). Although families with high burden of atherosclerosis/ MI were extensively studied, the real genetic cause could be identified for only a few of them. Moreover, the found variants were rather rare, family-specific, with a strong effect, and they did not explain the incidence of atherosclerosis/ MI in the wide population (Mayer et al., 2007; Björkegren et al., 2015). This led to the assumption of atherosclerosis as being a complex disease. Complex diseases are certainly also caused by rare, familial (or mendelian) variants, but mainly driven by an interplay of many genetic factors (Chakravarti, 1999). These non-rare, or common genetic variants do not necessarily cause an MI themselves. Instead, they rather modify the susceptibility of an organism to conditions that can favour the onset of the disease (Björkegren et al., 2015; Schadt & Björkegren, 2012), such as high blood pressure (Lieb et al., 2013), blood cholesterol levels, or diabetes. This means that even the controllable risk factors (see section 1.3) are under genetic control, underlining the complexity of atherosclerosis/ MI as a disease.

Common variants normally have a lower effect than rare variants (F. S. Collins et al., 1998; Reich & Lander, 2001), hence the relatively wide distribution throughout the population. Rare, familial variants, due to their much larger impact, which usually leads to a disease phenotype that emerges early in life (Boer et al., 1999), underlie a quite strong negative selection (Altshuler et al., 2008). The lower effect strength of common

variants, as well as the complexity of the interaction of genetic and environmental risk factors (W. Y. S. Wang et al., 2005; Björkegren et al., 2015), however, account for a late onset-disease pattern (Altshuler et al., 2008). This can indeed be observed in atherosclerosis and MI, where age is one of the major risk factors (Assmann et al., 2002; J. C. Wang & M. Bennett, 2012).
Studying the influence of common genetic variants on complex, late onset-diseases, is difficult, especially for atherosclerosis and MI, as the sample size within families is generally too small to detect variants with low effect (Laird & Lange, 2006). In addition, their effect is strongly intertwined with environmental conditions (Schadt & Björkegren, 2012). What complicates matters even further is the occurrence of death – premature and in young ages in case of rare, strong effect variants, or mainly in the second half of the life in case of common, low-effect variants – leading to a difficulty in accessing ancestral generations for sample taking (Mayer et al., 2007).

To overcome these limitations, a new approach was developed, testing genetic variations for their association to a disease in larger cohorts rather than families (Risch & Merikangas, 1996).

1.4.1. Genomewide Association Study

A Genomewide Association Study (GWAS) is a tool to study the genetics of complex diseases. GWAS are used to analyse the association of variations in the human genome to a disease. They are based on the idea that genetic markers, Single Nucleotide Polymorphisms (SNPs), can be used as tags for small genomic regions, and on the assumption that a genetic variation with a disease-causing influence would be found with a higher rate in patients with this disease than in people without the disease (Risch & Merikangas, 1996). Hence, they represent an unbiased approach (Chakravarti, 1999; Sachidanandam et al., 2001), not driven by prior knowledge of the functionality of the analysed regions.

Several developments within the last decade of the 20th century have paved the way for genome wide association studies:

The identification of a large number of SNPs SNPs are point mutations that, by traditional definition, occur in at least 1% of a population (Brookes, 1999). They

are alterations in the DNA sequence, changing a single nucleotide at one position, called allele, from an A (or a C, G or T) to one of the other three nucleotides. Rare cases are known in which three different nucleotides at one allele have been observed; usually, SNPs are biallelic (Brookes, 1999). They might be positioned in intergenic DNA, or non-coding or coding regions of genes. An intergenic SNP lies in regions between genes. Intergenic regions might still contain elements regulating the expression of genes, like enhancers or promotors, which can be affected by the SNP. Non-coding SNPs lie within protein-coding genes, but in regions that will not end up in the protein. They can also have effects on protein expression by changing transcription factor-binding sites, splice sites or mRNA stability. Coding SNPs lie in the sequence of a gene that codes for the amino acid chain of the protein. They can be synonymous or non-synonymous. Synonymous SNPs do not change the amino acid sequence – due to the ambiguity of the genetic code, some amino acids are encoded by several codons. Non-synonymous SNPs might either alter an amino acid (missense), or lead to a premature stop codon (nonsense). Depending on the chemical properties and the location of the amino acids, missense SNPs can have moderate or quite strong effects. Nonsense SNPs usually have the greatest impact, as they lead to a loss of protein sequence, which in turn can result in only partially or even mal-functioning proteins, or a complete loss of a protein due to nonsense-mediated decay.

In the first decade of the 21st century, SNPs were genotyped and identified in large numbers by the SNP Consortium (Altshuler et al., 2000; Sachidanandam et al., 2001), the Human Genome Project (Venter et al., 2001) and the International HapMap Consortium (International HapMap Consortium, 2005), and information was collected and publicly shared in a database called dbSNP (`http://www.ncbi.nlm.nih.gov/SNP/`, Sherry et al., 2001). To date, there are about 1.5×10^8 SNPs in the 3×10^9 nucleotide long human genome (dbSNP build 149; Nov 07, 2016).

The selection of tag SNPs based on haplotypes If SNPs combined randomly, the small number of 10 SNPs would already have $2^{10} = 1024$ combinatory possibilities. Luckily, since populations emerged from common ancestors, not all possible combinations are observed in nature (Johnson et al., 2001). In fact, SNPs seem to be inherited in specific patterns (Gabriel et al., 2002). These patterns, which were termed haplotypes, allow the prediction of SNPs nearby a given SNP (International HapMap Consortium, 2005). This SNP association is called Linkage Disequilibrium (LD) (Reich et al., 2001). SNP patterns are changed by recombination events that occur during meiosis (Jeffreys et al., 2001; A. Collins, 2009). The

genome consists of hotspots for recombination, leading to a block-like structure of LD (International HapMap Consortium, 2005). The more SNPs are identified, the finer gets the resolution of LD-blocks. This can in turn improve the outcome of a GWAS, as the signals can be mapped more precisely (Mackay, 2001).
Haplotypes were identified by the International HapMap Project, and substantially reduced the amount of SNPs necessary to be genotyped for a GWAS (Patil et al., 2001), while preserving the highest explanatory power – from more than 4 million (Barrett & Cardon, 2006) to about 500.000 in the year 2006, before the first GWAS for CAD was undertaken.

Rapid SNP genotyping using DNA Microarray Chips The number of SNPs selected by the HapMap consortium as tag SNPs would have still been far too high to be genotyped for large numbers of cases and controls (Syvänen, 2001), if it wasn't for the development of Microarray Chips (D. G. Wang et al., 1998; Broman & Feingold, 2004). These chips are capable of genotyping hundreds of thousands of SNPs at once. Currently available chips cover around 1 million SNPs or more (Ha et al., 2014). Sample DNA is fragmented by digestion with a restriction enzyme, and fragments are then labelled with a fluorescent dye. The chip contains SNP-specific antisense-oligonucleotides, to which the marked fragments will bind with high specificity regarding to their genotype. Elaborate analysis allows then to detect fluorescence signals and determine the genotypes of all SNP positions in a sample.

The design of a GWAS requires large groups of cases and controls, i.e. people with or without a phenotype or disease (Hirschhorn & Daly, 2005). DNA samples from every individual will then be genotyped for the SNPs of interest, and frequencies of the SNPs are calculated. With the large number of SNPs, the statistical significance level needs to be corrected for multiple testing – each SNP is treated like one hypothesis itself – leading to a significance threshold of $p < 5 \times 10^{-8}$ (Bonferroni-correction) (Risch & Merikangas, 1996; Jannot et al., 2015).

Traditionally, a risk gene is assigned for each locus based on the proximity of the gene to the significant SNP (Yang, 2012).

1.4.2. GWAS for CAD

In 2007, the first large GWAS were published, independently identifying a risk locus on chromosome 9 (Helgadottir et al., 2007; McPherson et al., 2007; Samani et al., 2007). In the following years, many more loci were identified to confer to the risk of CAD/ MI (R. Clarke et al., 2009; CARDIoGRAMplusC4D Consortium et al., 2013; Erdmann et al., 2009; Erdmann et al., 2011; Lu et al., 2012; Myocardial Infarction Genetics Consortium et al., 2009; Schunkert et al., 2011; Soranzo et al., 2009; CARDIoGRAMplusC4D Consortium, 2015; Coronary Artery Disease (C4D) Genetics Consortium, 2011; The IBC 50K CAD Consortium, 2011; Wellcome Trust Case Control Consortium, 2007; Trégouët et al., 2009; F. Wang et al., 2011).

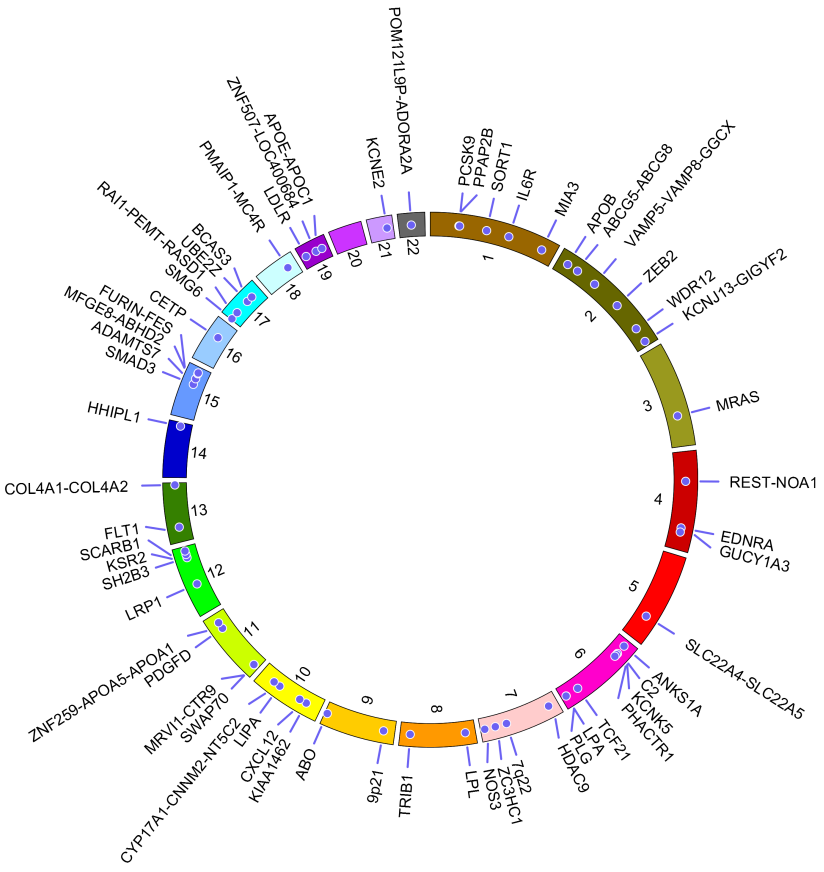

Figure 1.2.: Circular representation of CAD-risk loci, created using the Circos tool (Krzywinski et al., 2009). For each locus, the most likely gene underlying the signal is assigned either by proximity, expression Quantitative Trait Locus (eQTL), or nonsynonymous change in the encoded protein. Count as of February 2017 (Webb et al., 2017).

Surprisingly, the majority of the mapped genes were of unknown function, or were involved in pathways so far not suspected to contribute to CAD/ MI. Less than 25% of the mapped genes are related to the so called traditional risk factors (see table 1.1) (McPherson & Tybjaerg-Hansen, 2016); those that are, however, mainly associate to lipid metabolism or blood pressure (Lieb & Vasan, 2013).

1.4.3. GWAS and beyond

GWAS data serve as a starting point for further analyses (McCarthy & Hirschhorn, 2008) – the most basic one being the replication of the results in an independent population. As the effect sizes of the variants are small, more power, i.e. a larger number of genotyped individuals, could help to detect signals missed so far (Altshuler & Daly, 2007). To this end, GWAS can be combined into large meta-analyses, in which cohorts are pooled. Further improvement in digging out variants can be achieved by using expression Quantitative Trait Locus (eQTL)-data to find the causal genes behind the GWAS signals (Yang, 2012; Civelek & Lusis, 2014; Brænne et al., 2015).
An effort to improve gene mapping in GWAS for CAD/ MI using eQTL data was made in 2015, which confirmed several loci, but assigned many new genes, in many cases far away from the lead SNP, as the most likely candidates underlying the GWAS signals (Brænne et al., 2015).

Another approach is to find out how gene-gene or gene-environment interactions modulate the effects of risk genes (McCarthy & Hirschhorn, 2008; Schadt & Björkegren, 2012).

All these steps are used to identify the most likely candidate genes, which are worth being tested in the wet-lab, either *in-vitro* using atherosclerosis-relevant cell types (Nurnberg et al., 2016), such as SMCs, or in appropriate mouse models to capture the complex character of the disease *in-vivo* (Reardon & Getz, 2001; Fazio & Linton, 2001; Daugherty, 2002; Allayee et al., 2003; Maeda, 2011).
The experimental follow-up is the most crucial step in understanding and interpreting the association of a SNP with the disease phenotype (Maouche & Schunkert, 2012; Welch, 2012).

1.5. The candidate gene *Zc3hc1*

In this thesis, the gene *Zc3hc1* was investigated. It is located in the risk locus on human chromosome 7q32.2, which was reported in 2011 (see figure 1.3) and contains only one SNP, rs11556924 ($p = 2.22 \times 10^{-9}$, C⟶T), with genomewide significant association with CAD/ MI (Schunkert et al., 2011) and diastolic blood pressure (CARDIoGRAMplusC4D Consortium et al., 2013). No other SNPs are found in high LD (see figure 1.4).

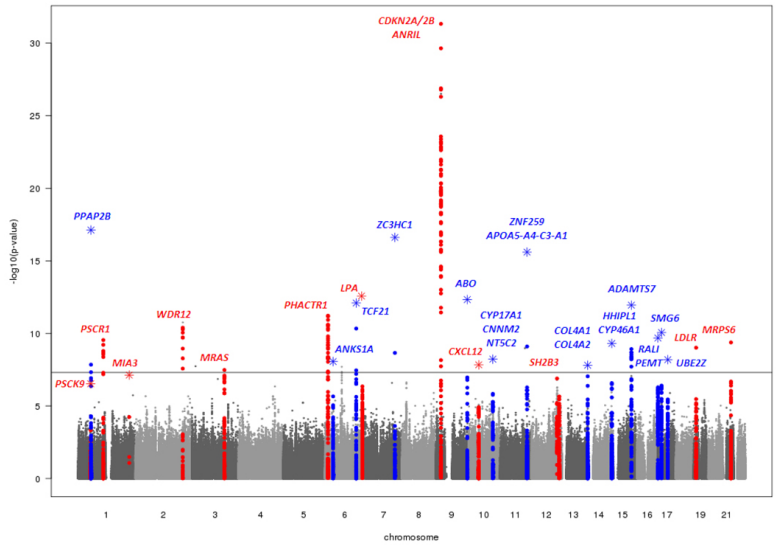

Figure 1.3.: Manhattan plot of CAD-risk loci. The graph shows the -$\log_{10}$ p-values for each SNP (y-axis). The x-axis represents the chromosomes. Cut-off: genomewide significance level. Blue: new loci identified by Schunkert et al. (2011), among them, on chromosome 7, the locus containing the gene *Zc3hc1*.

The SNP rs11556924 lies within the coding region of the gene *Zc3hc1*, and the major allele, C, is associated with a higher risk of CAD/ MI. The minor allele, T, has a frequency of 15.58% (1000 Genomes). The SNP is non-synonymous, causing an amino acid exchange in the encoded protein in position 363 from Arginine to Histidine. Although there is an eQTL-effect of the SNP rs11556924 on the neighbouring gene KLHDC10 (Erbilgin et al., 2013), *Zc3hc1* is believed to be the better candidate gene for functional analyses, as the SNP leads to an amino acid exchange in the encoded protein. This was recently emphasised (Brænne et al., 2015).

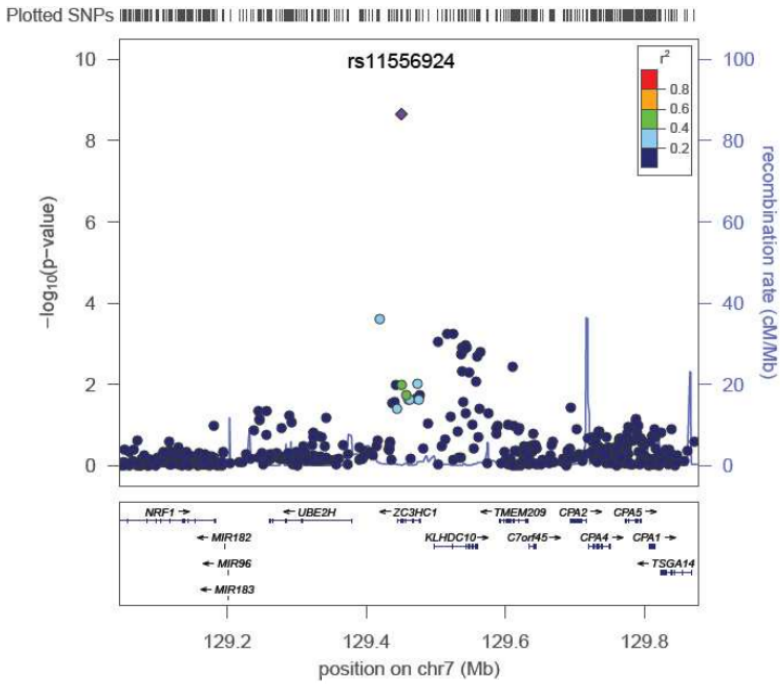

Figure 1.4.: Regional association plot of rs11556924. The locus contains only one genomewide significant SNP, and no other SNPs are in high LD ($r^2 > 0.8$). x-axis: position of the locus and the contained genes on chromosome 7. y-axis: -$\log_{10}$ p-values for each SNP (left), and recombination rates (right). LD of the other SNPs with the lead SNP, given as r^2, is color-coded. Image from Schunkert et al. (2011).

1.5.1. What is known about *Zc3hc1*?

Zc3hc1 encodes the protein Nuclear Interaction Partner of ALK (NIPA), which is involved in cell cycle control. It was first described in 2003 as a possible nuclear downstream target of the oncogenic tyrosine kinase nucleophosmin-anaplastic lymphoma kinase (NPM-ALK) (Ouyang et al., 2003). NPM-ALK, a fusion protein created by a chromosomal translocation (t(2;5)(p23;q35)), leads to the development of anaplastic large-cell lymphoma, a type of cancer emerging in lymphocytes. It was shown that phosphorylation of NIPA can have an antiapoptotic effect in a murine pro-B cell line (Ouyang et al., 2003). Although NIPA directly binds NPM-ALK (hence the name), it was not seen to be phosphorylated by this kinase. In following studies, NIPA was found to be a part of an SCF-type E3-Ubiquitin Ligase, interacting with Cyclin B1 (Bassermann et al., 2005b). SCF-type ligases have four subunits: Skp1, Cullin protein 1, RING-finger protein and an interchangeable F-Box protein (Cardozo & Pagano, 2004). The F-Box protein defines substrate specificity (Craig & Tyers, 1999). As can be seen in figure 1.5, NIPA contains both an F-Box domain and a binding site for Cyclin

B1 (Bassermann et al., 2007). Interestingly, the SNP rs11556924 lies within this region (see arrow in figure 1.5).

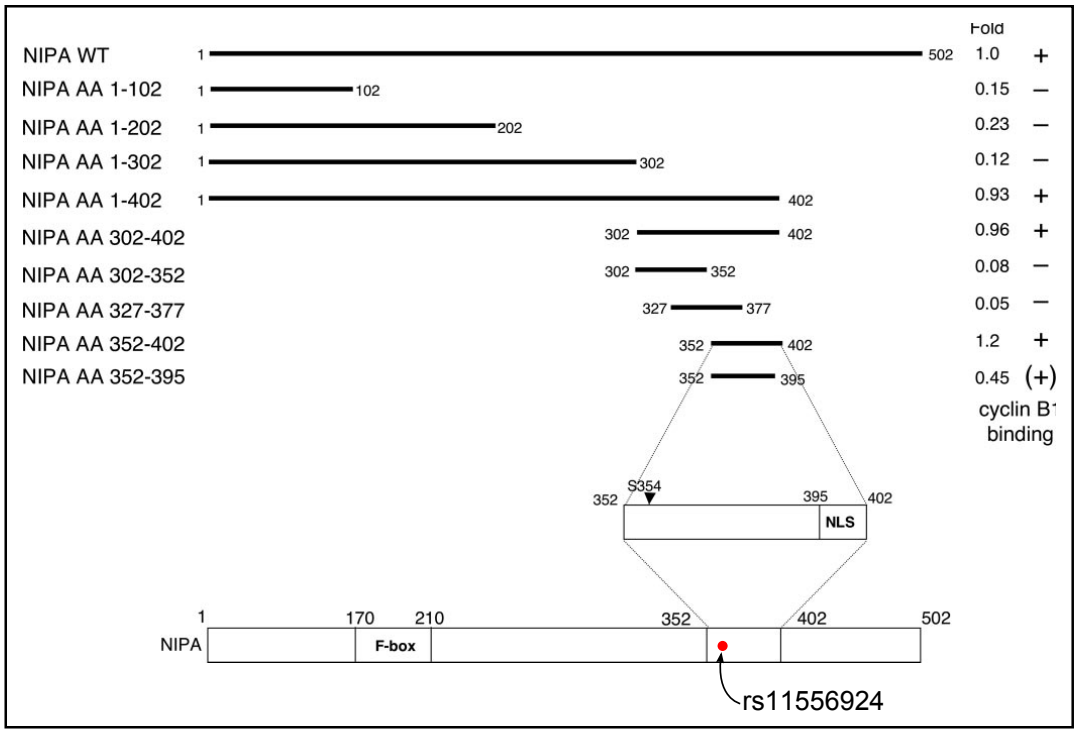

Figure 1.5.: NIPA contains a binding site for Cyclin B1. The SNP rs11556924 lies within the region that shows the strongest Cyclin B1-binding. Modified from Bassermann et al. (2007), by marking the position of rs11556924. NLS: nuclear localization sequence.

Cyclin B1 is a cell cycle regulating protein. In a complex together with Cyclin-dependent kinase Cdk1, named maturation promoting factor (Nurse, 1990), it induces mitosis in a switch-like manner (Ferrell, 1998). Maturation promoting factor is involved in early mitotic processes such as chromosome condensation, breakdown of the nuclear envelope, and assembly of the spindle poles, mediated by phosphorylation of 13S condensin (Kimura et al., 1998), lamins (Peter et al., 1990; Mall et al., 2012), and the kinetochores (Chen et al., 2008). During interphase, Cyclin B1 is localised in the cytoplasm. Prior to mitosis, it is upregulated (Hwang et al., 1995) and transferred to the nucleus (see figure 1.6). Phosphorylation of a cytoplasmic retention signal mediates translocation to, and also blocks the export from, the nucleus (Hagting et al., 1999).

Cyclin B1 is also associated with cancer (Yuan et al., 2006), as high levels of Cyclin B1 were found in a variety of cancerous tissues (A. Wang et al., 1997).

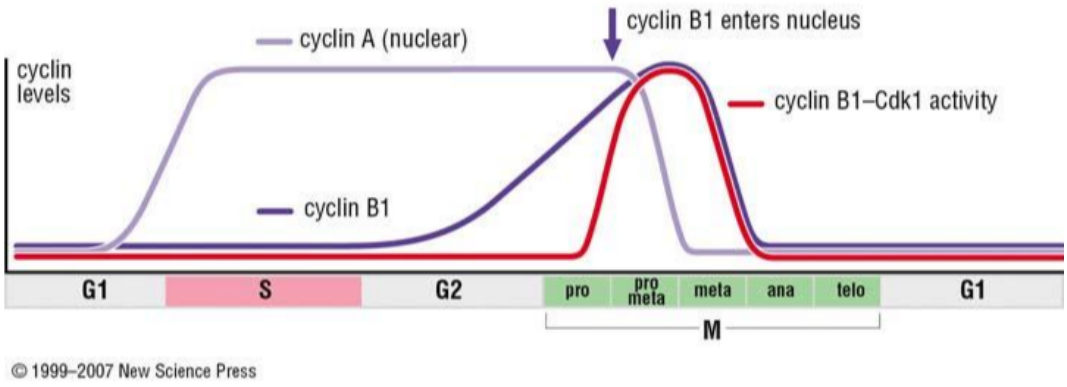

Figure 1.6.: Levels of Cyclin B1 through the cell cycle. At the end of the S phase, Cyclin B1 is upregulated, but remains inactive. After relocation to the nucleus, Cyclin B1 is activated and carries out its mitosis-promoting functions. Towards the end of M phase, Cyclin B1 activity decreases as it is degraded. (from: Morgan, 2007)

SCF-NIPA contributes to the regulation of Cyclin B1 (see figure 1.7), by targeting nuclear Cyclin B1 and leading to its degradation (Bassermann et al., 2005b). Upon entry of M phase, Cyclin B1 massively enters the nucleus (see figure 1.7, right panel), whereupon NIPA is inactivated through phosphorylation at different serine residues by Cyclin B1/ Cdk1 (Bassermann et al., 2007), and also by APC/C (Klitzing et al., 2011) and ERK2 (Illert et al., 2012a). After inactivation of NIPA, Cyclin B1 can subsequently carry out its function in promoting early events in mitosis (Bassermann et al., 2005a).

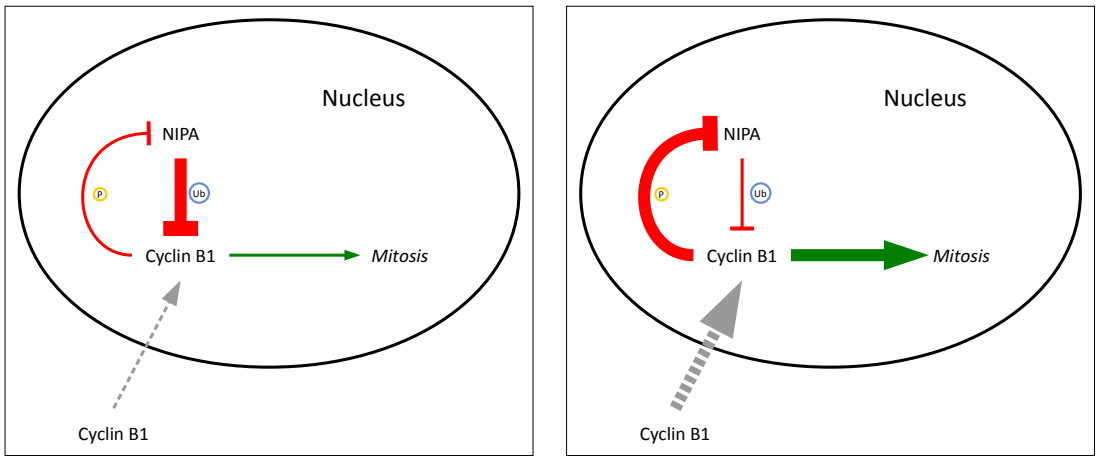

Figure 1.7.: NIPA controls entry of mitosis. During interphase (left), NIPA targets nuclear Cyclin B1 for degradation through ubiquitinylation. At the beginning of M phase (right), Cyclin B1 massively enters the nucleus, inhibits NIPA by phosphorylation, and promotes mitosis.

1.5.2. *Zc3hc1* and CAD/ MI

Recent publications have linked the SNP rs11556924 to hypertension in a Finnish population (Kunnas & Nikkari, 2015), and to a higher carotid intima-media-thickness (cIMT) (López-Mejías et al., 2013). Although both publications seem to have contradictory results – López-Mejías et al. saw the homozygote *non-risk* genotype to be associated with higher cIMT, an indicator of atherosclerosis, whereas Kunnas et al. reported the homozygote *risk* genotype to be correlated with higher blood pressure - they consolidate the link between the locus and CVD.

1.6. Aims of this thesis

Many GWAS have linked genomic regions to CAD/ MI (see section 1.4.2). However, the causal genes, as well as the underlying patho-mechanisms and functional links to CAD/ MI, are still unclear. This thesis addresses the question if *Zc3hc1*, one of these CAD-risk genes, plays a role in atherosclerosis, and if so, by which mechanism.
The locus containing the gene *Zc3hc1* was identified by only one SNP, rs11556924, with no other variants in high linkage. The SNP lies within the sequence of *Zc3hc1* and is a missense-variant, causing an aminoacid-exchange in the encoded protein NIPA. It is thus considered a good candidate for functional analyses.

The first aim is to study the effect of the SNP on the binding of NIPA and its interaction partner Cyclin B1.

The second and main part of this thesis is to investigate the role of the gene *Zc3hc1* in atherosclerosis using a mouse model. For this, the *Zc3hc1*-knockout (KO) mouse line will be established, confirmed, and phenotyped. Then, the mice will be backcrossed to the proatherogenic Apolipoprotein E (ApoE)-KO background, and the development of atherosclerosis will be analysed in order to assess the impact of the gene *Zc3hc1* on the disease.

2. Material and Methods

2.1. Mammalian Two-Hybrid assay

The Mammalian Two-Hybrid assay can be used to detect, and also quantify, protein interaction. The two proteins of interest are fused to either the Gal4 DNA-binding domain (origin species: yeast) or the NF-κB transcription-activating domain (origin species: mouse) in the plasmids pCMV-BD or pCMV-AD, respectively. Insertion of the proteins of interest has to occur in the same reading frame as the fusion proteins in the plasmids pCMV-BD and -AD. This can be achieved by amending the cloned cDNA sequences of the proteins with restriction enzyme sites that define the direction of insertion into the plasmids. The plasmids are then cotransfected into mammalian cells, together with the reporter plasmid containing the firefly luciferase gene with a synthetic promoter region consisting of several repeats of the Gal4 binding sites. If the proteins interact, they form a functional transcription activator that binds to the Gal4 promoter (see figure 2.1), and induces the expression of firefly luciferase, which can then be detected in a luminometer.

The assay includs four control plasmids, pBD-NF-κB, pBD-p53, p-AD-SV40T, and pAD-TRAF. pBD-NF-κB contains both the Gal4 DNA binding and the NF-κB transcription activating domains, and serves as a positive control, resulting in a strong signal. p53 and SV40T show protein interaction (moderate positive control), while p53 and TRAF do not (negative control). As an internal control, the plasmid pRL-TK, containing the Renilla luciferase under the HSV-thymidine kinase promoter, is transfected along with the other plasmids. It is expressed constitutively yet moderately, and the activity of firefly luciferase is normalised to the activity of the Renilla luciferase.

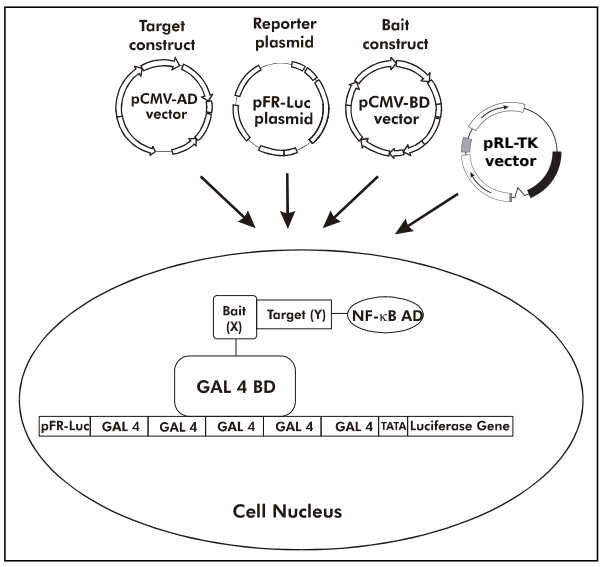

Figure 2.1.: Overview of Mammalian Two-Hybrid assay. The two proteins of interest are inserted into pCMV-AD (target construct) and -BD (bait construct), respectively. If successful transfection together with the reporter plasmid pFR-Luc occurs, and the proteins show interaction, the firefly luciferase gene will be activated and expressed. Resulting firefly luciferase activity can be measured in a luminometer. Cotransfected and constitutively expressed Renilla luciferase (pRL-TK) is used for normalization. Image modified from manufacturer's manual (http://www.chem-agilent.com/pdf/strata/211344.pdf).

2.1.1. Material, Buffers, Devices

Table 2.1.: Material, Buffers and Devices for Mammalian Two-Hybrid assay

Category	Name	Company/ Composition
Material	Reaction tubes (0.2, 0.5, 1.5 and 2.0ml)	Sarstedt
	Reaction tubes (15 and 50ml)	Sarstedt
	Biosphere Filter Tips (10, 100 and 1000µl)	Sarstedt
	Serological Pipettes (2, 5, 10 and 25ml)	Sarstedt
	Petri dish (94/16 MM)	greiner bio-one (# 633181)
	24-Well plate	greiner bio-one (# 662160)
	Disposable Scalpel No. 22	Feather (# 02.001.30.022)
	UV-Cuvette micro	Brand (# 759210)
	Inoculation loop (1µl)	Sarstedt (# 86.1567.010)
	Inoculation spreader	Sarstedt (# 86.1569.001)
	QIAprep® spin Miniprep Kit	Qiagen (# 27106)
	QIAfilter™ Plasmid Midi Kit	Qiagen (# 12243)
	Nucleospin® DNA and PCR Clean-up	Macherey-Nagel (#740609)

Continued on next page

Category	Name	Company/ Composition
	TOPO® TA Cloning® Kit	Invitrogen (# 450641)
	QuikChange II XL Mutagenesis Kit	Stratagene (# 200522)
	Chemically competent *E. coli* DH5α™	NEB (# C2987I)
	Mammalian cells	HeLa
	Restriction enzyme BamHI	NEB (# R0136S)
	Restriction enzyme SalI	NEB (# R0138S)
	rAPid Alkaline Phosphatase	Roche (# 4898133001)
	T4 DNA Ligase (1U/µl)	Roche (# 10716359001)
	Microplates 96 well, white	Berthold Technologies GmbH & Co. KG (# 23300)
Buffers	PCR Mastermix	5-Prime (# 2200110), 2.5x Master-Mix
	MyTaq™ DNA Polymerase	Bioline (# 21107), with separate 5x buffer
	TBE-Buffer	100mM Tris-Base + 80mM Boric Acid + 1.3mM EDTA in Aqua dest.
	1.5% Agarose	Biozym (# 840040), in TBE
	Dextran Blue Buffer	99% Formamide, 1% Dextran Blue, and 80µl Bio-Rad 5x Nucleic Acid Sample Loading Buffer (# 1610767) per ml final volume
	SYBR-Green I	diluted 1:200 in DMSO
	Loading Dye	SYBR-Green I diluted 1:2 in Dextran Blue Buffer
	100bp DNA Ladder plus (44ng/µl)	Peqlab (# 25-2020), 500ng/µl, diluted in Aqua dest.
	LB agar (Lennox)	Sigma (# L2897-250G)
	LB (Lennox)	Sigma (# L3022-250G)
	Antibiotics	Ampicillin (100mg/ml); Kanamycin (100mg/ml)
	Restriction enzyme buffer NEBuffer 3	NEB (# B7003S)
	BSA, 100x (10mg/ml)	NEB
	S.O.C. Medium	Thermo Fisher (# 15544034)
	Culture Medium	Gibco (# 31966), DMEM (1x), supplemented with 10% FBS and 1% P/S

Continued on next page

Category	Name	Company/ Composition
	FuGene HD Transfection Reagent	Promega (# E2311)
	Dual-Luciferase® Reporter Assay System	Promega (# E1960)
Devices	PCR Cycler	SensoQuest labcycler
	Elektrophoresis Power Supply	Micro-Bio-Tec Brand
	Chemidoc XRS documentation	Bio-Rad
	Transilluminator Flu-O-Blu	Biozym, (460 to 490nm)
	Thermomixer 5436	Eppendorf
	Biofuge pico	Heraeus
	Centrifuge Rotanta 460 R	Hettich
	Compact shaker KS 15 control	Edmund Bühler GmbH
	Incubator Hood TH 15	Edmund Bühler GmbH
	Laminar Flow Clean Bench	CleanAir
	Biophotometer	Eppendorf
	TriStar^2 Multimode Reader LB 942	Berthold Technologies GmbH & Co. KG

Table 2.2.: Primer pairs for amplification of the cDNAs of human NIPA and Cyclin B1. Primers were diluted with Aqua dest. in pairs, to a concentration of 5pmol/µl each. Amplicon: the size of the expected PCR product length in basepairs.

Target	Forward Primer	Reverse Primer	Amplicon
NIPA	`ggatccATGGCGGCGCCCTGTG`	`gtcgacTCAGCATGAGCACAGAG`	1521
Cyclin B1	`ggatccATGGCGCTCCGAGTCACCAG`	`gtcgacTTACACCTTTGCCACAGCC`	1314

Table 2.3.: Primers for mutagenesis. Each primer was diluted with Aqua dest. to a concentration of 10pmol/µl.

Target	Forward Primer	Reverse Primer
NIPA-811	`GCTCTCCCTGATAaCATGTTCGCAATGTATG`	`CATACATTGCGAACATGtTATCAGGGAGAGC`
NIPA-1088	`CCAGTCCTGTTGACCgTCCTGAGCCAGAGGC`	`GCCTCTGGCTCAGGAcGGTCAACAGGACTGG`

Table 2.4.: Primers for insertion control and sequencing. Most primers are commercially available under following names: M13(-20) (M13 forward), AD 5' (AD forward), and BD 5', and BD 3' (BD forward, and reverse, respectively). Each primer was diluted with AQUA DEST. to a concentration of 10pmol/µl.

Target	Forward Primer	Reverse Primer
M13	GTAAAACGACGGCCAG	CAGGAAACAGCTATGAC
pCMV-AD	GGAGATGAAGACTTCTCCT	AATACGACTCACTATAG
pCMV-BD	AGCATAGAATAAGTGCGAC	TAATACGACTCACTATAGGG

2.1.2. Protocol

Amplification and Isolation of cDNA

To amplify the cDNAs for human NIPA and Cyclin B1, and to amend the sequences with restriction enzyme sites, specific primer pairs were designed (see table 2.2). The forward primer was extended by GGATCC for the restriction enzyme BamHI, and the reverse primer by GTCGAC for SalI. Both enzymes produce sticky ends, thus enabling the specific ligation of the cDNAs in the desired orientation.

The plasmid pCMV-BD does not contain an in-frame stop codon. As the full cDNA sequences of both NIPA and Cyclin B1 were cloned including their own stop codons, there was no need to add a stop codon for a proper termination of translation.

The primer pairs were then used in PCRs (see table 2.5 for the recipe, and table 2.6 for the PCR-program) with cDNA from human coronary artery SMCs. The PCR products were separated on an agarose gel, identified, and cut out from the gel over a blue light-emitting transilluminator. The PCR products were then isolated using the Nucleospin® DNA and PCR Clean-up Kit according to manufacturer's instructions, and eluted in 25µl elution buffer.

Cloning into shuttle vector Topo

To verify the sequences of the amplified cDNAs, the PCR products were cloned into the shuttle vector pCR™2.1-TOPO® TA (or Topo). Topo vector contains resistance genes

Table 2.5.: Ingredients for a PCR reaction for cDNA-amplification. Values given in µl.

	Volume
2.5x 5-Prime-Mix	4
Primer mix	1
Aqua dest.	4
cDNA	1
Total	10

Table 2.6.: PCR program *TD61 1:45 35* for cDNA-Amplification. Primer annealing temperature is lowered stepwise, from 61°C to 55°C.

Purpose	[°C]	[min]	Repeats
Denaturation	94	5:00	1x
Denaturation	94	0:30	3x
Annealing	61	0:30	
Elongation	72	1:45	
Denaturation	94	0:30	3x
Annealing	59	0:30	
Elongation	72	1:45	
Denaturation	94	0:30	3x
Annealing	57	0:30	
Elongation	72	1:45	
Denaturation	94	0:30	35x
Annealing	55	0:30	
Elongation	72	1:45	
Elongation	72	10:00	1x
Cooling	4	∞	1x

against the antibiotics Ampicillin and Kanamycin to restrict growth on agar plates containing either of the antibiotics only to successfully transformed bacteria. Cloning into Topo vector resembles a sticky end-cloning, as the plasmid is already linearised and has `T`-overhangs, which ligate easily with the `A`-overhangs of the PCR products that are left there by the Taq DNA polymerase.

Each PCR product was ligated individually into a linearised Topo vector (see table 2.7). The tubes were incubated for 5 min at room temperature, then put on ice. 3µl per ligase reaction were each added to a 50µl aliquot of competent *E. coli* bacteria, and left on ice for 15min. Bacteria were then transformed by heat-shock at 42°C for 40s, and again put on ice. To start proliferation, 125µl S.O.C. medium were added to each tube, and bacteria were then placed in a shaking incubator for 1h at 37°C. Finally, 100µl of each reaction were plated on LB-agar plates containing 100µg/ml Ampicillin and incubated overnight at 37°C.

Table 2.7.: Recipe for ligation of PCR products into Topo-vector. Values given in µl.

	Volume
cleaned-up PCR product	3
Salt	1
linearised Topo-vector	0.8
Aqua dest.	1.2
Total	6

Insertion Control

After overnight incubation, individual clones were picked using a small pipette tip, and gently moved to a new LB-agar plate with a raster in order to identify the clones. The pipette tips were then swirled in a PCR tube with a premixed PCR reaction (20µl, see table 2.8). For this PCR, the M13 primer pair was used. These primers bind within the plasmid sequence, outside of the Multiple Cloning Site (MCS) (see figure 2.2), hence excluding false positive PCR results which could arise from unligated PCR product when using the same primers as for the amplification.

PCR was performed with the same program as for amplification (see table 2.6), only

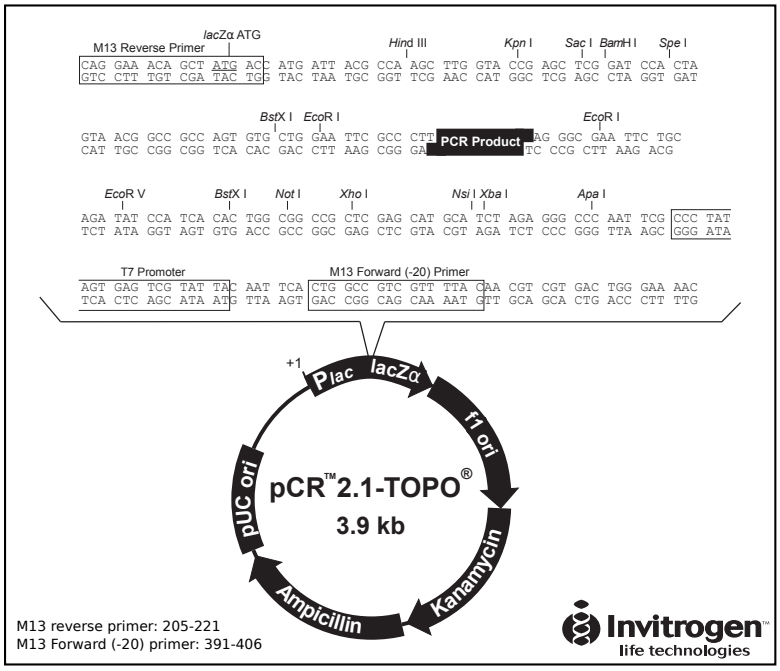

Figure 2.2.: Multiple cloning site of the pCR™2.1-TOPO® TA-vector. Position and sequence of the M13 primer pair are denoted. Image modified from manufacturer's manual (https://tools.thermofisher.com/content/sfs/manuals/topota_man.pdf).

the first step at 94°C was changed to 10min. After the PCR, samples were put on an agarose gel, positive clones containing the desired inserts were identified and selected for plasmid isolation via Miniprep.

Table 2.8.: Ingredients for a PCR reaction for insertion control (20µl reaction volume). Values given in µl.

	Volume
5x MyTaq™ buffer	4
M13(-20) forward primer (10pmol/µl)	1
M13 reverse primer (10pmol/µl)	1
MyTaq™ DNA Polymerase (5U/µl)	0.1
Aqua dest.	13.9
Total	20

Plasmid Isolation using Miniprep

Clones selected for plasmid isolation were transferred into 5ml liquid LB-medium containing 100µg/ml Ampicillin, and incubated overnight in a shaking incubator at 37°C and 225 rpm. On the next day, tubes were centrifuged for 10min at 3000 rcf to pellet the bacteria. After that, plasmids were isolated using the QIAprep® spin Miniprep Kit according to manufacturer's instructions, and eluted in 50µl elution buffer. Concentration of the samples was measured using a biophotometer.

Sequencing

Sequencing was performed to ensure clones containing the correct inserts were used. Samples were prepared and sent to Seqlab - Sequence Laboratories Göttingen GmbH (Göttingen). Sequences longer than 500 bp were sequenced with more than one primer, with each primer mixed into an individual reaction.
700 to 1000ng of purified plasmid DNA were filled up to 12µl with AQUA DEST., 3µl of 10µM primer solution were added, reaching a final volume of 15µl, and samples were then sent for sequencing.

Mutagenesis

Single bases in the plasmids were changed using Mutagenesis. First, primers containing the desired change (denoted by a small letter, see table 2.3), and sufficiently long flanking regions, were designed, and then used in a PCR reaction (see tables 2.9 and 2.10). For a higher efficiency, the reverse complement to each primer was also used in the mutagenesis reactions.

After the PCR, the parental plasmids were digested using the restriction enzyme DpnI, which can recognise methylated and hemimethylated DNA. 0.2µl of the enzyme solution were added to each reaction, and placed in a thermocycler for 1h at 37°C, followed by a cooling step at 16°C. The mutated plasmids were then individually transformed according to manufacturer's instructions into XL-10-Gold ultracompetent cells for nick repair, spread on LB-agar plates containing 100µg/ml Ampicillin, and incubated at 37°C for $>$ 16 h. On the next day, clones were picked and precultivated in 4.5ml liquid

Table 2.9.: Ingredients for a mutagenesis PCR reaction. Values given in µl.

	Volume
10x Buffer	1
Plasmid (50ng/µl)	1
Forward primer (10pmol/µl)	1
Reverse primer (10pmol/µl)	1
Deoxyribose Nucleoside Triphosphate (dNTP) mix	0.2
QuikSolution reagent	0.6
Aqua dest.	5.2
PfuUltra DNA Polymerase	0.2
Total	10.2

Table 2.10.: PCR program *Pointmutation* for mutagenesis. The program is designed according to manufacturer's instructions, with the elongation step within the 18x-cycle lasting for 1min /kbp of the plasmid length (3.9kbp Topo-vector + 1.5kbp biggest insert).

Purpose	[°C]	[min]	Repeats
Denaturation	95	1:00	1x
Denaturation	95	0:50	18x
Annealing	60	0:50	
Elongation	68	6:00	
Elongation	68	7:00	1x
Cooling	16	∞	1x

LB-medium containing 100µg/ml Ampicillin for Miniprep (see section 2.1.2). After isolation of the plasmids, they were sequenced (see section 2.1.2) to ensure a successful mutagenesis.

Subcloning into Target and Bait Plasmids pCMV-AD & -BD

Plasmids containing the cDNA of NIPA-Wildtype (WT), NIPA-R363H, or Cyclin B1 (see table 2.2 and section 2.1.2) were selected for subcloning into the plasmids pCMV-AD (target construct) and pCMV-BD (bait construct) for the mammalian two-hypbrid assay. Each cDNA was ligated into both vectors.
First, the cDNAs were cut out from the shuttle vector via digestion with the restriction enzymes BamHI and SalI. The volume for the required amount of plasmid DNA (1µg) was calculated for each cDNA, and then used for the digestion reaction. The samples were pipetted together according to the recipe (see table 2.11), and then incubated for 1h at 37°C, followed by a deactivation step for the enzymes at 65°C for 20min.

Table 2.11.: Restriction enzyme digestion to cut out cDNAs. Values given in µl, except for the required plasmid amount, which is denoted in µg, and for which the volume needs to be adjusted accordingly.

	Volume
Shuttle plasmid (µg)	1
BamHI (20U/µl)	0.5
SalI (10U/µl)	1
NEBuffer 3	4
BSA (10x)	4
Aqua dest.	ad 40
Total	40

After digestion, the samples were separated on an agarose gel, and the bands containing the digested cDNAs were cut out. The cDNAs were isolated from the gel bands using the Nucleospin® DNA and PCR clean-up kit, and their concentration was measured using a biophotometer.

The cDNAs containing the restriction enzyme sites for BamHI and SalI were then cloned into the plasmids pCMV-AD and -BD. First, the plasmids were linearised using the

same restriction enzymes. Each sample was mixed according to table 2.12, and then incubated at 37°C for 10min, followed by an inactivation step at 65°C for 15min. After that, the ends of the linearised plasmids were dephosphorylated; 1µl rAPid Alkaline Phosphatase and 1µl 10x dephosphorylation buffer were added to each reaction, and then incubated at 37°C for 10min, followed by an inactivation step at 65°C for 15min. Then, the cDNAs were ligated into the plasmids using the T4 DNA ligase; for each cDNA, the mix was pipetted according to table 2.13, and then added to the linearised and dephosphorylated plasmids (final volume $\leq$ 25µl). After incubation for 1h at room temperature, the plasmids were then transformed into competent *E. coli* bacteria. For each ligation reaction, 5µl were added to an aliquot of 50µl of bacteria, and incubated on ice for 10min. After heat-shock transformation for 40s at 42°C, 250µl of room-temperatured S.O.C. medium were added, and the bacteria were incubated for 1h at 37°C while shaking. After that, 150µl were spread on LB-agar plates containing either 100µg/µl Ampicillin (for bacteria transformed with pCMV-AD) or 50µg/µl Kanamycin (for bacteria transformed with pCMV-BD), and incubated overnight at 37°C.

Table 2.12.: Linearization of Target and Bait plasmids. Both plasmids, pCMV-AD and -BD were digested with the restriction enzymes BamHI and SalI. Amounts are sufficient for one reaction. Values given in µl.

	Volume
Plasmid (50ng/µl)	1
BamHI (20U/µl)	0.7
SalI (10U/µl)	1.4
NEBuffer 3	0.7
BSA (10x)	0.7
Aqua dest.	2.5
Total	7

From each plate, clones were picked using a small pipette tip, and gently moved to a new LB-agar plate with a raster in order to identify the clones; plates contained either 100µg/µl Ampicillin for bacteria transformed with pCMV-AD, or 50µg/µl Kanamycin for bacteria transformed with pCMV-BD. The pipette tips were then swirled in a PCR tube with a premixed PCR reaction (20µl, see table 2.14).

PCR was performed with the same program as the amplification of the cDNAs (see table 2.6, only the first step at 94°C was changed to 10min. After the PCR, samples were

Table 2.13.: Ligation of cDNA into Target and Bait plasmids. The volume for 150ng of cDNA should not exceed 10µl. Each cDNA was ligated into both plasmids. Values given in µl.

	Volume
cDNA (ng)	150
Ligation Buffer (10x)	2
T4 DNA ligase (1U/µl)	2
ATP (10mM)	2
Total	$\leq$ 16

Table 2.14.: Ingredients for a PCR reaction for insertion control (20µl reaction volume). Primers are given in table 2.4. Values given in µl.

	Volume
5x MyTaq™ buffer	4
Forward primer (10pmol/µl)	1
Reverse primer (10pmol/µl)	1
MyTaq™ DNA Polymerase (5U/µl)	0.1
Aqua dest.	13.9
Total	20

put on an agarose gel, and positive clones containing the desired cDNAs were identified. These clones were selected for plasmid isolation via Miniprep, and were cultivated in liquid LB-medium containing Ampicillin (pCMV-AD) or Kanamycin (pCMV-BD). Plasmid isolation was performed as decribed above (see section 2.1.2). To check for clones containing the correct cDNAs, the plasmids were sent for sequencing, as decribed above (see section 2.1.2).

Plasmid Isolation using Midiprep

Clones containing the correct plasmids were selected for MidiPrep in order to obtain sufficient concentrations for use in the Mammalian Two-Hybrid assay. The clones were precultivated overnight at 37°C in 50ml liquid LB-medium containing the appropriate antibiotics. On the next day, the tubes were pelleted in a cooled centrifuge (4°C) for 15min at 6000 rcf. Supernatant was discarded, and the plasmid DNA was isolated from the pellets using the QIAfilter™ Plasmid Midi Kit according to the manufacturer's instructions. Finally, the concentrations were measured using a biophotometer, and plasmids were stored at −20°C.

Mammalian Two-Hybrid assay

Per well of a 24-well plate, 6–8 $\times$ 10^4 mammalian cells (HeLa) were seeded in 1 ml Culture Medium, and incubated in a CO_2-incubator for 24 h at 37°C. Prior to transfection, the medium was changed. Each transfection was performed in triplicates. The desired plasmids were mixed according to the recipe in table 2.15, gently swirled, and incubated for 15–20 min at room temperature. Then, the mix was added to the cells, the plate was gently rocked to allow for even distribution, and the cells were again incubated for 24 h.

For analysis, the cells were lysed and the cell lysate was analysed for luciferase activity. First, the cells were washed twice with 0.5 ml Phosphate-Buffered Saline (PBS). PBS was removed as thoroughly as possible, and 100 µl of 1x passive lysis buffer were added to each well, gently swirled, and incubated for 20 min at room temperature while gently shaking. After that, a 20 µl aliquot from the lysate was transferred to a luminometer plate and measured for firefly and Renilla luciferase activity (see table 2.16 for measurement details).

Separate wells were used for protein isolation and subsequent analysis of the expression of the fusion proteins by staining against the Protein NIPA (for the antibody, see section 2.9.1).

Table 2.15.: Ingredients for the Mammalian Two-Hybrid assay. Amounts are given for the transfection of cells in a single well of a 24-Well plate.

	per Well	
Bait plasmid	250	ng
Target plasmid	250	ng
pFR-Luc	250	ng
pRL-TK	7.5	ng
FuGene	1	µl
DMEM pure	100	µl

Table 2.16.: Program of the Multimode Reader for measuring Luciferase activity. The buffers are automatically dispensed into the wells.

Step	time
Dispense 50µl Luciferase Assay Buffer II	
Delay	2s
Integrate Firefly activity	10s
Dispense 50µl Stop & Glo Buffer	
Delay	2s
Integrate Renilla activity	10s

2.2. Generation of *Zc3hc1*-deficient mice

Heterozygous (HET) *Zc3hc1* mice (Zc3hc1$^{tm1a(KOMP)Wtsi}$, background: C57BL/6N) were obtained from the UC Davis Knockout Mouse Project (KOMP) Repository (California). There, they were created using a promoterless targeting cassette, inserted into the intron between exons 4 and 5 of *Zc3hc1*. The targeting construct is composed of a neomycin selection gene, a splice acceptor, the reporter gene lacZ, which is surrounded by two self-cleaving peptide sequences, and two loxP sites flanking exon 5 of the mouse *Zc3hc1* gene (see figure 2.3).

The obtained female and male HET mice were mated to generate *Zc3hc1*-deficient, or knockout (KO), animals. PCR screenings of DNA samples isolated from ear biopsies (see sections 2.3.1 and 2.4.1) were used to determine the genotypes.

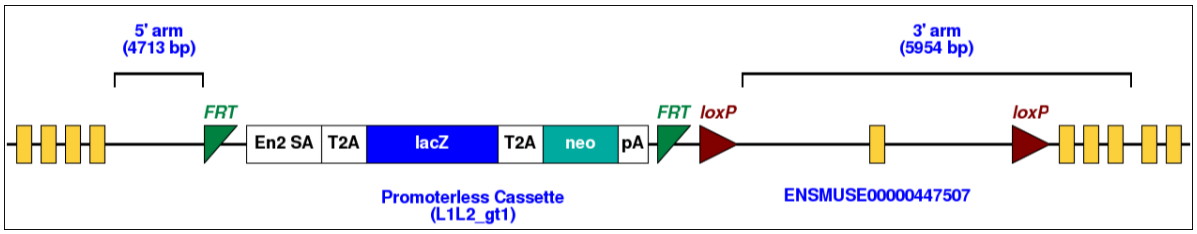

Figure 2.3.: Targeting vector for knocking-out *Zc3hc1*. This vector was used by the UC Davis KOMP Repository to modify mouse embryonic stem cells, introducing the targeting cassette into the gene *Zc3hc1* by homologous recombination. It contains the homology regions (5' and 3' arms), a reporter gene (lacZ), and an antibiotic resistance gene (neo) for selection. The cassette also contains a splice acceptor site (En2 SA), and two sequences for self-cleaving 2A peptides (T2A, Thosea asigna virus 2A), surrounding the reporter gene, as well as a transcriptional termination sequence (pA, poly-adenylation). Furthermore, the vector contains recognition sequences for DNA recombinase enzymes (FRT, for S. cerevisiae FLP recombinase; loxP, for bacteriophage P1 Cre recombinase), which can be used to cut out the targeting cassette (FRT) or an exon (loxP). In combination with cell type-specific expression of the recombinases, this vector could also be used for a conditional knock-out of the targeted gene. Image from: https://www.mousephenotype.org/data/alleles/MGI:1916023/tm1a(KOMP)Wtsi.

2.3. DNA isolation

2.3.1. Material, Buffers, Devices

Table 2.17.: Material, Buffers and Devices for DNA isolation

Category	Name	Company/ Composition
Material	Reaction tubes (1.5ml)	Sarstedt
Buffers	Buffer A	1.52ml 1M NaOH + 24µl 0.5M EDTA + 58.6ml Aqua dest.
	Buffer B	2.4ml 1M Tris-HCl (pH 7.5) + 57.6ml Aqua dest.
Devices	Thermomixer 5436	Eppendorf
	Biofuge pico	Heraeus

2.3.2. Protocol

DNA was isolated by Alkaline Lysis. Ear punch biopsies, taken for animal numbering and identification, were dissolved in 50µl Buffer A, incubated for 15min at 95°C, and stabilised with 50µl Buffer B. Samples were then centrifuged to pellet remaining tissue, and stored at room temperature.

2.4. Genotyping

2.4.1. Material, Buffers, Devices

Table 2.18.: Material, Buffers and Devices for genotyping

Category	Name	Company/ Composition
Material	Reaction tubes (0.2, 0.5 and 1.5ml)	Sarstedt
	96-well PCR plate	Sarstedt
Buffers	PCR Mastermix	5-Prime MasterMix 2.5x, (# 2200110)
	TBE-Buffer	100mM Tris-Base + 80mM Boric Acid + 1.3mM EDTA in Aqua dest.

Continued on next page

Category	Name	Company/ Composition
	1.5% Agarose	Biozym (# 840040), in TBE
	Dextran Blue Buffer	99% Formamide, 1% Dextran Blue, and 80µl Bio-Rad 5x Nucleic Acid Sample Loading Buffer (# 1610767) per ml final volume
	SYBR-Green I	diluted 1:200 in DMSO
	Loading Dye	Dextran Blue Buffer:SYBR-Green I (2:1)
	100bp DNA Ladder plus (44ng/µl)	500ng/µl (Peqlab, # 25-2020), diluted in Aqua dest.
Devices	PCR Cycler	SensoQuest labcycler
	Elektrophoresis Power Supply	Micro-Bio-Tec Brand
	Chemidoc XRS documentation	Bio-Rad

Table 2.19.: Primers for Genotyping. Corresponding forward and reverse primers were mixed and diluted in Aqua dest. to a final concentration of 5pmol/µl each.
*) https://www.komp.org/pdf/Genotyping_of_KOMP_CSD_targeted_alleles_Protocol.pdf
**) https://www2.jax.org/protocolsdb/f?p=116:5:0::NO:5:P5_MASTER_PROTOCOL_ID,P5_JRS_CODE:221,002052

Target	Forward Primer	Reverse Primer	Product Size
Zc3hc1	TTGACTGACAGAGGATGAGAGC	GGGCCTTTAATCCCAACACT	260^{WT} ; 298^{KO}
LoxP	GAGATGGCGCAACGCAATTAAT*	TGACAGCATTGTTTTCTGACCTGTGG	534
LacZ	GACGTCTCGTTGCTGCATAA	CAGCAGCAGACCATTTTCAA	399
ApoE**	GCCTAGCCGAGGGAGAGCCG	TGTGACTTGGGAGCTCTGCAGC	155^{WT}
		GCCGCCCCGACTGCATCT	245^{KO}

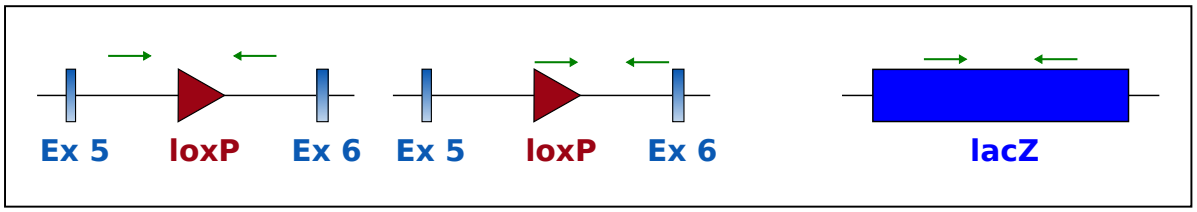

Figure 2.4.: Location of genotyping primers. Left: primer pair targeting the intron between exons 5 and 6 of *Zc3hc1*, which in the targeted allele contains a loxP site. In KO animals (−/−), the resulting PCR product has a size of 298 bp, compared to 260 bp in WT (+/+). HET mice (+/−) have both alleles. Two additional primer pairs (middle and right), one with a primer binding within the loxP site, and one with both primers within the lacZ gene sequence, result in products only in trangene animals.

2.4.2. Protocol

Samples were pipetted according to the protocol (see table 2.20), carefully to avoid bubbles, placed in the thermocycler, and the PCR program *TD61 30 35* was started (see table 2.21).
After the PCR reaction, each sample was mixed with 3µl of Loading Dye, and pipetted into a pocket of a 1.5% agarose gel. Each row was headed by a 100bp-ladder (7µl + 3µl Loading Dye). DNA was separated through Gel-electrophoresis at 120V for 1h, and visualised under UV-Light.

Table 2.20.: Ingredients for a PCR reaction. Values given in µl.

	Zc3hc1/ LoxP/ LacZ	ApoE
2.5x 5-Prime-Mix	4	4
Primer-Mix	1	1.5
Aqua dest.	4	3.5
DNA	1	1
Total	10	10

Table 2.21.: PCR program *TD61 30 35* for Genotyping. Primer annealing temperature is lowered stepwise, from 61°C to 55°C.

Purpose	[°C]	[min]	Repeats
Denaturation	94	5:00	1x
Denaturation	94	0:30	3x
Annealing	61	0:30	
Elongation	72	0:30	
Denaturation	94	0:30	3x
Annealing	59	0:30	
Elongation	72	0:30	
Denaturation	94	0:30	3x
Annealing	57	0:30	
Elongation	72	0:30	
Denaturation	94	0:30	35x
Annealing	55	0:30	
Elongation	72	0:30	
Elongation	72	10:00	1x
Cooling	4	∞	1x

2.5. RNA isolation

2.5.1. Material, Buffers, Devices

Table 2.22.: Material, Buffers and Devices for RNA isolation

Category	Name	Company/ Composition
Material	Reaction tubes (0.2, 1.5, 2.0 and 50ml)	Sarstedt
	Biosphere Filter Tips (10, 100 and 1000µl)	Sarstedt
	Stainless Steel Beads (7mm)	Qiagen (# 69990)
	RNeasy Plus Mini Kit	Qiagen (# 74136)
	UV-Cuvette micro	Brand (# 759210)
Buffers	β-mercaptoethanol	Gibco
	Ethanol abs.	Th. Geyer
	TBE-Buffer	100mM Tris-Base + 80mM Boric Acid + 1.3mM EDTA in RNase-free water
	1.5% Agarose	Biozym (# 840040), in TBE

Continued on next page

Category	Name	Company/ Composition
	Dextran Blue Buffer	99% Formamide, 1% Dextran Blue, and 80µl Bio-Rad 5x Nucleic Acid Sample Loading Buffer (# 1610767) per ml final volume
	SYBR-Green I	diluted 1:200 in DMSO
	Loading Dye	Dextran Blue Buffer:SYBR-Green I (2:1)
	100bp DNA Ladder plus (44ng/µl)	500ng/µl (Peqlab, # 25-2020), diluted in AQUA DEST.
Devices	Tissuelyser LT	Qiagen
	Biofuge pico	Heraeus
	Biophotometer	Eppendorf
	Elektrophoresis Power Supply	Micro-Bio-Tec Brand
	Chemidoc XRS documentation	Bio-Rad

2.5.2. Protocol

RNA from fresh tissue was isolated with the Qiagen RNeasy Plus Mini Kit, which is suitable for not more than 30mg of tissue, as otherwise the capacity of the gDNA-Eliminator Columns is exceeded. Two buffers from the kit need preparatory steps: β-Mercaptoethanol must be added to the RLT Plus-Buffer (10µl/ml, under the fume hud), and RPE-Buffer, prior to first use, needs an addition of a 4-fold of its volume of 96 to 100% ethanol. All steps were performed under the fume hud at room temperature.

Tissue samples were placed in 2ml-tubes, 600µl RLT Plus-buffer and a steel bead were added. Tubes were then placed in the Tissue-Lyser LT and disrupted for 5min at 50Hz. Samples were centrifuging for 5 to 10min at maximum speed in a tabletop centrifuge, or longer if foam persisted. The supernatant was then carefully pipetted into the gDNA Eliminator columns, and centrifuged for 30s at 8000 rcf. Columns were discarded and Flow-Through was kept. Equivalent volume of 70% ethanol, about 600µl, was added to each sample, and stepwise transferred to and centrifuged in the RNA-binding RNeasy-Column (15s at 8000 rcf), until the whole sample was processed. Flow-Through was discarded each time. Bound RNA was then washed by adding 700µl of Buffer RW1 to the column and centrifuging for 15s at 8000 rcf. Flow-Through was discarded. Two additional washing steps, each by applying 500µl of Buffer RPE, followed; samples

were centrifuged at 8000 rcf for 15s after the first, and for 2min after the second step, respectively. Flow-Through was discarded each time. RNeasy-columns were then placed on new Collector Tubes and dried by centrifuging 1min at maximum speed. Finally, after again placing the columns on new Collector-Tubes, RNA was eluted with 30µl of RNase-free water by spinning for 1min at 8000 rcf. Eluted RNA was transferred into smaller tubes (0.2ml) for storage, aliquots were taken for measuring the concentration, and samples were immediately frozen at −80°C.

Concentration of RNA-samples was determined in a UV-photometer. Aliquots were diluted 1:50 in RNase-free water, and measured at a wavelength of 260nm. Additionally, samples were measured at 280nm (absorbance of protein), and the purity of the RNA-sample was assessed by the ratio of Absorbance_{260}/ Absorbance_{280} (2.0 for pure RNA).

RNA integrity was analysed in an RNase-free agarose gel. 1µl aliquots of the RNA samples were filled up to 10µl with RNase-free water, and 5µl of Loading Dye were added. Samples were then pipetted into the agarose gel, and electrophoresis was performed at 105V for 50min. To determine size of the observed bands, visualised under UV-Light, a 100bp-ladder (7µl + 3µl Loading Dye) was used.

2.6. Reverse Trancription

2.6.1. Material, Buffers, Devices

Table 2.23.: Material, Buffers and Devices for Reverse Transcription of RNA to cDNA

Category	Name	Company/ Composition
Material	Reaction tubes (0.2 and 1.5ml)	Sarstedt
	Biosphere Filter Tips (10 and 100µl)	Sarstedt
Buffers	M-MLV Reverse Transcriptase Kit	ThermoFisher (# 28025021)
	dNTP mix (100mM each)	Promega (# U1240)
	Hexanucleotide Random-Primer Mix	Carl Roth (# HP28.1)
	RiboLock RNase Inhibitor	Thermo Scientific (# EO0382)
Devices	PCR Cycler	SensoQuest labcycler

2.6.2. Protocol

RNA was reverse transcribed into cDNA with the M-MLV Reverse Transcriptase Kit from ThermoFisher.
1 to 5µg of total RNA per sample, filled up to a volume of 10µl with RNase-free water, were used. First, RNA samples were denatured at 68°C for 5min in the PCR-cycler, then cooled on ice. The MasterMix (see table 2.24) was prepared on ice, adding the M-MLV-RT at the end, and pipetted to the RNA-samples; total reaction volume was 20µl. Samples were then incubated in the PCR-cycler for 1h at 37°C, followed by an inactivation step for 5min at 95°C, and then frozen at −20°C.

Table 2.24.: Ingredients for an RT-PCR reaction to reverse transcribe RNA into cDNA. Values given in µl.

	Volume
5X First Strand Buffer	4
Ribolock	1
dNTP mix (100mM each)	1
Random-Primer Mix	1
DTT (100mM)	2
M-MLV RT	1
Total	10

2.7. Qualitative PCR with cDNA

2.7.1. Material, Buffers, Devices

Table 2.25.: Material, Buffers and Devices for qualitative PCR with cDNA

Category	Name	Company/ Composition
Material	Reaction tubes (0.2, 0.5 and 1.5ml)	Sarstedt
	96-well PCR plates	Sarstedt
Buffers	PCR Mastermix	5-Prime MasterMix 2.5x, (# 2200110)
	TBE-Buffer	100mM Tris-Base + 80mM Boric Acid + 1.3mM EDTA in Aqua dest.
	1.5% Agarose	Biozym (# 840040), in TBE
	Dextran Blue Buffer	99% Formamide, 1% Dextran Blue, and 80µl Bio-Rad 5x Nucleic Acid Sample Loading Buffer (# 1610767) per ml final volume
	SYBR-Green I	diluted 1:200 in DMSO
	Loading Dye	Dextran Blue Buffer:SYBR-Green I (2:1)
	100bp DNA Ladder plus (44ng/µl)	500ng/µl (Peqlab, # 25-2020), diluted in Aqua dest.
Devices	PCR Cycler	SensoQuest labcycler
	Elektrophoresis Power Supply	Micro-Bio-Tec Brand
	Chemidoc XRS documentation	Bio-Rad

Table 2.26.: Primer pairs for Qualitative PCR with cDNA. Expected product sizes of the amplified cDNA-fragments for each exon-spanning primer pair are given. Product size of primer pair Exon3 & Exon9 is given for the WT sequence only. Primers were individually diluted in Aqua dest. to a concentration of 10pmol/µl.

Target	Primer Name	Function	Sequence	Product Size [bp]	
Zc3hc1	Exon3	Forward	TCTGCGCTAAATATGGTTGG	152	WT: 1042
	Exon4	Reverse	GGCACTGCACAAGGATTTCT		
	Exon8	Forward	AGCATGGGAACAGGAGATTC	207	
	Exon9	Reverse	TCCACTTCTGTTTCCCCATT		
GAPDH	GAPDH_F	Forward	TCACCACCATGGAGAAGGC	169	
	GAPDH_R	Reverse	GCTAAGCAGTTGGTGGTGCA		

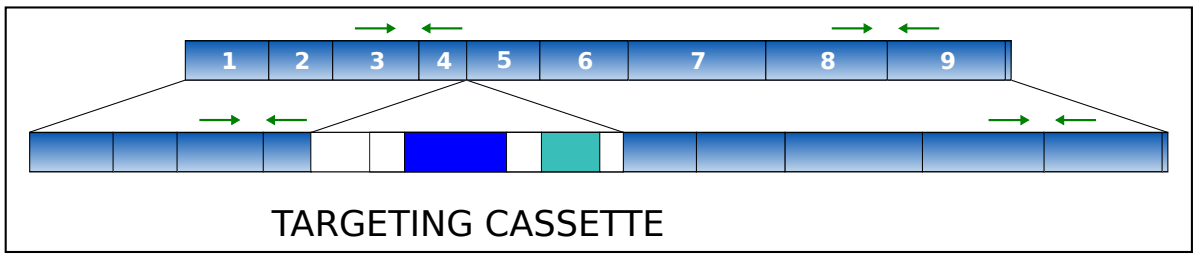

Figure 2.5.: Location of primers in *Zc3hc1*-cDNA. Exon spanning primer pairs, indicated by green arrows, are positioned between exons 3 and 4, and exons 8 and 9, respectively. A long range PCR between the primers in exon 3 and 9 can be used to distinguish between WT and transgene cDNA.

2.7.2. Protocol

To examine the expression of *Zc3hc1* on transcript level, cDNA, reverse transcribed from RNA (see section 2.6.1), was used. Reactions were pipetted according to protocol (see table 2.27), and placed in the thermocycler to carry out the PCR. The same program as for genotyping was used (see table 2.21). For the primer combination *Zc3hc1* Exon3/Exon9, though, the elongation time was set to 1:15min (see table 2.28).

Table 2.27.: Ingredients for a PCR reaction. Values given in µl.

	Volume
2.5x 5-Prime-Mix	4
Primer Forward (10pmol/µl)	0.5
Primer Reverse (10pmol/µl)	0.5
Aqua dest.	4
cDNA	1
Total	10

After the PCR-reaction, each sample was mixed with 3µl of Loading Dye, and pipetted into a pocket of a 1.5% agarose gel. Each row was headed by a 100bp-ladder (7µl + 3µl Loading Dye). Gel-electrophoresis was carried out at 120V for 1h, and bands were then visualised under UV-Light.

Table 2.28.: PCR program *TD61 1:15 35* for amplification of cDNA, with an elongation time of 1:15min. Primer annealing temperature is lowered stepwise, from 61°C to 55°C.

Purpose	[°C]	[min]	Repeats
Denaturation	94	5:00	1x
Denaturation	94	0:30	3x
Annealing	61	0:30	
Elongation	72	1:15	
Denaturation	94	0:30	3x
Annealing	59	0:30	
Elongation	72	1:15	
Denaturation	94	0:30	3x
Annealing	57	0:30	
Elongation	72	1:15	
Denaturation	94	0:30	35x
Annealing	55	0:30	
Elongation	72	1:15	
Elongation	72	10:00	1x
Cooling	4	∞	1x

2.8. Protein isolation

2.8.1. Material, Buffers, Devices

Table 2.29.: Material, Buffers and Devices for protein isolation

Category	Name	Company/ Composition
Material	Reaction tubes (1.5 and 2.0ml)	Sarstedt
	Stainless Steel Beads (7mm)	Qiagen (# 69990)
	Strip Plate	greiner bio-one (# 756070)
Buffers	RIPA Buffer (10x)	Cell Signaling (# 9806S)
	cOmplete™ Protease Inhibitor Cocktail (25x)	Roche (# 11697498001); stock solution prepared by dissolving one tablet in 2ml Aqua dest.
	PMSF	Sigma (# P7626)
	DC Protein Assay	Bio-Rad (# 5000116)
	Protein Standard, 2mg/ml BSA	Sigma Aldrich (# P0834)
Devices	Tissuelyser LT	Qiagen

Continued on next page

Category	Name	Company/ Composition
	Biofuge pico	Heraeus
	Synergy HT Microplate Reader	Biotek

2.8.2. Protocol

Tissue samples were placed in 2ml Eppendorf tubes. 350µl of Protein Isolation Buffer (see table 2.30) and a steel bead were added. Tubes were then placed in the Qiagen Tissuelyzer and homogenised for 10min at 50Hz. Afterwards, samples were centrifuged for 5min at 16 000 rcf and 4°C, and supernatant was transferred into a new tube. They were kept on ice, until all samples were collected, and then stored at −80°C.

Table 2.30.: Ingredients for Protein Isolation Buffer. Amounts are given for a total volume of 5ml. Values given in µl.

	Volume
RIPA Buffer (10x)	500
cOmplete™ Protease Inhibitor Cocktail (25x)	200
PMSF	50
Aqua dest.	4250
Total	5000

Concentration was measured in duplicates with the Bio-Rad DC Protein Assay, according to protocol. In a 96-Well strip plate, 5µl of sample (or water, or standard) were placed in a well each. 25µl of S:A-mix (1:50), and 200µl of buffer B were added. Samples were incubated for 15min in the dark, and then measured in the plate reader at 750nm.

2.9. SDS-PAGE and Western blot

2.9.1. Material, Buffers, Devices

Table 2.31.: Material, Buffers and Devices for SDS-PAGE and Western blot

Category	Name	Company/ Composition
Material	Reaction tubes (1.5, 15 and 50ml)	Sarstedt
	Drying Block	Schleicher & Schuell (# 310-992), 37 × 100mm
	Chromatography paper (3mm)	Th.Geyer (# 7637916)
	Immobilon-P PVDF Transfer Membrane	Merck (# IPVH00010)
Buffers	Acrylamid:Bisacrylamid (37.5:1)	Carl Roth (# 3029.2)
	Separation Gel Buffer	1.5M Tris pH 8.8 + 0.4% SDS
	Stacking Gel Buffer	0.5M Tris pH 6.8 + 0.4% SDS
	TEMED	Sigma Aldrich (# T9281)
	10% APS	Carl Roth (# 9592.3), (w/v) in Aqua dest.
	Electrophoresis Buffer	12.5mM Tris-Base + 9.6mM Glycin + 1.75mM SDS, adjust pH to 8.3, and fill up to 1l with Aqua dest.
	Precision Plus Protein™ Dual Color Standard	Bio-Rad (# 1610374)
	Blue Loading Buffer (3x)	NEB (# B7703S)
	DTT	1.25M in Aqua dest.
	Sample Loading Buffer	Blue Loading Buffer:1.25M (10:1)
	Blot Buffer	25mM Tris-Base + 192mM Glycin + 200ml Methanol, add Aqua dest. to 1l
	Methanol	Carl Roth
	TBS/ TBS-Tween	150mM NaCL + 10mM Tris, add Aqua dest. to 1l, adjust pH to 7.3; add 500µl Tween 20 for TBS-Tween

Continued on next page

Category	Name	Company/ Composition
	5% Skimmed Milk	2.5g Skimmed Milk Powder (Carl Roth, # T145.3) in 50ml TBS
	ECL Prime Western Blotting Detection Reagent	GE Healthcare (Amersham, # RPN2232)
Devices	Mini Protean Tetra Cell System	Bio-Rad
	Power Pac 300	Bio-Rad
	Trans-Blot Turbo	Bio-Rad
	Duomax 1030 Shaker	Heidolph
	Shaker Vibrax-VXR	IKA
	Chemidoc XRS Documentation	Bio-Rad

Table 2.32.: Antibodies for Western blot.

Desription	Dilution	Company
rabbit polyclonal anti-NIPA (phospho S354)	1:500 in 5% Skimmed Milk	ab63557, abcam
rabbit polyclonal anti-GAPDH	1:2000 in 5% Skimmed Milk	ab9485, abcam
goat anti-rabbit IgG, HRP-linked	1:2000 in 5% Skimmed Milk	7074, Cell Signaling

2.9.2. Protocol

Protein samples were analysed with Sodium Dodecyl Sulfate Polyacrylamide Gel Electrophoresis (SDS-PAGE) and subsequent immunoblotting. Gels consist of two parts, a separation gel and a stacking gel, which has pockets for individual samples and is on top of the separation gel. The gels have different percentages of acrylamide: 5% in the stacking gel, and 10% for the separation gel.

First, the gels for the electrophoresis were prepared in the casting frames. Two glass plates, one having 1mm spacers, were pressed together and clamped into the casting frame; a sponge under the plates closed the chamber from the bottom. The separation gel was then poured between the glass plates, and covered with ethanol to obtain a horizontal edge. After polymerisation of the separation gel, ethanol was discarded, and

Table 2.33.: Composition of SDS-PAGE gels. Volume is sufficient for two 1mm thick gels, and a rest for control of polymerisation. Note: TEMED and APS should be added right before use. Values given in µl.

	stacking gel (5 %)	separation gel (10 %)
Stacking gel buffer	1500	
Separation gel buffer		3125
Acrylamide	1000	4156.25
AQUA DEST.	3500	5218.75
TEMED	10	12.5
APS	60	75
Total	6070	12 587.5

remaining ethanol was removed with drying block paper. The stacking gel was then poured into the chamber, and the well-forming comb was inserted, avoiding air bubbles. When the stacking gel polymerised, glass plates were carefully taken out from the casting frame and placed in the buffer dam, which was then positioned in the electrophoresis chamber. After filling the inner chamber between the glass plates with electrophoresis buffer, the combs were removed carefully. Protein samples were prepared by mixing them 2:1 with loading buffer, followed by a denaturating step at 95°C for 5min. Samples were then pipetted into the wells of the gel. Each lane was loaded with 15µg total protein. Every gel contained a protein marker (Precision Plus Protein Dual Color). Proteins were then separated at 100V for 30min, and at 120V until the blue loading buffer reached the bottom of the gel.

After the electrophoresis, the separated proteins were first blotted to a Polyvinylidene Fluoride (PVDF)-membrane using the Semidry-technique, and then immunostained with specific antibodies. Five sheets of chromatography paper were cut in half, and all ten pieces were soaked in transfer buffer. The PVDF-membrane was washed in methanol and equilibrated in transfer buffer. For the transfer of the proteins, the the transfer sandwich, consisting of 5 sheets of chromatography on the bottom, the membrane, the gel, and the other 5 sheets of soaked chromatography paper, was assembled in a Turboblotter cassette. Air from between the layers was removed using the blot roller. The gel, kept between the glass plates in the electrophoresis chamber filled with buffer was taken out and placed in the sandwich, after removing the stacking gel. The proteins were transferred at 25V for 40min.

After the transfer, the membranes were incubated in 5% skimmed milk for 1h at 4°C on a shaker, to prevent unspecific binding of the antibodies (blocking). In order to stain one membrane with different primary antibodies, the membranes were cut horizontally

between 37 and 50kDa as determined by the marker bands. The upper half was used for staining with the anti-NIPA-antibody, while the lower was used for anti-GAPDH-staining. Membranes were then incubated with the primary antibodies on a shaker for 1h at room temperature. After three washing steps in TBS-Tween, each for 15min on a shaker at room temperature, the membranes were incubated with the secondary antibody (1h at room temperature, on a shaker). After another three washing steps in TBS-Tween, the protein bands were visualised with the ECL detection reagent and documented in the Chemidoc XRS. ECL detection reagent was mixed according to the manual; each membrane was incubated with 1ml, and image recording started after 1min.

2.10. X-Gal staining

2.10.1. Material, Buffers, Devices

Table 2.34.: Material, Buffers and Devices for X-Gal staining

Category	Name	Company/ Composition
Material	Reaction tubes (15ml)	Sarstedt
	Cover Slips 24 × 50mm, #1	Menzel (# 9161050)
	Dako Pen	Dako (# S2002)
Buffers	β-Gal Staining Kit	Invitrogen (# K1465-01)
	X-Gal solution	20mg/ml in DMF
	Nuclear fast red	Carl Roth (# N096.1)
	Cytoseal XYL	Thermo Scientific (# 8312-4)
Devices	Incubator	Memmert

2.10.2. Protocol

X-Gal (5-bromo-4-chloro-3-indolyl-β-D-galactopyranoside) staining was carried out using a commercial kit (Invitrogen, Germany) and performed according to the instruction of the manufacturer. Cryosections of organs were dried at room temperature for 1 to 2h, and circled with the Dako Pen to provide a barrier for liquids. They were then washed

with PBS for 10min at room temperature, fixed in the fixative solution containing 2% formaldehyde and 0.2% glutaraldehyde at room temperature for 10min, and washed again twice with PBS. The slides were then incubated overnight at 37°C in the X-Gal staining solution (see table 2.35).

Table 2.35.: Ingredients for X-Gal staining solution. Values given in µl.

	Volume
Solution A	25
Solution B	25
Solution C	25
X-Gal solution (20mg/ml in DMF)	125
PBS	2300
Total	2500

After rinsing the slides once with PBS and once with AQUA DEST., the nuclei were counterstained. The sections were incubated with Nuclear fast red in a staining cuvette for 5min at room temperature, rinsed twice in AQUA DEST. to remove excess staining, and then dried for 6h. Finally, slides were dipped in Xylene, mounted with Cytoseal XYL and covered with cover slips.

2.11. Phenotyping *Zc3hc1*-deficient mice

A group of *Zc3hc1*-KO mice, and a control group of WT mice, starting at the age of 3 weeks, were weighed for over 44 weeks to compare weight gain over time.

From the animal database, all offspring of *Zc3hc1*-HET matings were extracted and the genotype frequencies were calculated. From the same data, the average litter size was calculated.

Zc3hc1-KO mice, both male and female, were mated with WT or *Zc3hc1*-HET mice, respectively, to examine fertility of *Zc3hc1*-KO and HET mice.

Two groups of mice, *Zc3hc1*-KO and WT, were left to die of age. Life span was calculated and compared in a Kaplan-Meier survival curve.

2.12. Backcrossing to ApoE-KO mouse line

To generate animals for the atherosclerosis study, the *Zc3hc1* mouse line was backcrossed to the pro-atherogenic Apolipoprotein E (ApoE)-KO mouse line from Jackson Laboratories (B6.129P2-ApoE^{tm1Unc}/J, Stock-# 002052). First, Male ApoE-KO and female *Zc3hc1*-KO mice were bred (see step I, figure 2.6), resulting in double HET animals. Male double HET mice were then picked and mated with female ApoE-KO animals (step II), and resulting male *Zc3hc1*-HET ApoE-KO offspring were selected and again crossed with female ApoE-KO mice (step III). This mating step generated either *Zc3hc1*-WT ApoE-KO or *Zc3hc1*-HET ApoE-KO animals. This generation was ready to breed animals usable for experiments. Female and male *Zc3hc1*-HET ApoE-KO mice (step IV) were mated in high numbers to obtain sufficient animals for the experimental groups (step V). Genotypes were always confirmed via PCR (see sections 2.3.1 and 2.4.1). The *Zc3hc1* mouse line was backcrossed for more than five generations to ensure the C57BL/6J background of the ApoE mouse line.

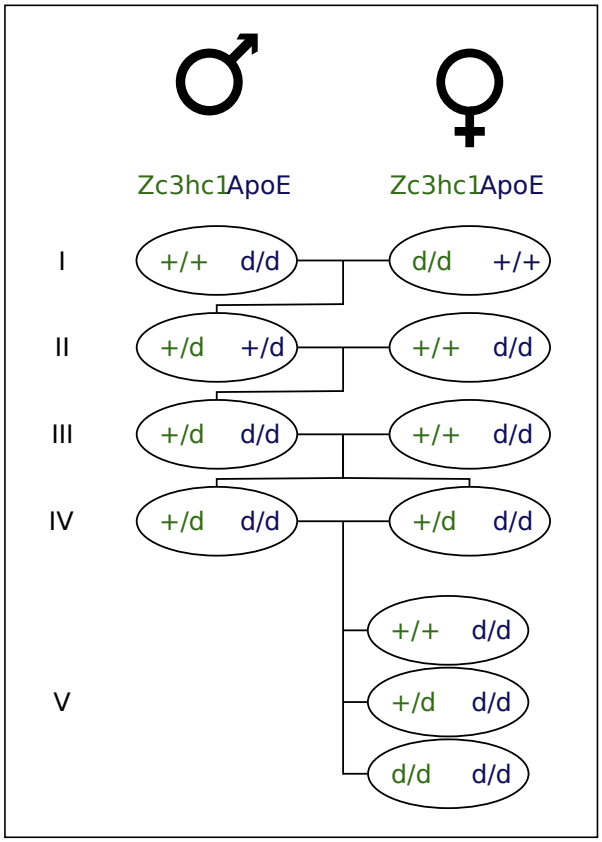

Figure 2.6.: Schematic representation of the breeding plan for backcrossing the *Zc3hc1*-mouse line to the ApoE-KO background.

2.13. Atherosclerosis Study

2.13.1. Material, Buffers, Devices

Table 2.36.: Material, Buffers and Devices for atherosclerosis study

Category	Name	Company/ Composition
Material	Operation tools	various
	Microvette 100 K3E	Sarstedt (# 20.1278)
	Haematocrit capillaries	Hirschmann Laborgeräte (# 9100260)
	Reaction tubes (1.5, 15 and 50ml)	Sarstedt
	Cell culture dish (60mm)	greiner bio-one
	Microslides SuperFrost® Plus	Hecht (# 42409110)
	Dako Pen	Dako (# S2002)
	Cover Slips 24 × 50mm, #1	Menzel
	Minutien Pins	Fine Science Tools (# 26002-10); base diameter: 0.1mm, tip diameter: 0.0125mm
	Western type highfat diet	ssniff Spezialdiäten GmbH (# EF TD88137 mod.)
Buffers	Isofluran	Baxter
	4% PFA	Morphisto (# 11762.01000)
	Tissue freezing medium	Leica Biosystems
	60% Isopropanol	Carl Roth, diluted in Aqua dest.
	Oil Red O Stock solution	Sigma (# O0625), 0.5g in 100ml 100% Isopropanol
	Oil Red O Staining solution	60% ORO stock solution, in Aqua dest., filtered
	TBE-Buffer	100mM Tris-Base + 80mM Boric Acid + 1.3mM EDTA in Aqua dest.
	2.5% Agarose	Biozym (# 840040), in TBE
	Mayer's Hematoxylin	Roth (# T865.1)
	Aquatex	Merck (# 1.08562.0050)
	Masson's Trichrome Staining Kit	Sigma (# HT15-1KT)
	Weigert's Hematoxylin	Weigert A (Ferric-Hematoxylin, Carl Roth, # X906.1), Weigert B (Ferri-Hematoxylin, Carl Roth, # X907.1), (1:1)

Continued on next page

Category	Name	Company/ Composition
	1% Acetic Acid	J. T. Baker, in Aqua dest.
	Xylene	J. T. Baker
	Cytoseal XYL	Thermo Scientific (# 8312-4)
	ice-cold Methanol:Acetone	Merck (# 1.00014.1000) and Carl Roth (# 8388.6), (1:1)
	0.3% H_2O_2	Sigma (# 216763), 30%; diluted 1:100 in Aqua dest.
	0.025% Trypsin	PAA (# L11-658), diluted 1:10 in PBS
	Block buffer (MoMa)	5% (w/v) skimmed milk powder (Carl Roth, # T145.3), 0.05% Tween20 (Merck, # 8.22184.1000), in PBS
	Block buffer (α-SMA)	5% normal goat serum (Dako, # X0907), in PBS
	Immpact NovaRed HRP Substrate	Vector (# SK-4805)
	Liquid DAB+ Substrate	Dako (# K3468)
Devices	PCR Cycler	SensoQuest labcycler
Software	GIMP	version 2.8.16
	Matlab	builds R2015a, R2015b, R2016a

Table 2.37.: Antibodies for staining cryosections.

Desription	Dilution	#, Company
rat monoclonal anti-Monocyte + Macrophage [MOMA-2]	1:500 in block buffer	ab33451, abcam
rabbit polyclonal anti-rat IgG, HRP-linked	1:2000 in PBS	P0450, Dako
rabbit polyclonal anti-α-SMA	1:100 in PBS	ab5694, abcam
goat anti-rabbit IgG, HRP-linked	1:500 in PBS	sc-2004, Santa Cruz

2.13.2. Induction of atherosclerosis by feeding a Western-type diet

The atherosclerosis study was carried out using groups of *Zc3hc1*-KO ApoE-KO and ApoE-KO animals, matched by age and gender. At the age of 10 weeks, they were put on a Western type highfat diet (HFD, see table 2.38) for 8 weeks, weighed weekly, and then sacrificed for organ retrieval and subsequent quantification of atherosclerosis. Mice were put on starvation for at least ten hours (overnight) before sacrification, in order to collect fasting blood samples for plasma lipid analysis.

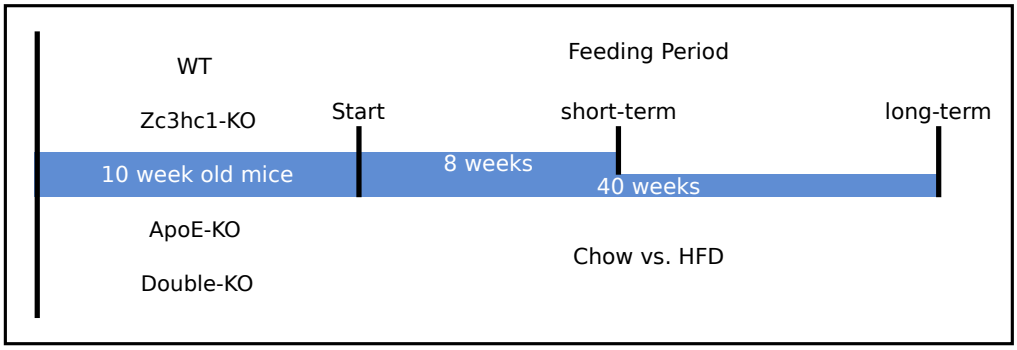

Figure 2.7.: Experiment outline for the *in-vivo* atherosclerosis study. Groups of mice, at the age of ten weeks, are put on a Western type high fat diet (HFD) or continued with normal (Chow) diet, for 8 weeks (short-term) or 40 weeks (long-term), respectively. At the end of the feeding period, mice are set on starvation overnight to collect fasting blood samples, and then sacrificed for organ retrieval.

Table 2.38.: Composition of the ssniff Western type diet.

Crude Nutrients	%
Crude Protein	17.3
Crude fat	21.2
Crude fibre	5.0
Crude ash	4.5
Starch	14.5
Sugar	32.8

2.13.3. Atherosclerosis Quantification

Atherosclerosis was quantified in the aortic root and in the thoracic aorta. From each mouse, the heart, with the aorta attached, were taken out and fixed in Paraformaldehyde (PFA). Prior to sectioning the hearts, the aortas were cut off and stored for *en-face* analysis. Hearts were then embedded in Cryo-Section Medium overnight at room temperature. Each heart was cut in 10µm sections, which were collected from before the appearence of the aortic valves, until the aorta emerged from the heart (see figure 2.8, left). Sections were distributed over four groups, A-D (see figure 2.8, right), leading to a distance of 40µm between sections within a group. Each group was used for a different staining: group A with Oil Red O (ORO) for Plaque Size, group B with Masson's Trichrome for quantification of Collagen content, group C with MoMa-2 antibody for Monocytes and Macrophages, and group D with α-SMA antibody for SMCs.

Thoracic aortas were used for quantification of Plaque Coverage in the en-face analysis.

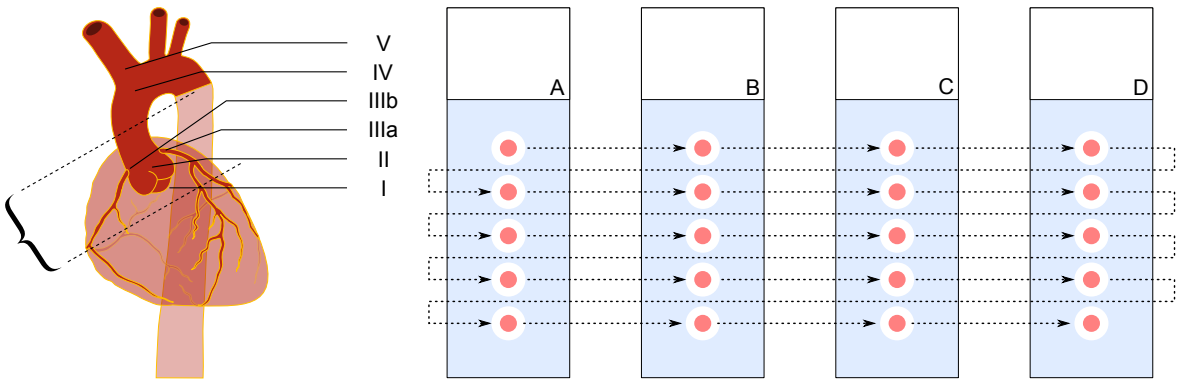

Figure 2.8.: Heart sectioning strategy. Left: Anatomy of the cross-sectioned region of the heart; I: aortic root; II: aortic valves; IIIa: left coronary artery; IIIb: right coronary artery; IV: aortic arch; V: brachiocephalica. Dotted lines mark the region that was sectioned and collected, starting from the aortic root. Right: Collection of the sections was carried out in the order represented by the dotted arrows. One batch (A-D) consists of 20 sections; in total, 5 to 6 batches, or 100 to 120 sections (= 1000 to 1200µm), were collected. Image of Aorta and Heart taken from Aorta_scheme_noTags by Edoarado via Wikimedia Commons, and used under the Creative Commons Attribution-Share Alike 3.0 Unported license.

Plaque Size

Ten consecutive sections of group A, starting from the appearance of all three aortic valves, were used per mouse to assess Plaque Size.

Cryosections were thawed and dried for 1 to 2h at room temperature. They were then dipped 10x in 60% isopropanol, incubated in the ORO staining solution for 15min, and again dipped 10x in 60% isopropanol. Afterwards, sections were washed under running tap water for 5min, counterstained in Mayer's Hematoxylin for 3min, and washed again under running tap water for 5min. Slides were then mounted whith Aquatex, covered with cover slips, and left overnight at 4°C to ensure an even polymerisation of the mounting medium.

To analyse plaque size in aortic cross-sections, images of the ORO-stained sections, counterstained with Mayer's Hematoxylin, were recorded at 4-fold magnification, ensuring homogenous white balance and brightness. The images were then edited using the open source image software GIMP (v2.8.8), selecting first the aorta area including the lumen and deleting the surrounding into white as background. In the next step, the plaque area was selected manually; due to its inhomogenous structure, the plaque area was not selectable with a threshold operation. Hence, it was painted over with a specific color, and the resulting image was exported. These images were then used in the analysis with a self-written algorithm in Matlab (script A.1 and A.2), first selecting the aorta area as non-white pixels, then counting the pixels with the defined color for the plaque area, and finally normalizing the plaque area to the aorta area. The analysis was performed automatically, and results were saved in text-files for further statistical analysis. Averages over all ten images were used to compare individuals.

Plaque Coverage

Plaque Coverage was analysed in the thoracic aorta, the part between the heart and the renal branches. Aortas were freed from the surrounding fat tissue and the adventitia under a stereomicroscope. They were then stained with ORO to visualise plaques. First, they were equilibrated in 60% isopropanol for 10min, then stained in ORO staining solution for 30min, and, after another 10min in isopropanol, they were washed in Aqua dest. for 1min. They were then opened longitudinally and spanned with

minutien pins on 2.5% agarose in a 60mm culture dish, covered with PBS, and photographed.

Images were then analysed analogous to ORO-stained cross-sections. Plaque Coverage was calculated as the percentage of the aorta covered by ORO stained plaques.

Collagen Content

For Collagen quantification, five consecutive sections, out of the ten sections of group B corresponding to those used for the plaque size quantification, were analysed.

Cryosections were thawed and dried for 1 to 2h at room temperature. To rehydrate the sections, they were dipped in AQUA DEST. for 5 times. The duration of each of the following staining or washing steps was 5min, if not stated otherwise. First, sections were incubated in Weigert's Hematoxylin, and washed under running tap water. After dipping 5x in AQUA DEST., they were stained in Biebrich Scarlet-Acid Fuchsin solution, then washed under running tap water, and dipped in AQUA DEST. for 5 times. After that, they were incubated in Phosphomolybdenic/ Phosphotungstic Acid solution (1:1:2 in AQUA DEST.), and then stained with Anilin Blue. After washing under running tap water and 5x dipping in AQUA DEST., they were treated for 2min with 1% Acetic acid, washed for 1 to 2min under running tap water and dried overnight. On the next day, they were dipped in Xylene and mounted with Cytoseal.

To quantify the collagen content, the stained cross-sections were recorded with a microscope (at 4-fold magnification) while maintaining homogenous white balance and brightness. The plaque area was then selected in the image editing software GIMP while comparing the current selection with the plaque area from the ORO-staining. For the automated analysis, the non-plaque area was erased and left as white background (see figure 2.9, step 1). The analysis was performed with a self-written algorithm in Matlab (script A.3 and A.4); this algorithm first calculates the plaque area in pixel (as non-white area), transforms the picture into the ycbcr color code and then extracts blue pixels for collagen (script A.3 and A.4) from the individual color channels through given thresholds (see figure 2.9, step 2). These thresholds were manually adjusted with a few images prior to analysis of all samples. For each image, collagen content was normalised to plaque area, and the results were then automatically stored in text-files for further

statistical analysis. Averages from five sections were used to compare individuals.

Monocytes and Macrophage Content

Five sections of group C, corresponding to the sections used for Collagen analysis, were used for Monocytes and Macrophages (MoMa) staining.

Cryosections were fixed in ice-cold Methanol:Acetone for 10min at room temperature, dried for 2 to 3min, and then circled with Dako Pen. To block endogenous peroxidase activity, sections were incubated in 0.3% H_2O_2 for 20min. After three times washing in PBS for 5min, slides were incubated in pre-warmed 0.025% Trypsin solution for 5min at 37°C, and then washed again three times for 5min in PBS. After blocking of unspecific binding sites with blocking buffer (MoMa) for 1h at room temperature, the slides were incubated with the MOMA-2 antibody overnight at room temperature. Next day, slides were washed three times in PBS for 5min, incubated with the secondary antibody for 1h at room temperature, and washed again three times in PBS. Antibody staining was then visualised using the ImmPACT NovaRED Peroxidase Substrate for 5:30min. After a washing step with running tap water, slides were counterstained with Mayer's hematoxylin for 3min, and again washed in running tap water for 7min. Slides were then dried overnight, and, on the next day, dipped in Xylene and mounted with Cytoseal, and photographed at 4x-magnification.

MoMa content was analysed similarly to collagen, with thresholds for brown as the color for positive MoMa staining (script A.5 and A.6). Averages from five images were used to compare individuals.

Smooth Muscle Cell Content

For the analysis of SMC content per plaque, 5 sections of group D, corresponding to the sections used for Collagen and for MoMa analysis, were used.

Cryosections were fixed in ice-cold Methanol:Acetone for 10min at room temperature, dried for 2 to 3min, and then circled with Dako Pen. Endogenous peroxidase activity was then blocked with a specific Peroxidase Block for 10min at room temperature. After

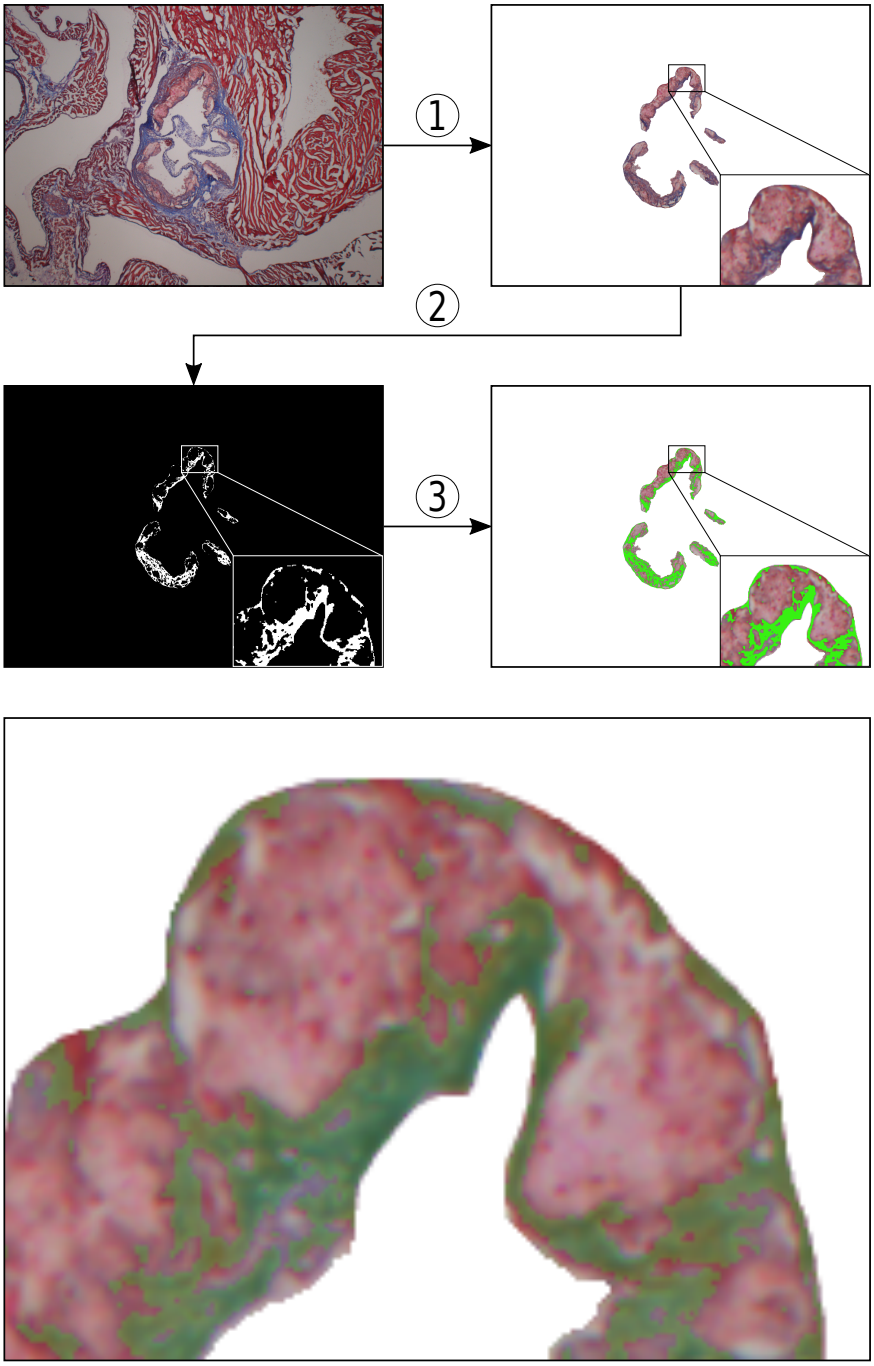

Figure 2.9.: Workflow for analysing plaque composition; shown here is the analysis of collagen in Masson's Trichrome stained images. MoMa2 and α-SMA stainings were analysed similarly. Step 1: the original image (top left) is edited manually, selecting plaque region and deleting the rest into white background (top right). Step 2: these images are then automatically analysed with the respective Matlab algorithm which extracts the color for positive stainings using a threshold operation, and saves the result as a black-and-white mask (middle left). Step 3: prior to analysis of all images, overlays (middle right) are created manually to verify the selected areas and, if necessary, adjust the threshold. Bottom: semi-transparent overlay showing the reliablity of the algorithm in selecting, in this case, collagen fibers on the basis of their color.

washing in PBS for 5min, sections were incubated in block buffer (α-SMA) for 1h at room temperature. Block buffer was discarded, and sections were then incubated with the primary antibody overnight at room temperature. Next day, sections were washed 3x for 5min in PBS, incubated with the secondary antibody for 1h at room temperature, and again washed 3x for 5min in PBS. Bound antibody was then visualised with HRP substrate, DAB+, for 15min at room temperature. After washing under running tap water for 5min, sections were stained with Mayer's hematoxylin for 3min, washed again under running tap water for 10min, and mounted with Aquatex.

Analysis of SMC content was performed analogous to MoMa-content, restricting the positive stained area to high intensity brown only (script A.7 and A.8). For this reason, thresholds for the red-channel of the RGB-map, and the luminance-channel of the ycbcr-map were combined. The α-SMA positive area was normalised to Plaque Size, and the ratio for every image was then automatically saved in a file. Averages from five images were used to compare individuals.

2.14. Isolation and Cultivation of primary aortic SMCs

2.14.1. Material, Buffers, Devices

Table 2.39.: Material, Buffers and Devices for Isolation and Cultivation of aortic SMCs

Category	Name	Company/ Composition
Material	Reaction tubes (1.5, 15 and 50ml)	Sarstedt
	Biosphere Filter Tips (10, 100 and 1000µl)	Sarstedt
	Sterile Operation tools	various
	Cell culture dish (60mm)	greiner bio-one (# 628160)
	Nunclon Delta Multidish (6-Well plate)	Thermo Scientific (# 140675)
	Nunclon Delta Multidish (12-Well plate)	Thermo Scientific (# 150628)
	Cell culture flask (25cm^2)	Sarstedt (# 83.3910.002)
	Cell culture flask (75cm^2)	Sarstedt (# 83.3911.302)
	Cell scraper (25cm)	Sarstedt (# 83.1830)
	Cell Strainer 40µm Nylon	BD Falcon (# 352340)
Buffers	Isofluran	Baxter
	Culture Medium	DMEM (# 31966, Gibco), supplemented with 20% FBS and 1% P/S
	Collagenase Type II (10mg/ml)	Cellsystems (# LS004176), in Culture Medium, sterile filtered
	0.1% Gelatin	pork skin (# G1890, Sigma), in PBS, sterile autoclaved
	0.05% Trypsin/ 0.02% EDTA	Thermo Fischer (# 15400054), diluted 1:10 in PBS
Devices	Stereomicroscope M80	Leica
	Thermomixer 5436	Eppendorf
	Biofuge pico	Heraeus
	Inverse Microscope Wilovert A	Hund
	Centrifuge 5702 R	Eppendorf
	Varifuge 3.0R	Heraeus
	Shaking Water bath 1083	GFL
	CO_2-Incubator Hera cell	Heraeus
	Laminar Flow Clean Bench	CleanAir

Continued on next page

Category	Name	Company/ Composition
	Neubauer Counting Chamber	Marienfeld

2.14.2. Protocol for Isolation of primary mouse aortic SMCs

Primary aortic SMCs were isolated from 8-10 thoracic aortas per group. First, one mouse was narcotised with Isofluran and euthanised with cervical dislocation, then fixed with needles on a dissection tray (see figure 2.10, top left), and sprayed with ethanol. The fur was incised at the abdomen and cut open to the chin. Next, the peritoneum, the diaphragm, and the ribcage were opened; for these steps, one set of tools was used ('outside tools'). Another set of tools ('inside tools') was used to remove organs from, and take out the aorta. The heart was grabbed carefully with tweezers, and cut off from the aorta. The trachea and the esophagus were also cut off at the throat, and everything was then pulled down, together with the lungs, leaving just the aorta in the chest. The aorta was then grabbed and pulled very softly, and carefully cut from the spine until reaching the diaphragm. This step was performed with high precaution in order not to cut the aorta. At the diaphragm, the aorta was cut off, washed in PBS, and then put into a cell culture dish with Culture Medium (see figure 2.10, top middle). The previous steps were repeated for each mouse, until all aortas were collected.
Aortas were then cleaned from blood, fat and adventitia under an operation microscope with illumination from below. First, blood and fat were removed by grabbing the aorta with two precision tweezers and carefully squeezing out the blood. Then, fat was removed (see figure 2.10, top right), and the aorta was placed in a new cell culture dish with Culture Medium. After cleaning all aortas from blood and fat, they were predigested in Collagenase II (10min at 37°C), in order to make removing the adventitia easier, and then placed back in a cell culture dish with Culture Medium. Adventitia was removed from each aorta under the microscope – which compares to 'pulling a sock from a leg' – and aortas were placed in a new cell culture dish with Medium until all were done (see figure 2.10, bottom left).
Under the sterile bench, each 4 to 5 aortas were transferred to one reaction tube containing 1ml of Collagenase II-solution. With a fresh, sterile pair of scissors, the aortas were cut into very small and fine pieces (< 1mm) in the tubes. To digest the aortas, the tubes were placed in a thermo-shaker at 37°C for at least 6h, until all tissue pieces were dissolved.
For each group, one well of a 6-Well plate was coated with gelatin before the end of the

digestion. Each well was incubated with 1ml of gelatin for 30min at room temperature. Gelatin was then aspirated, and each well was washed three times with 2ml PBS. After removing the PBS, 1ml of Culture Medium was put into each well, and the plate was placed in an incubator.
After the digestion, tubes were centrifuged at 1000 rcf for 10min. The supernatant was discarded, and the cells were resuspended in 1ml Culture Medium; after resuspending the first pellet of a group, the medium was taken into the second tube to resuspend the second pellet. Cells were then pipetted into their respective well in the 6-Well plate, and kept in the incubator for 3 to 5 days without moving before the first medium change.

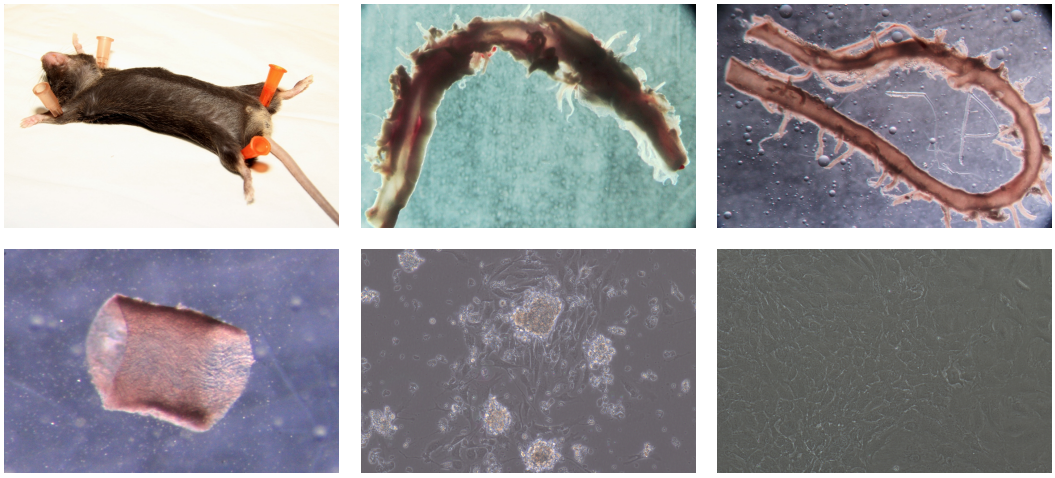

Figure 2.10.: Isolation and Cultivation of primary mouse aortic SMC. Top row: pinning the mouse (left); aorta with surrounding fat tissue and blood (middle); aorta after removing fat (right). Bottom row: piece of aorta after removal of adventitia (left); primary aortic SMCs, 1 day after the first passage (middle); confluent layer of aortic SMCs, P6 (right).

2.14.3. Protocol for Cultivation of primary mouse aortic SMCs

Primary aortic SMCs were first passaged when the cells in the 6-Well plate were 100% confluent (see figure 2.10, bottom middle).

Medium was removed, and cells were washed once with 2ml PBS. After removing PBS, 0.5ml Trypsin/ EDTA per well were added and incubated for 20 to 30s. This duration was not changed until the cells reached Passage 4 (P4). Trypsin was neutralised with 2ml of Culture Medium, and cells were carefully detached in small chunks using a cell

scraper. After resuspending the cells carefully yet thoroughly, they were passed into a 15ml tube and centrifuged for 10min at 1000 rcf. Supernatant was discarded. Cells were then resuspended in 1ml of fresh Culture Medium and plated on a new gelatin-coated culture dish (see section 2.14.2). Split ratio for the first passages was 1:2, e.g. cells from 1 well of a 6-Well plate were plated into 2 wells of a 6-Well plate.

Further subcultivation was performed accordingly, with slight adjustments of volumes and culture dishes: Higher volumes of Trypsin were used in larger culture dishes: 1ml in a 25cm^2 culture flask, and 3ml in a 75cm^2 culture flask, respectively. Accordingly, the volume of Culture Medium to neutralise Trypsin was adjusted to 3ml in 25cm^2, and 6ml in 75cm^2 culture flasks, respectively. After P4, the incubation time of Trypsin was prolonged to 1min at 37°C, and cells were split in the ratio of 1:3.

To ensure only single cells were used for experiments, the cell solution was filtered through a 40µm pore size cell filter to remove remaining chunks of cells.

2.15. Flow Cytometry

2.15.1. Material, Buffers, Devices

Table 2.40.: Material, Buffers and Devices for Flow Cytometry

Category	Name	Company/ Composition
Material	Reaction tubes (1.5, 15 and 50ml)	Sarstedt
	FACS tubes (5ml	Sarstedt (# 55.476.013)
	Cell scraper (25cm)	Sarstedt (# 83.1830)
Buffers	Accutase® solution	Sigma (# A6964)
	Culture Medium	DMEM (# 31966, Gibco), supplemented with 20% FBS and 1% P/S
	Trypan Blue (0.4%)	Sigma (#T8154)
	BD Cytofix/Cytoperm™	BD Biosciences (# 554714)
Devices	Neubauer Counting Chamber	Marienfeld
	Flow Cytometer LSRII	BD Biosciences
Software	FlowJo	version 10.0.4

Table 2.41.: Antibodies for Flow Cytometry analysis of SMCs.

Desription	Company
mouse monoclonal anti-α-SMA – FITC	F3777, Sigma
mouse IgG2a-FITC Isotype Control	F6522, Sigma

2.15.2. Protocol

Expression of SMC marker α-SMA was quantified in primary aortic SMCs using Flow Cytometry. For each group, cells cultivated in one T75 were harvested, stained with the FITC-labeled antibody, and measured.
First, medium was aspirated and cells were washed with 6ml PBS. Then, they were incubated with 4ml Accutase solution for 2min at 37°C. After that, they were detached by gently beating the flask and scraping the cells off using a cell scraper. The cell solution was then centrifuged for 5min at 1000 rcf. The supernatant was removed and cells were washed three times in PBS. An aliquot of 10µl for counting live cells was taken, mixed with 10µl Trypan Blue solution, and cells were immediately counted using a Neubauer chamber.
After the last washing step, the cells were resuspended in Fixation/ Permeabilization solution at a concentration of 1×10^6cells/ml. Three tubes per group were filled with 0.5ml each, and then incubated on ice for 30min to permeabilise the cells. Cells were then washed by adding 1ml BD Perm/Wash™ Buffer (1x, in AQUA DEST.), and centrifuged for 8min at 400 rcf in a cooled centrifuge at 4°C. Supernatant was removed, and the cells were resuspended in 300µl Wash Buffer.
For each group, one tube was stained with the Isotype control antibody, one tube with the FITC-labeled anti-α-SMA antibody, and one tube was left unstained as the negative control. 1µl of each antibody (final dilution: 1:300) was pipetted into the corresponding tubes; the tubes were gently mixed, and incubated in the dark for 1h at 4°C. After that, cells were washed twice with 1ml Wash Buffer, and centrifuging for 8min at 400 rcf in a cooled centrifuge at 4°C. They were then resuspended in 700µl Wash Buffer, put on ice, and measured in the Flow Cytometer. Data analysis was performed using the software FlowJo (version 10.0.4).

2.16. Proliferation assay

2.16.1. Material, Buffers, Devices

Table 2.42.: Material, Buffers and Devices for proliferation assay

Category	Name	Company/ Composition
Material	Reaction tubes (15 and 50ml)	Sarstedt
	Biosphere Filter Tips (10, 100 and 1000µl)	Sarstedt
	Nunclon Delta Multidish (12-Well plate)	Thermo Scientific (# 150628)
	Cell scraper (25cm)	Sarstedt (# 83.1830)
Buffers	Culture Medium	DMEM (# 31966, Gibco), supplemented with 20% FBS and 1% P/S
	0.1% Gelatin	pork skin (# G1890, Sigma), in PBS, sterile autoclaved
	0.05% Trypsin/ 0.02% EDTA	Thermo Fischer (# 15400054), diluted 1:10 in PBS
	4% PFA	Morphisto (# 11762.01000)
	Triton-X-100	Sigma (# T-8787), 0.1% in PBS
	DAPI Staining solution	0.01% in PBS
Devices	Inverse Microscope Wilovert A	Hund
	Shaking Water bath 1083	GFL
	CO_2-Incubator Hera cell	Heraeus
	Laminar Flow Clean Bench	CleanAir
	Neubauer Counting Chamber	Marienfeld
	Fluorescence Microscope BZ9000	Keyence
Software	ImageJ	version 1.48v

2.16.2. Protocol

To quantify proliferation of aortic SMCs, cells were seeded at 40 to 50 cells/mm^2 in six wells of a 12-Well plate per group; three for manual counting, and three for an automated analysis of DAPI-stained images.
At each given timepoint, cells from the three wells for manual counting were counted using the Neubauer chamber. First, medium was aspirated, and the cells were washed

once with 1ml PBS. Then, they were incubated with 300µl Trypsin per well for 1min at 37degreeCelsius. Trypsin was neutralised with 700µl of Culture Medium, the cells that remained attached were carefully detached using a cell scraper, and an aliquot was taken for counting. Values for three wells were averaged.

For the automated analysis, the cells were stained with DAPI, photographed, and analysed with ImageJ. First, the medium was aspirated, and the cells were washed once with 1ml PBS. Then, they were fixed with 0.5ml PFA for 5min, and, after removing the PFA, permeabilised with 0.5ml Triton-X-100 10min. Cells were then washed with 1ml PBS and stained with 0.5ml DAPI solution for 10min in the dark. DAPI was replaced with 0.5ml PBS, and the wells were then photographed.

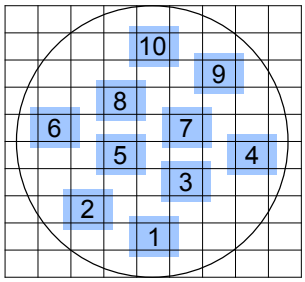

Figure 2.11.: Recorded image positions for automated counting. The circle depicts the area of a well in a 12-well plate, the blue rectangles, numbered in the order of recording, represent the recorded images.

Ten fixed, non-overlapping positions per well (see figure 2.11) were recorded for the analysis with a self-written ImageJ-algorithm (see script A.9). This algorithm detects blue stained areas as objects on a black background, counts each area as a signal (= cell), and automatically saves the results (see figure A.4). Recorded images had a resolution of 4080×3072 pixel, and a calibration of 1µm/pixel. Accordingly, a single image contained 12 533 760 pixel, which equals to 12 533 760µm^2, or 12.533 76mm^2. The total recorded area of 10 images was 125.3376mm^2. A well of a 12-Well plate has a bottom diameter of 22.1mm, and an area of 383.596 317mm^2. Compared to the total recorded area of 10 images, the well area is 3.06 times as big, or, in other words, images cover a representative fraction of 32.674% of a well. Hence, the total cellnumber per well was extrapolated by adding the values from 10 images and multiplying this number by 3.06. For each timepoint, the average of three wells was calculated.

2.17. Migration assay

2.17.1. Material, Buffers, Devices

Table 2.43.: Material, Buffers and Devices for migration assay

Category	Name	Company/ Composition
Material	Reaction tubes (1.5 and 15ml)	Sarstedt
	Biosphere Filter Tips (10, 100 and 1000µl)	Sarstedt
	Cell scraper (25cm)	Sarstedt (# 83.1830)
	Transwell Migration Plate	CIM-Plate 16 (ACEA Biosciences, Inc., # 05665817001)
Buffers	Culture Medium	DMEM (# 31966, Gibco), supplemented with 20% FBS and 1% P/S
	serumfree Medium	DMEM (# 31966, Gibco)
	0.1% Gelatin	pork skin (# G1890, Sigma), in PBS, sterile autoclaved
	0.05% Trypsin/ 0.02% EDTA	Thermo Fischer (# 15400054), diluted 1:10 in PBS
Devices	Shaking Water bath 1083	GFL
	CO_2-Incubator Hera cell	Heraeus
	Laminar Flow Clean Bench	CleanAir
	Neubauer Counting Chamber	Marienfeld
	xCELLigence RTCA DP	ACEA Biosciences

2.17.2. Protocol

Migration of aortic SMCs was analysed with the xCELLigence RTCA DP system (ACEA Biosciences), a real-time impedance-based cell quantification device, using electronically integrated transwell migration plates, or Boyden chambers (*CIM-Plate 16*, see figure 2.12, top). Each well contains a membrane which is coated with electrodes on the bottom. Cells are seeded in the top compartment, and a signal is generated only if cells migrate through the pores and attach at the bottom of the membrane. The read-out is given as Cell Index (CI), resembling the change in impedance of the electrodes, which correlates in a cell type-specific manner with number and size of the cells.

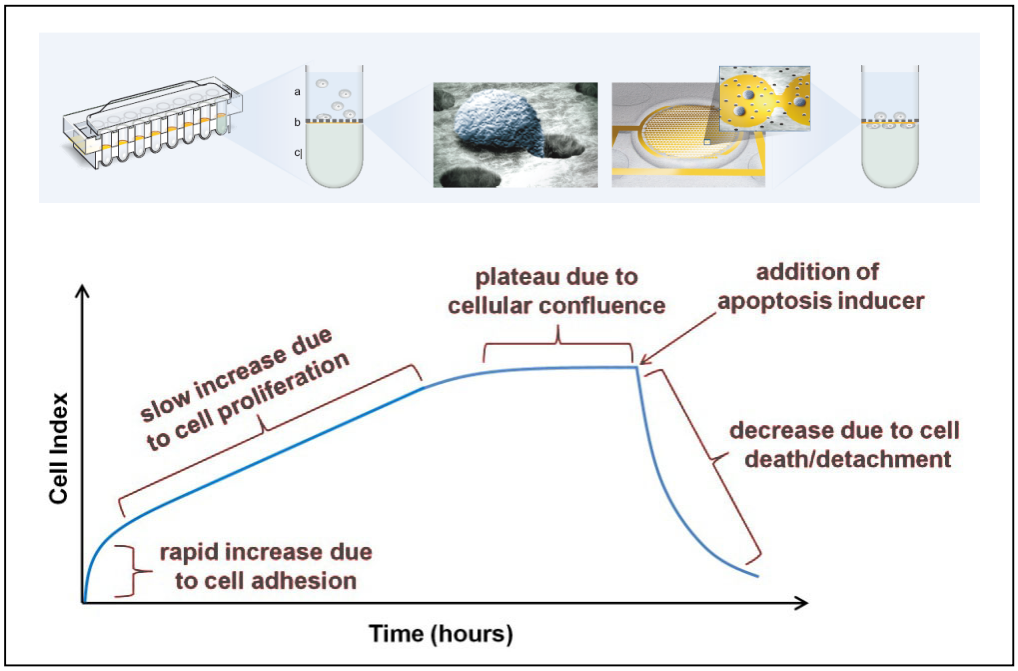

Figure 2.12.: Schematic overview of the xCELLigence migration assay. Top: cells are seeded in the upper compartment, and will give a signal only when they migrate through the membrane. The pores are sufficiently small to prevent cells from simply falling through. The signal generated on the electrodes is recorded, and the read-out is given as the unitless parameter Cell-Index. Bottom: the curve generated from an experiment can be divided into different stages. Images are taken from manufacturer's website (https://aceabio.com/product/rtca-dp/) and product presentation http://icob.sinica.edu.tw/pubweb/data/xCelligence_%B2%D3%A5%CDpdf).

First, the electrode side of the membrane was coated with gelatin. 30µl of 0.1% gelatin solution were carefully pipetted on each membrane, incubated for 15min, and carefully aspirated while touching the electrodes was avoided. After the membranes were dried for 15min at room temperature, the bottom compartment of each well was filled with 165µl of either Culture Medium or serum-free medium as control, and the membrane compartment was mounted. The upper wells were then filled with 50µl of serum-free medium, and equilibrated for 1h at 37°C in an incubator. Cells were passaged as described in section 2.14.2, and resuspensed in serum-free medium. Cell concentration was then adjusted to 400 000 cells/ml; and 100µl of this cell suspension, or 40 000 cells, were pipetted into each well.
Data was recorded for at least 24h, or until there was no change in CI (plateau phase).

3. Results

3.1. Interaction of human NIPA and Cyclin B1

To test whether the CAD-risk SNP rs11556924 has an influence on the interaction of NIPA and Cyclin B1, the two proteins were expressed in a mammalian two-hybrid assay.

3.1.1. Cloning of NIPA and Cyclin B1 cDNAs

First, the cDNA sequences of Cyclin B1, NIPA-WT and NIPA-R363H were amplified by PCR. They were then inserted into the shuttle vector Topo. After sequencing, and correction via mutagenesis with a subsequent resequencing step, clones were chosen for subcloning into the plasmids for the mammalian-two-hybrid assay, and the interaction was measured.

Amplification and isolation of cDNAs of NIPA and Cyclin B1

To amplify cDNAs of NIPA and Cyclin B1, primers were designed by taking the beginning (forward) and reverse-complement of the ending (reverse) of each cDNA sequence (16 and 17 bp for NIPA, and 20 and 19 bp for Cyclin B1, respectively). They were amended by recognition sequences for restriction enzymes; forward primers with `GGATCC` for BamHI, and reverse primers with `GTCGAC` for SalI, respectively (see table 2.2). These primers were then used to amplify the cDNAs in duplicate PCR reactions. A cDNA library from human coronary artery SMCs served as template for amplification of Cyclin

B1, while plasmids with known sequences of NIPA cDNA were used to amplify NIPA-WT and NIPA-R363H, respectively. The PCR products were separated on an agarose gel (see figure 3.1), and one band for each cDNA was cut out and cleaned up.

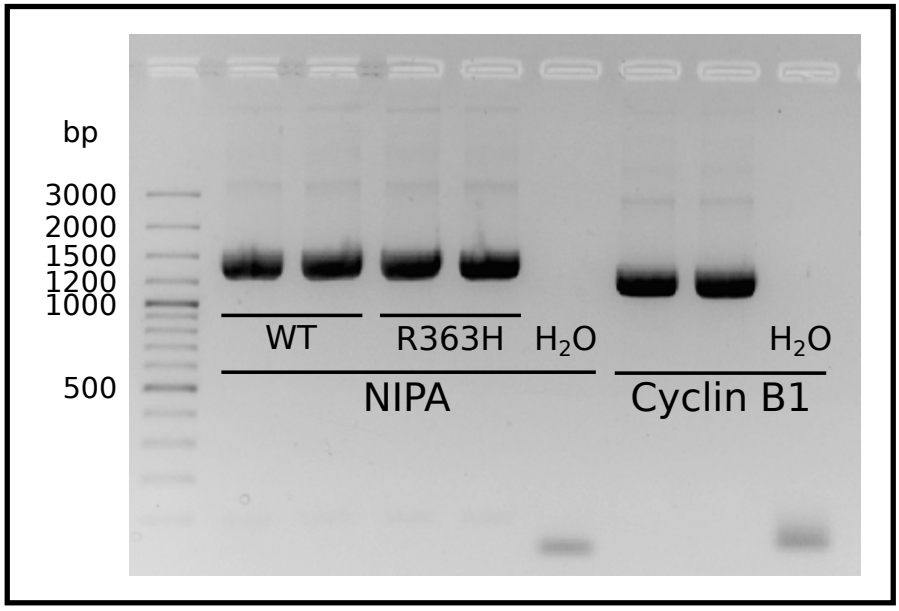

Figure 3.1.: Amplification of cDNAs by PCR. Each cDNA was amplified in duplicates. Bands can be observed at 1500 bp (NIPA), and between 1200 to 1500 bp (Cyclin B1).

Cloning cDNAs of NIPA and Cyclin B1 into shuttle vector Topo

Cleaned up PCR products were then ligated into the shuttle vector Topo, and transformed into bacteria. After overnight cultivation of the bacteria on agar plates containing Ampicillin, clones were observed (see figure 3.2). For each transformation, 5 clones were selected for insertion control via PCR to ensure uptake of the desired cDNAs. As can be seen by PCR products at around 1500 bp (see figure 3.3), clones NIPA-WT 1 and 2, NIPA-R363H 3 to 5, or Cyclin B1 1 to 4 contain the transformed plasmids with the inserted cDNAs, while the others do not.

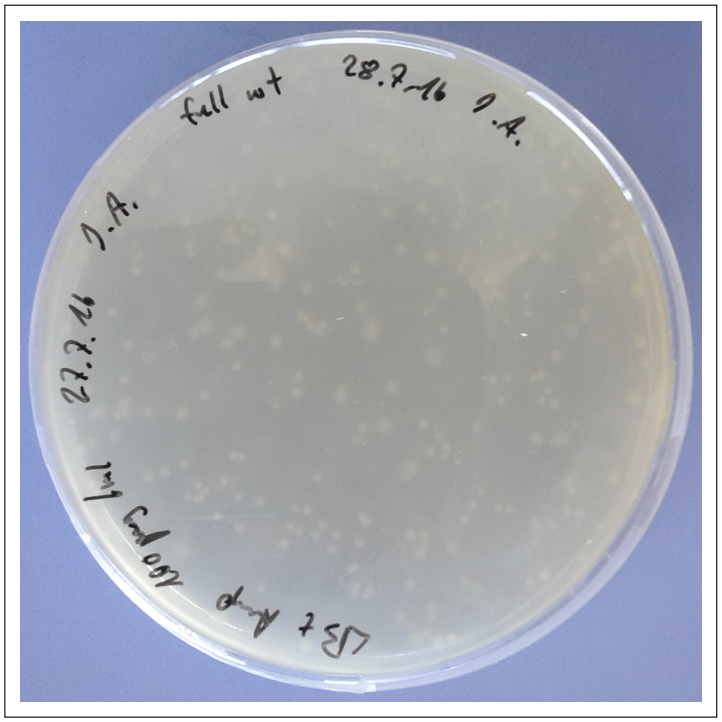

Figure 3.2.: Bacterial clones on a selective agar plate. The plate contains 100µg/ml Ampicillin.

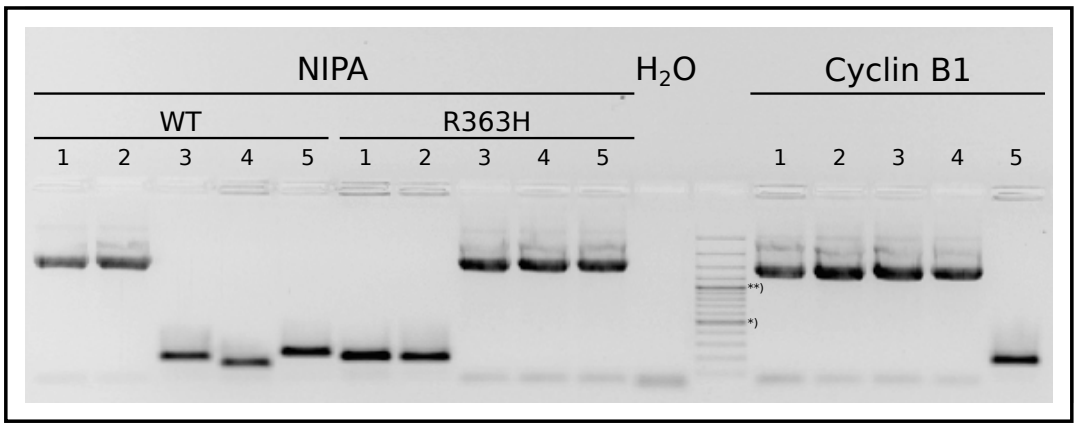

Figure 3.3.: Insertion control by PCR with M13 primers. *) 500 bp; **) 1000 bp; the bands above 1000 bp are 1200, 1500, 2000 and 3000 bp.

Isolating and sequencing clones for NIPA and Cyclin B1

Following clones were selected for sequencing from plasmid: NIPA-WT 2, NIPA-R363H 3, and Cyclin B1 3 and 4 (see figure 3.3).
They were first isolated and purified using Plasmid Miniprep, and then sent for sequencing.

The isolated plasmid for NIPA-WT 2 contained 4 mutations (at the bases 775, 811, 973 and 1196; see sequencing alignment below), NIPA-R363H 3 contained only one mutation (the same mutation at base 811 as in NIPA-WT 2; the `A` at position 1088 is the SNP rs11556924), while Cyclin B1 3 and 4 were correct (see appendix A.2.1).

```
                    770        780        790        800
NIPA_WT_ref   CTGGGCGTGTAGTTCCTCTTTGGAATCCATGCAGCTCTCCCTGAT
NIPA_WT_2     ..........gg..................................
NIPA_R363H_3  ..........a...................................

                810        820        830        840        850
NIPA_WT_ref   AACATGTTCGCAATGTATGAGGAAGGTGGGGCTCTGGGGCTTCCA
NIPA_WT_2     gg..........................................
NIPA_R363H_3  gg..........................................

                    860        870        880        890
NIPA_WT_ref   GCAGATTGAATCGTCCATGACTGACCTGGATGCATCCTTTGGCCT
NIPA_WT_2     ..........a...................................
NIPA_R363H_3  ..........a...................................

              900        910        920        930        940
NIPA_WT_ref   GACCAGCTCCCCAATCCCAGGCCTTGAGGGGCGACCAGAGCGCTT
NIPA_WT_2     ..........a...................................
NIPA_R363H_3  ..........a...................................

                    950        960        970        980
NIPA_WT_ref   ACCTCTGGTGCCTGAATCTCCTCGGAGGATGATGACCCGGAGCCA
NIPA_WT_2     ..............................gg..............
NIPA_R363H_3  ..............................a...............

              990        1000       1010       1020       1030
NIPA_WT_ref   GGATGCCACTTTCTCCCCAGGCTCAGAGCAGGCTGAAAAGAGCCC
NIPA_WT_2     ..........a...................................
NIPA_R363H_3  ..........a...................................
```

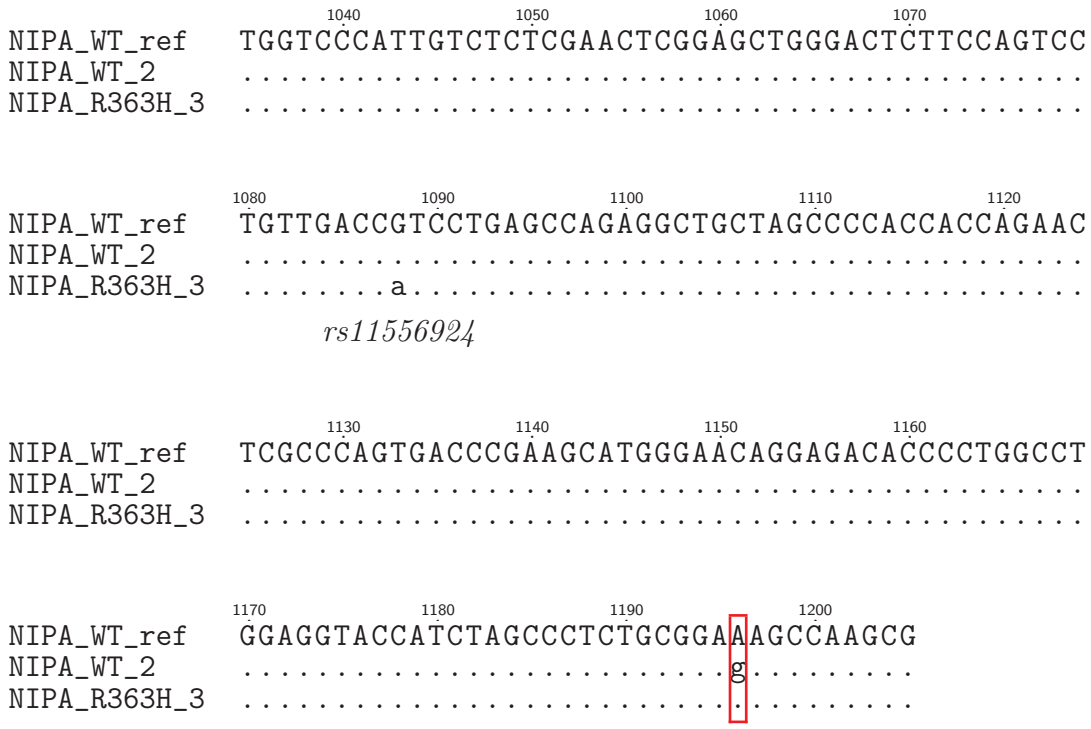

Figure 3.4.: Sequencing results for NIPA-WT clone 2 and NIPA-R363H clone 3, in comparison to the reference sequence. NIPA-WT clone 2 contains various mutations (red boxes), whereas NIPA-R363H clone 3 contains only one mutation besides the SNP rs11556924 at position 1088. Shown here is a part of the sequence, from base 765 to 1205.

Correcting NIPA-WT and NIPA-R363H per mutagenesis

The mutations in the plasmids NIPA-WT and -R363H were corrected by mutagenesis. First, the clone NIPA-R363H 2 was taken to change base 811 from G to A to obtain the correct sequence of NIPA-R363H. After mutagenesis, the plasmid was purified using Plasmid Miniprep, and samples from eight different clones were sequenced (see appendix A.2.2). Then, an aliquot of the corrected NIPA-R363H was taken to change the base at position 1088 from A to G to obtain NIPA-WT. After this second mutagenesis step, again plasmid DNA was isolated using miniprep, and six clones were sequenced. All but one (clone 2) were successfully changed to the wildtype sequence (see appendix A.2.3).

3.1.2. Subcloning NIPA and Cyclin B1 into fusion plasmids pCMV-AD & -BD

After successful identification of plasmids with the correct sequences, the cDNAs were subcloned into the fusion plasmids pCMV-AD and -BD. Each cDNA was ligated into both of the plasmids to test the mammalian two-hybrid in both directions, NIPA-AD with Cyclin B1-BD, and vice versa.

Subcloning

For subcloning, the first step is to cut out the cDNAs from the shuttle vector. Here, a double digestion with restriction enzymes BamHI and SalI was used. After the digestion, the cDNAs were separated on an agarose gel (see figure 3.5). For each cDNA, the digestion reaction was split into two lanes, and an additional lane contained undigested plasmid as a control. The digested plasmid shows two bands, one slightly over 3000 bp, the other at around 1500 bp (NIPA) or between 1200 and 1500 bp. The latter bands were cut out and cleaned up individually.

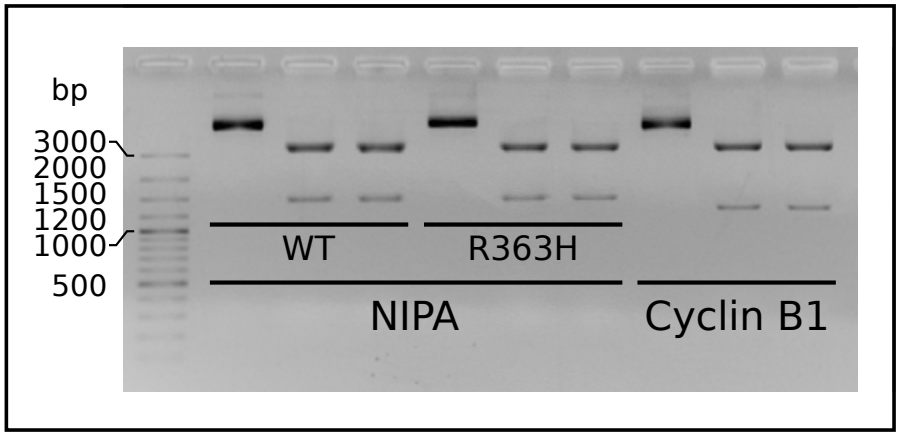

Figure 3.5.: Separation of excised cDNAs from plasmid on an agarose gel. For subcloning, the cDNAs were cut out from Topo-Vector by restriction enzyme digestion with BamHI + SalI, and separated on an agarose gel. For every cDNA, uncut plasmid was loaded into one lane, followed by the digestion reactions, which were equally distributed into two lanes. Uncut plasmids show only one band of more than 3kbp. Digested plasmids show two bands, one close to 3kbp, and one at 1.5kbp (NIPA) or 1.2kbp (Cyclin), respectively.

The ligation of the cDNAs into the fusion plasmids pCMV-AD and -BD was carried out

in a single-tube subcloning reaction. The fusion plasmids were first linearised using the same restriction enzymes BamHI and SalI, the nick ends were dephosphorylated, and the cDNAs were ligated into the plasmids. Then, the ligated plasmids were transformed into competent *E. coli* bacteria, and grown overnight on agar plates containing Ampicillin for transformations with pCMV-AD, or Kanamycin for pCMV-BD, respectively. From each plate, 10 clones were picked and controlled by PCR for uptake of the plasmid containing the inserted cDNA (see figures 3.6 and 3.7).

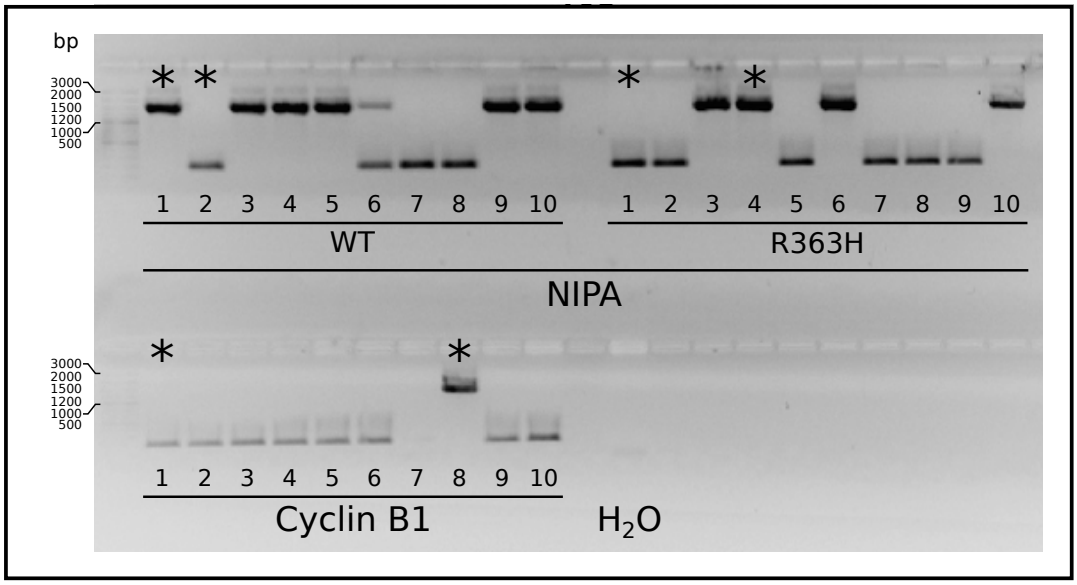

Figure 3.6.: Insertion control by PCR in pCMV-AD. From every plate, 10 clones were picked and tested by PCR. Some clones show large products at 1500 bp, some only smaller bands at 200 bp. Clones marked by asterisks were sequenced.

Plasmid isolation and sequencing

For each transformation, two clones were selected for sequencing; one with a large PCR product at around 1500 bp, and one with a smaller band between 200 to 300 bp (marked by asterisks in figures 3.6 and 3.7). They were first isolated and purified using Plasmid Miniprep and then sent for sequencing. All clones with larger PCR bands contained the correct sequences (pCMV-AD: NIPA-WT 1, NIPA-R363H 4, Cyclin B1 8; pCMV-BD: NIPA-WT 2, NIPA-R363H 9, Cyclin B1 2), and were then isolated using Plasmid Midiprep for a higher yield of plasmid.

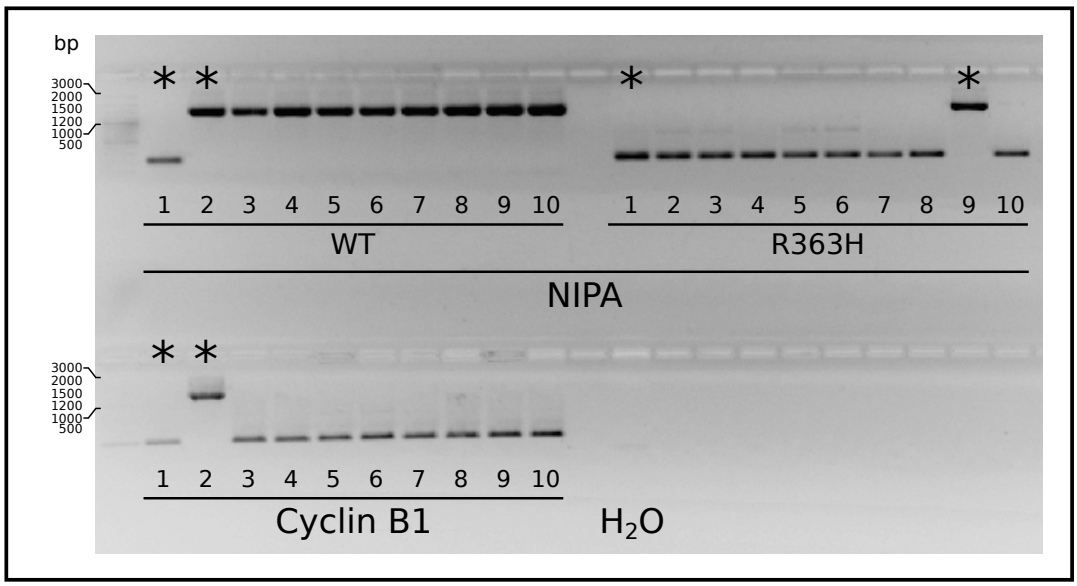

Figure 3.7.: Insertion control by PCR in pCMV-BD. From every plate, 10 clones were picked and tested by PCR. Some clones show large products at 1500 bp, some only smaller bands at 200 bp. Clones marked by asterisks were sequenced.

3.1.3. Mammalian Two-Hybrid with NIPA and Cyclin B1

The plasmids were transfected into HeLa cells. After 24h, cells from three wells per sample were lysed and the luciferase activity was measured (see figure 3.8). Firefly luciferase activity was observed in the positive controls (BD-p53 + AD-SV40, BD-NFκB, and BD-Nip1-300 + AD-Mau2), but not in the negative control (BD-p53 + AD-TRAF). NIPA-WT and Cyclin B1 showed only very low Firefly luciferase activity, both in absolute levels (see table A.1) and relative to Renilla luciferase. This experiment was performed twice; data shown here is from the second experiment (performed by the technician of the Institute for Human Genetics), the first had similar results.
Transfected cells from the second experiment were also lysed to isolate protein in order to analyse expression of the fusion proteins. Lysates were immunoblotted with an antibody against NIPA (see figure 3.9). A band at 75 kDa indicates the expression of the NIPA-fusion protein (NIPA: 55 kDa, AD/ BD-domains: about 20 kDa).

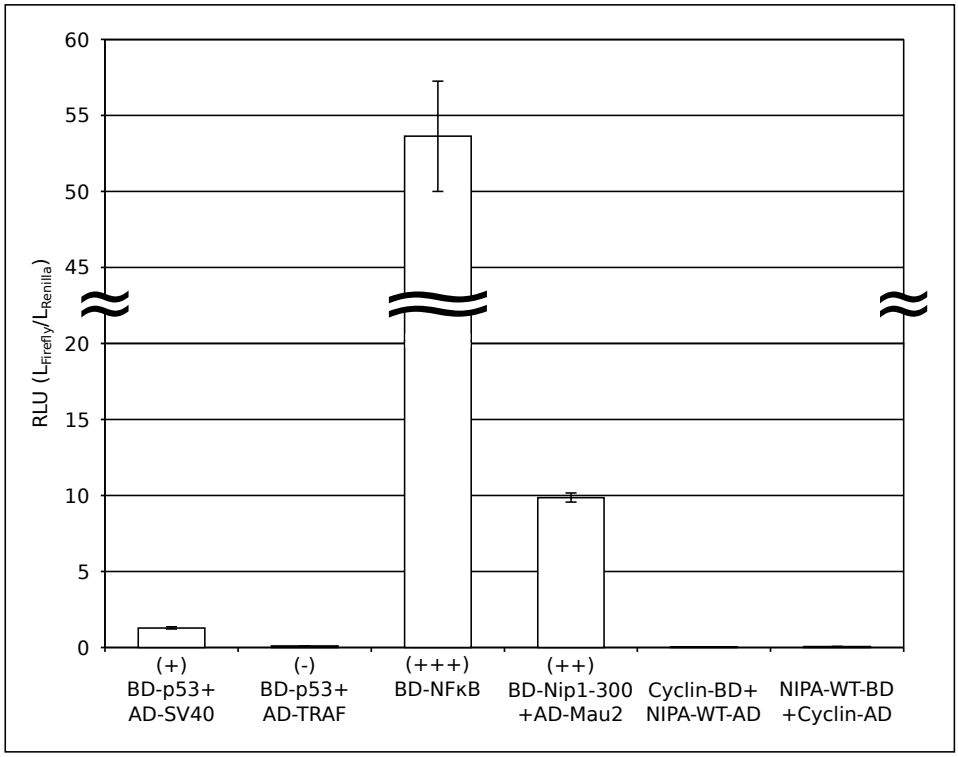

Figure 3.8.: Results of a Mammalian Two-Hybrid assay with NIPA and Cyclin B1; see table A.1 for raw data. Data shown from one experiment. $L_{Firefly}$: luminescence of firefly luciferase; $L_{Renilla}$: luminescence of Renilla luciferase; RLU: relative light unit, calculated as $L_{Firefly}/L_{Renilla}$.

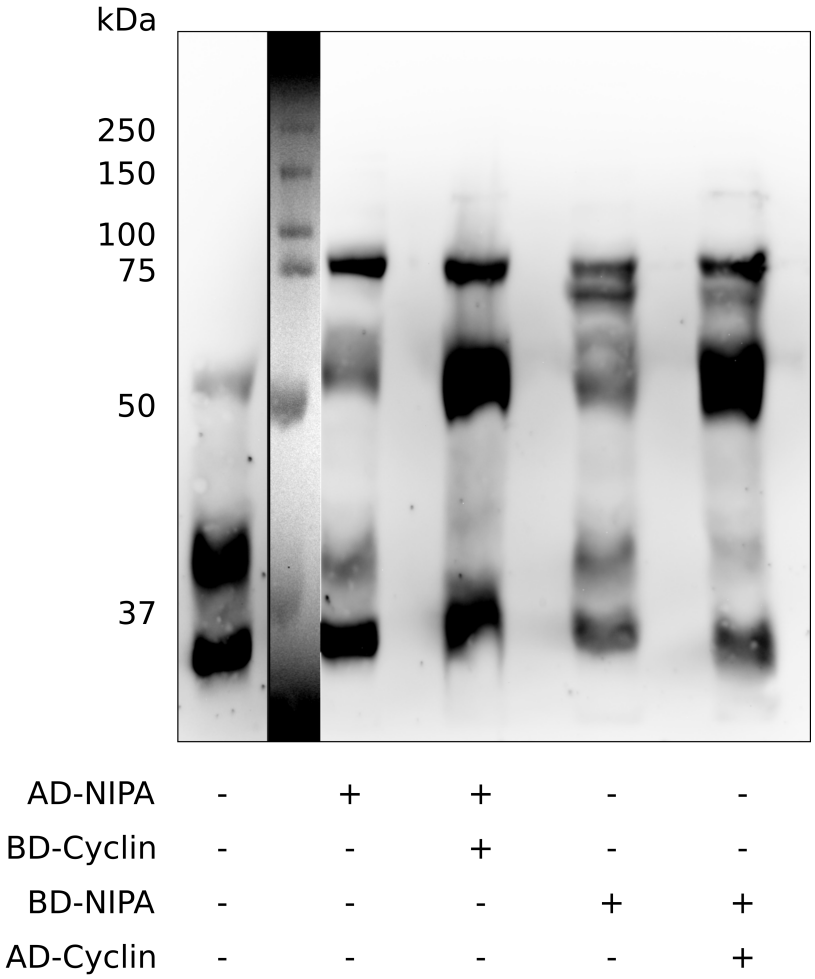

Figure 3.9.: Expression of transfected NIPA-fusion proteins. Immunoblot with an antibody against NIPA. At 75 kDa, a band is visible in the samples transfected with AD- or BD-NIPA, but not in the untransfected control (left). An additional, slightly smaller band can be seen in samples transfected with BD-NIPA. Endogenous NIPA has a size of about 55 kDa, the fusion domains AD and BD are about 20 kDa. Two additional bands are located around 37 kDa. Western Blot was performed by the technician of the Institute for Human Genetics, who also provided the image.

3.2. Establishing and phenotyping the *Zc3hc1*-knockout mouse model

All animal experiments were performed in accordance with the German animal studies committee of Schleswig-Holstein.

To create *Zc3hc1*-KO mouse line in order to study the effect of the CAD-risk gene *Zc3hc1* in an *in-vivo* experimental model, mice with a heterozygous deficiency were obtained and mated to produce homozygous *Zc3hc1*-deficient, or *Zc3hc1*-KO animals.
First, the extent of expression of *Zc3hc1* in a wildtype mouse was determined by analysing the mRNA-expression in a number of organs.
Then, in the knockout mice, the deficiency was confirmed at all levels possible; by genotyping the DNA to analyse the genetic modification, by analysing the changes in mRNA to verify the knockout on transcriptional level, by immunoblotting to confirm the functional loss of protein expression, and additionally with a staining for the induced reporter β-Gal as means to prove the functionality of the inserted disrupting cassette.
The KO-mice were phenotyped to assess the impact of the *Zc3hc1*-deficiency on the overall physiology of the animals.

3.2.1. Expression of *Zc3hc1*-mRNA in various tissues

To obtain an expression profile for *Zc3hc1*, mRNA from various organs of a wildtype mouse was isolated, transcribed to cDNA and used for a PCR-assay for *Zc3hc1*. The results are shown in figure 3.10. Both primer pairs used, one between exon 3 and 4, the other between exon 8 and 9, show bands in all organs, at the respective expected product size for each pair, indicating a ubiquitous expression of *Zc3hc1*-mRNA. GAPDH was used as a loading control.

3.2.2. Generation and confirmation of *Zc3hc1*-deficient mice

Mice with heterozygous deficiency of *Zc3hc1* were obtained (see section 2.2), and mated to generate homozygous deficient animals. The status of the deficiency, Wildtype (+/+

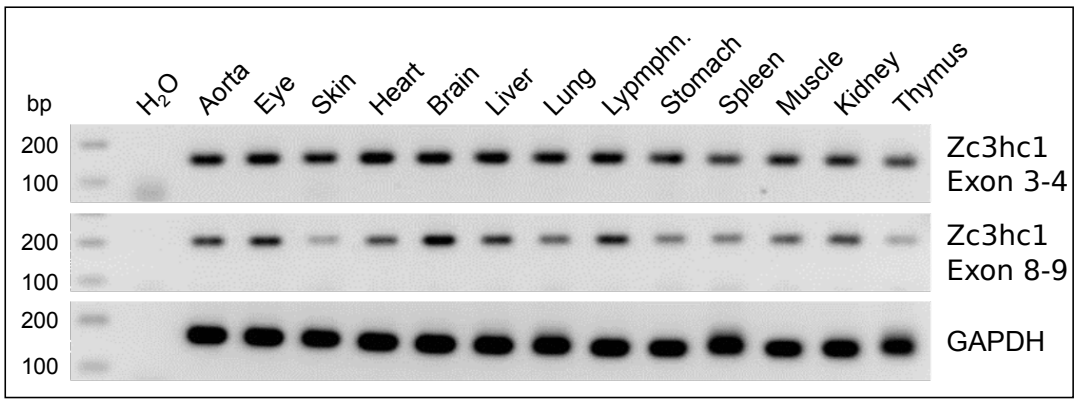

Figure 3.10.: *Zc3hc1*-mRNA is expressed ubiquitously. From different organs from one mouse, mRNA was isolated, reverse transcribed into cDNA and used for a PCR with primers for *Zc3hc1*. Two primer pairs were used, targeting exon 3 & 4, and exon 8 & 9. GAPDH was used as loading control. Lymphn.: Lymphnodes; H_2O: water control; bp: base pairs.

or WT), heterozygous (+/− or HET) or homozygous (−/− or KO), was determined by genotyping. *Zc3hc1*-KO mice were viable, and the deficiency of *Zc3hc1* was further confirmed at transcription and expression levels, and the impact on the phenotype was assessed.

Confirmation of the targeted *Zc3hc1*-allele on genomic DNA

Three primer pairs were used (see table 2.19 for sequences, and figure 3.11 for a schematic representation of the primer target sites): one pair surrounding a LoxP-site in the intron between Exon 5 and 6 (target: *Zc3hc1*), one pair with the forward primer inside the LoxP-site (target: LoxP), and the third pair inside the lacZ-gene. Results are shown in figure 3.11. The *Zc3hc1*-primers show different results for each genotype; one smaller band between 200 and 300 bp for a WT mouse (+/+), one larger band at 300 bp for *Zc3hc1*-KO mice (−/−), and both these bands in a *Zc3hc1*-HET mouse. *Zc3hc1*-HET and -KO samples show bands for LoxP and lacZ, at around 500 bp and 400 bp, respectively; only WT animals show no band for either of the two PCRs.

Targeted *Zc3hc1*-allele is transcribed into mRNA

To confirm if the introduced targeting cassette is not only present at DNA level, but is also transcribed to the *Zc3hc1*-mRNA, mRNA from heart and liver from *Zc3hc1*-WT,

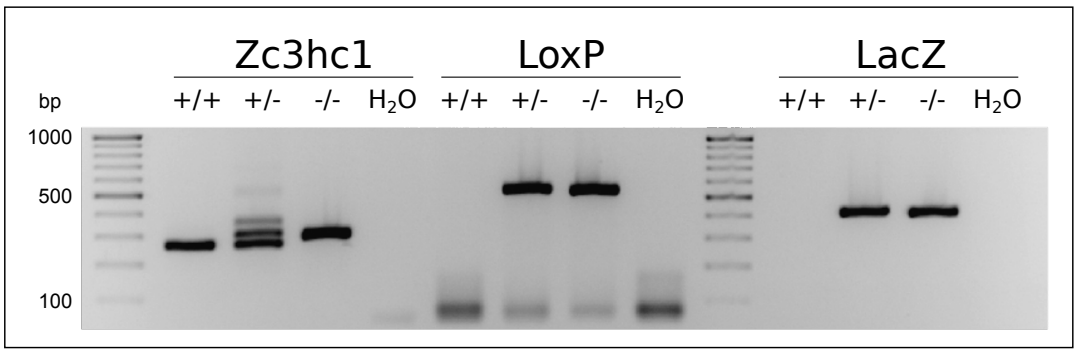

Figure 3.11.: Genotyping *Zc3hc1* mice, using DNA isolated from ear biopsies. Left: products of a PCR targeting the intron between exons 5 and 6 of *Zc3hc1*, which contains a loxP site; a larger band is observable in KO animals (−/−, around 300 bp) compared to WT (+/+, between 200 to 300 bp), while HET mice (+/−) have both. Middle: PCR products of a primer pair with the forward primer located inside the loxP sequence; a band is seen only in HET and KO animals. Right: a PCR product from a primer pair within the lacZ-sequence is also seen in HET and KO mice only. Data shown from one exemplary genotyping. H_2O: water control; bp: base pairs.

-HET, and -KO animals was isolated and transcribed into cDNA. Then, a PCR with the forward primer Exon3 and the reverse primer Exon9 was performed.
The expected product size is 1042 bp in the WT sequence, and much longer in the targeted allele due to the inserted targeting cassette. A PCR with an elongation time short enough to leave the amplification of the long range product impossible, showed the expected results. A band can be observed only in WT and HET animals, the latter with a weaker or, in case of the liver sample, very low intensity, and no band in KO animals (see figure 3.12). Loading control confirms the existence of cDNA in all samples. Also, short range PCRs, with primer pairs for exon 3 and 4, and exon 8 and 9, respectively, showed bands in all genotypes (see figure 3.13).

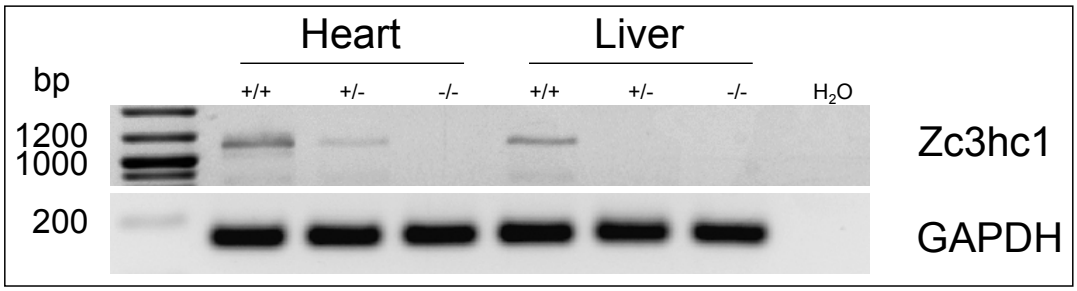

Figure 3.12.: Targeting cassette is transcribed into mRNA. A long range PCR with primers between exon 3 and 9 of *Zc3hc1*, and an elongation time of 1:15min, results in a band at 1042 bp in WT and HET animals; no band is produced using cDNA from KO animals within the given time. H_2O: water control; bp: base pairs.

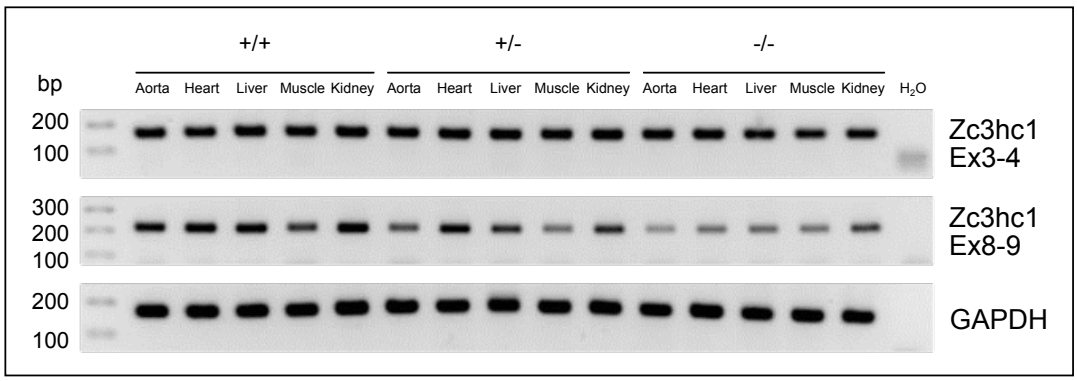

Figure 3.13.: Full-length mRNA is expressed also in transgene animals. cDNA from different organs was tested using primers targeting a sequence before (exon 3 & 4) and after (exon 8 & 9) the inserted cassette, respectively; both products are seen in all organs from all three genotypes. GAPDH was used as loading control. H_2O: water control; bp: base pairs.

Zc3hc1-KO mice show a loss of protein

To determine whether the KO of *Zc3hc1* leads to a loss of protein, an immunoblot with a specific antibody was performed. Total protein from several organs of either a *Zc3hc1*-WT or a *Zc3hc1*-KO mouse was isolated, separated in an SDS-PAGE and subsequently blotted on a PVDF-membrane. This membrane was then cut in half (see section 2.9.1), and the upper half was incubated with an antibody specific for NIPA, the protein encoded by *Zc3hc1*. GAPDH was stained in the lower half, and used as loading control.
Results are shown in figure 3.14. The band at the expected size for NIPA, 50-60 kDA (arrow), is clearly missing in the KO-lane in both heart and liver. GAPDH is present in all samples.
Additional bands are visible; one band between 75 and 100 kDa in all lanes, and several bands between 50 kDa and the NIPA-band in the liver samples.

Detection of β-Galactosidase using X-Gal staining

A reporter gene, lacZ, is introduced into the mouse genome during the generation of the KO mouse. It encodes the bacterial enzyme β-Gal , which metabolises β-galactosides, releasing the monosaccharide galactose. Galactose-derivates coupled with a colorful dye can be used to detect and visualise the enzymatic reaction of the β-Gal. One of these derivates is X-Gal, resulting in a blue staining after being cleaved by β-Gal. Heart

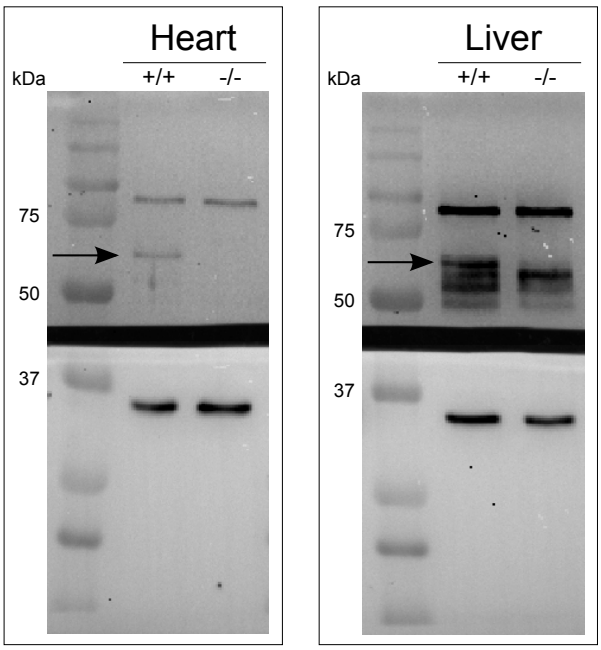

Figure 3.14.: Loss of protein expression. Immunoblotting with an antibody against NIPA shows a band at 55 to 60kDa (arrow) in WT but not in KO animals. The lower half of the membrane was stained with an antibody against GAPDH as a loading control. 15µg of total protein were used per lane.

cryosections from one mouse per genotype (*Zc3hc1* +/+, +/−, and −/−) were used to detect β-Gal-activity using X-Gal. figure 3.15 shows the results, blue dots are visible in sections from +/− and −/−, but not +/+ mice.

3.2.3. Phenotyping of *Zc3hc1*-KO mice

After confirming the *Zc3hc1*-deficiency, the impact on the phenotype was assessed.

Zc3hc1-KO mice show altered physical appearance

From the first litters, *Zc3hc1*-KO mice were noticeably different from their WT littermates. They were smaller, and a very low number of mice showed a shorter snout (see figure 3.16).

To follow up on the size difference, mice were weighed for a period of 44 weeks (see

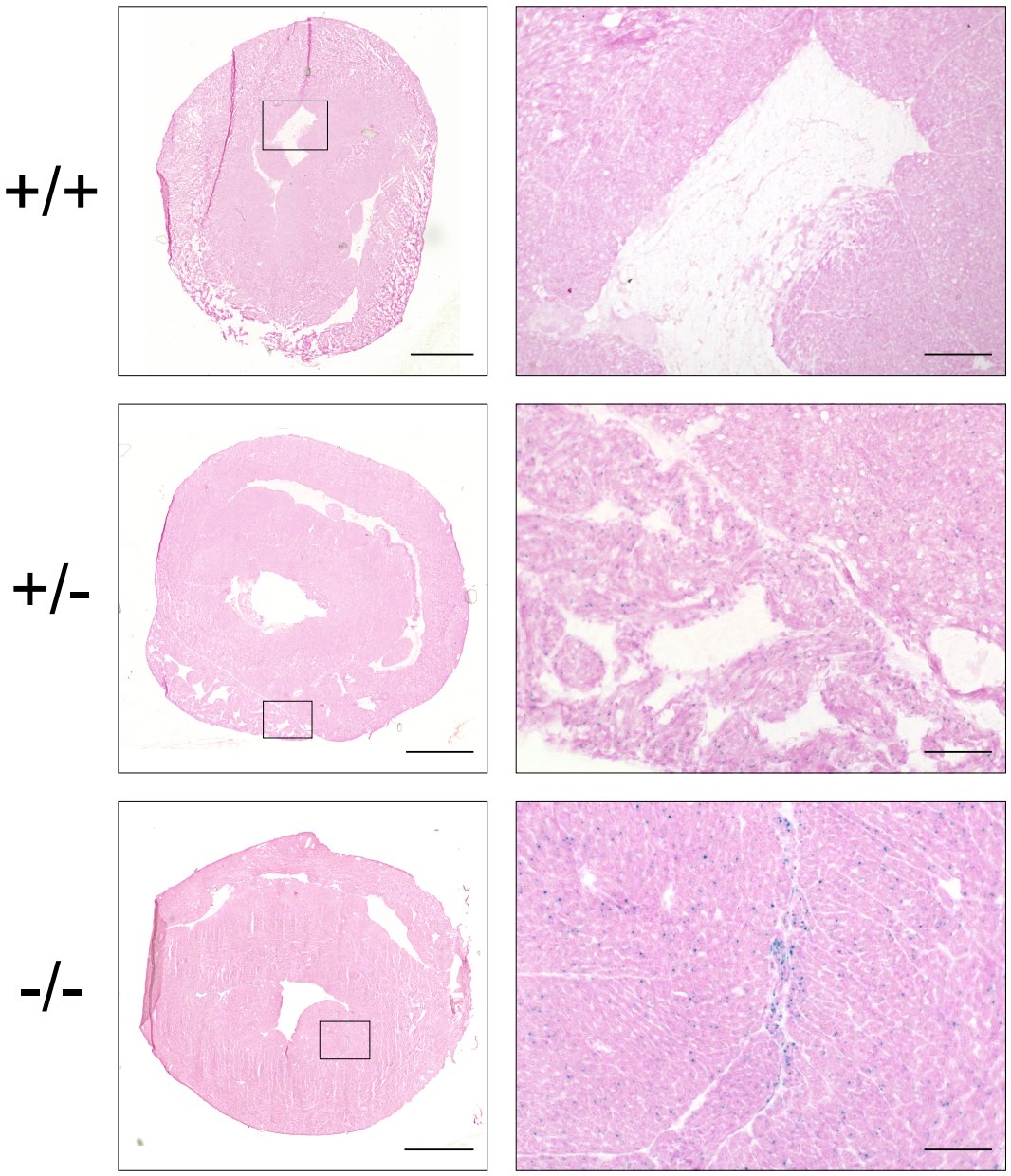

Figure 3.15.: Functional expression of the inserted lacZ-Gene. X-Gal staining shows expression of β-Gal, the enzyme encoded by the gene lacZ, in HET and KO but not in WT animals. Heart cryosections from animals of all three genotypes were stained with X-Gal, which releases a blue chromogen if metabolised by β-Gal. Left: overview of the heart section. Right: detailed view of the rectangular areas marked in the heart sections. Scale bar: 1mm (whole heart sections); 100µm (magnifications).

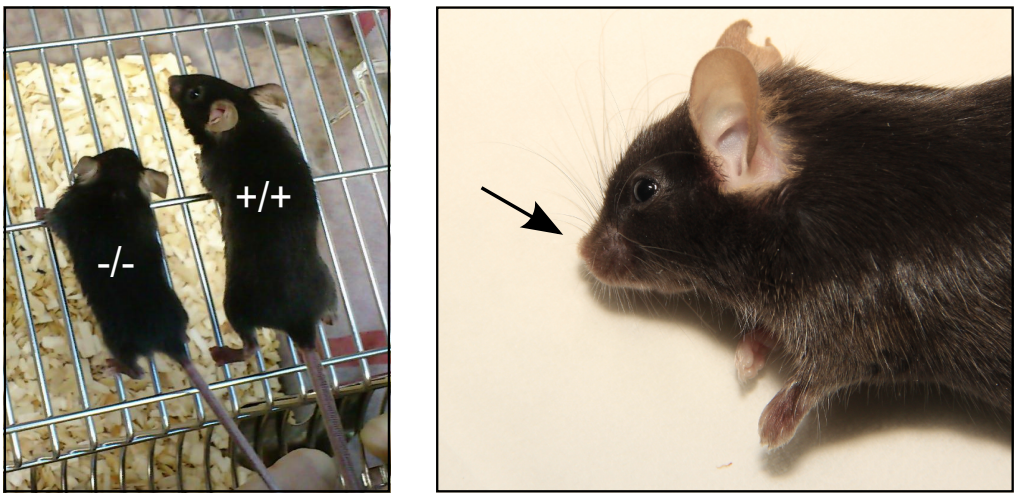

Figure 3.16.: *Zc3hc1*-KO mice are smaller, and can have a shorter snout. Left: KO animal is visibly smaller than its WT littermate. Right: Abnormally shortened snout, observed in only very few KO animals.

figure 3.17). Intervals were changed from weekly (for 10 weeks after weaning) to monthly (between 13 and 25 weeks of age), to one three-month interval (week 37), and a last timepoint to confirm that mice reached full growth (week 44). *Zc3hc1*-KO mice (n = 7) maintain a significantly lower bodyweight over their lifetime ($p < 0.0001$, paired t-test), compared to WT littermates (n = 16).

Impact of *Zc3hc1*-KO on birth rate and litter size

The genotyping results revealed a reduced birth rate for *Zc3hc1*-KO animals. To quantify the birth rate, the genotype frequencies were calculated for all genotyped offspring from matings of *Zc3hc1*-HET mice. The results are shown in table 3.1. The rate for *Zc3hc1*-KO mice was 10%, WT and HET animals were born with frequencies of 29 and 61% , respectively.
To determine whether this is a mendelian distribution or not, a Chi-square test was calculated. The Chi-square score was 12.06, and the p-value was 0.0024, showing that the observed genotype distribution is significantly non-mendelian.

The average litter size, the number of pups born divided by the number of litters, was 5.18. This number was derived from a total of 323 litters, which also includes litters that were not genotyped.

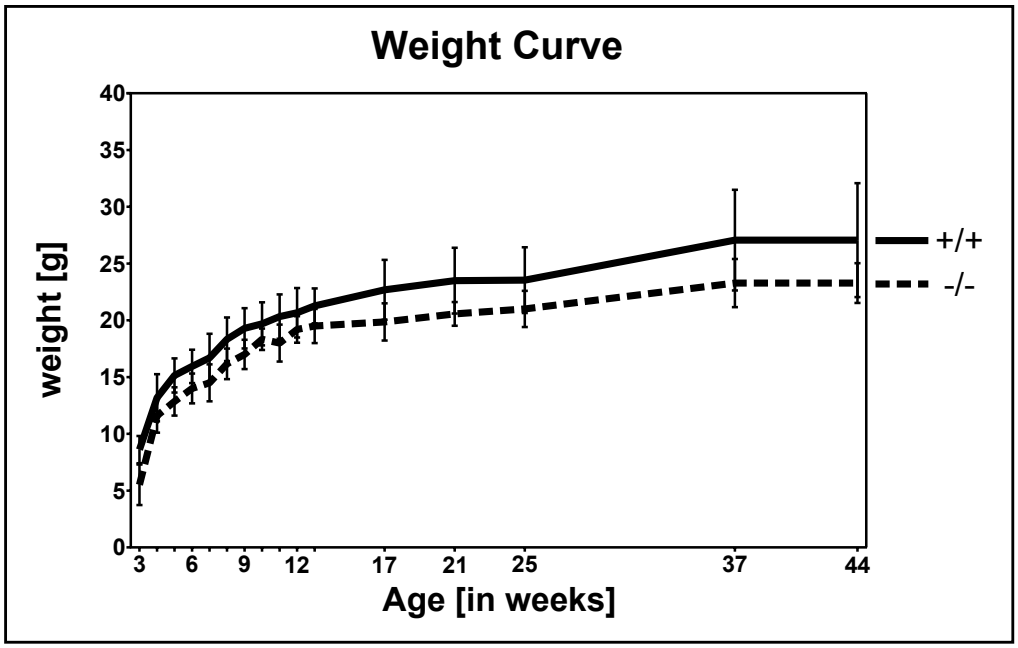

Figure 3.17.: *Zc3hc1*-KO mice have a significantly lower bodyweight ($p < 0.0001$, paired t-test). Initially, mice were weighed weekly (age 3 to 13 weeks), followed by weight controls at the depicted time points.

Table 3.1.: Genotype frequencies of offspring from *Zc3hc1*-HET matings. Shown are the total number of mice born per genotype, and the percentages of total, as well as the percentages per genotype.

		WT	HET	KO	$\sum$
total	n	355	757	131	1243
total	%	29	61	10	100
male	%	32	60	8	100
female	%	30	59	11	100

Zc3hc1-KO does not change life span

Zc3hc1-KO mice were viable. To assess long-term effects of the deficiency, a group of mice were left to observe their life span. *Zc3hc1*-KO mice ($n = 6$) showed no alteration in life span (see figure 3.18), compared with their WT littermates ($n = 5$).

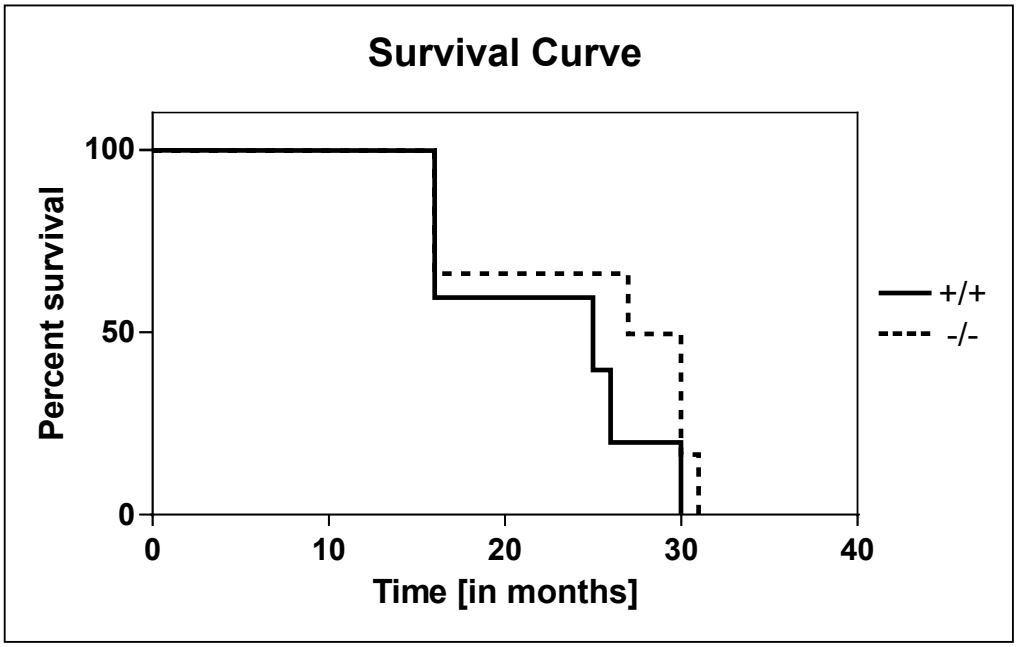

Figure 3.18.: KO-mice live as long as WT-littermates. Life times of mice were noted and compared in a Kaplan-Meier curve. No difference between KO ($n = 6$) and WT ($n = 5$) were seen.

3.3. Atherosclerosis Study

The second, major goal of this thesis was to determine the role of *Zc3hc1* in atherosclerosis. Therefore, the *Zc3hc1*-KO mouse line was backcrossed to the proatherogenic ApoE-KO background. Additionally, to induce atherosclerosis, double-KO mice, and ApoE-KO as controls, were put on a Western type diet. The extent of atherosclerosis was then analysed in the aortic root.

3.3.1. Backcrossing to the proatherogenic ApoE-KO mouse line

For the atherosclerosis study, the *Zc3hc1*-mouse line was backcrossed to the proatherogenic ApoE-KO background in several stages (see section 2.12).

Offspring of every mating step was genotyped, and animals for further breeding were selected accordingly.

The final mating step was performed with *Zc3hc1*-HET ApoE-KO mice to generate the animals for the atherosclerosis study. As can be seen in figure 3.19, the genotyped animals are all homozygous KO for ApoE, while they show all genotypes for *Zc3hc1*: WT (1 and 3), HET (4, 5, 7 and 8), and KO (2 and 6), allowing for the selection of animals matched in age and gender for the experimental and control groups, respectively.

The genotype frequencies were calculated as well (see table 3.2), using the numbers from matings between *Zc3hc1*-HET ApoE-KO mice. The distribution is similar to that from mice without ApoE-KO background (see table 3.1). However, male double-KO mice are born with only a 6% chance. The distribution was also significantly non-mendelian (Chi-square score: 15.42, p-value < 0.0001).

3.3.2. Atherosclerosis Experiment

As shown in section 2.13, 10 week old mice were put on a short-term highfat diet for 8 weeks, and then sacrificed for organ retrieval and subsequent analysis of the extent

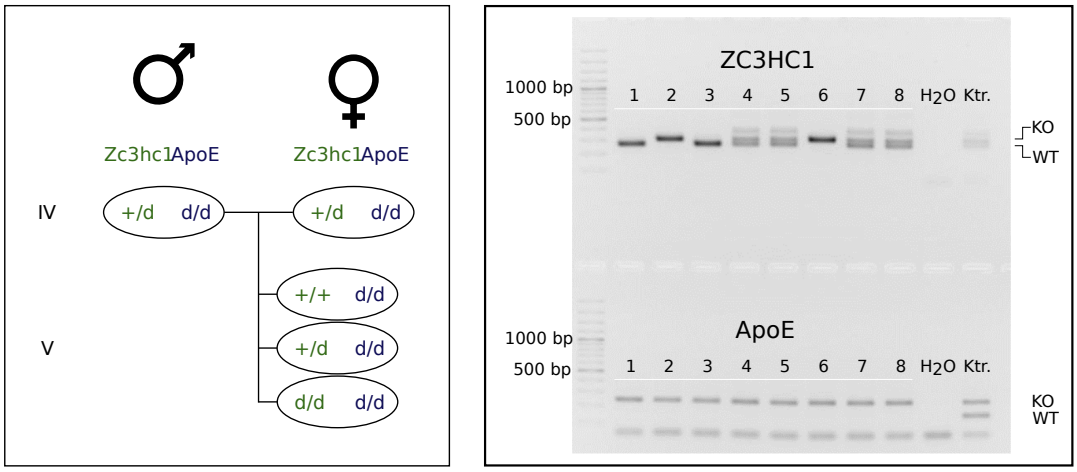

Figure 3.19.: Genotyping for confirmation of successful backcross. Left: Selected animals were used for the final mating step (IV) to generate *Zc3hc1*-WT, -HET, and -KO animals on the ApoE-KO background (V) for the atherosclerosis study. Right: Genotyping of mice from step V showed animals which were ApoE-KO, but had all genotype forms for *Zc3hc1*.

Table 3.2.: Genotype frequencies from matings of *Zc3hc1*-HET ApoE-KO mice. Shown are the total number of mice born per genotype, and the percentages of total, as well as the percentages per genotype.

ApoE		KO			
Zc3hc1		WT	HET	KO	$\sum$
total	n	263	513	72	859
total	%	31	61	8	100
male	%	31	63	6	100
female	%	31	58	11	100

of atherosclerosis. Parameters examined include body weight, plasma lipid levels, and plaque analysis at aortic root level.

Weight after HFD

Mice were weighed weekly for the duration of the highfat diet. Results are shown in figure 3.20; double-KO mice have a significantly lower weight compared to the ApoE-KO control mice ($p < 0.0001$). They also gain less weight, 3.9g, from 17.1 to 21g, compared to the ApoE-KO control animals, which gain almost 6g, from 23 to 28.67g.

In order to identify the influence of both genotype and diet on the weight gain, ApoE- and double-KO mice on HFD were compared to similar groups of mice which were fed normal, or Chow diet only. In addition, the weight gain of *Zc3hc1*-KO and wildtype mice on Chow was also compared (see figure 3.17). As can be seen from figure 3.21, all mice which lack the gene for *Zc3hc1* have a similar weight (light colors); neither diet nor the additional deficiency of the ApoE-gene have an influence on the weight. On the other hand, the knockout of ApoE increases the weight only slightly compared to wildtype mice (BL/6), whereas the HFD leads to a remarkable weight increase in ApoE-KO mice.

Plasma Lipids

Plasma levels of Total, HDL- and nonHDL-Cholesterol, Triglycerides and Phospholipids were compared at the end of the feeding period. There were no differences between the Double-KO and the ApoE-KO control mice (see table 3.3).

3.3.3. Quantitative plaque analysis

The extent of atherosclerosis was analysed in sections of the aortic root. First, plaque size was determined. Then, the plaque composition was analysed, quantifying the amount of Collagen, Monocytes and Macrophages, and SMCs, respectively, normalised to plaque area.

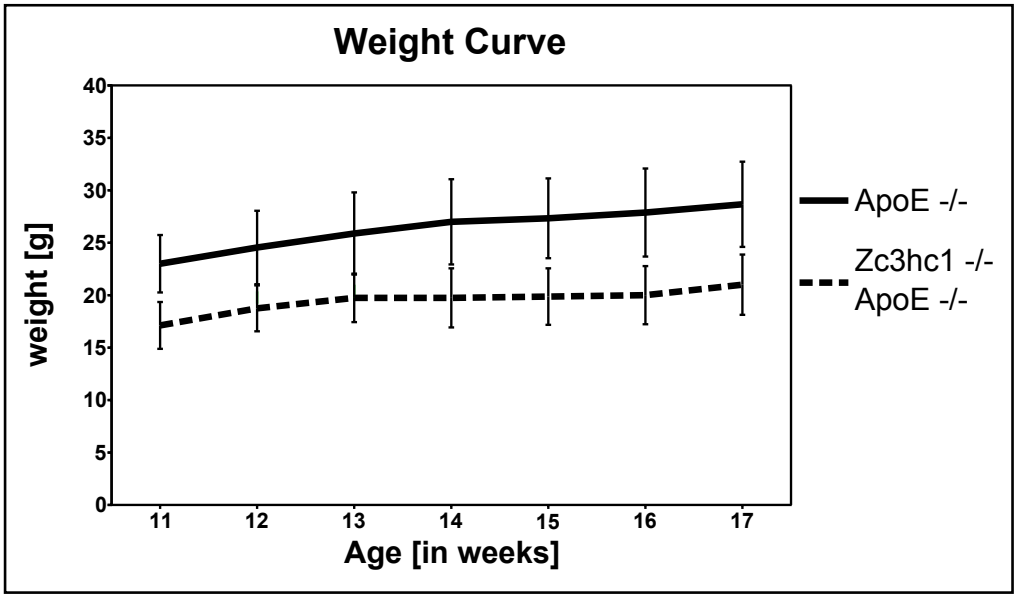

Figure 3.20.: Weight gain during HFD. During the feeding period, mice were weighed weekly; Double-KO animals ($n = 8$) maintain a lower bodyweight, and gain less (3.9g), compared to ApoE-KO control animals ($n = 9$, 5.67g).

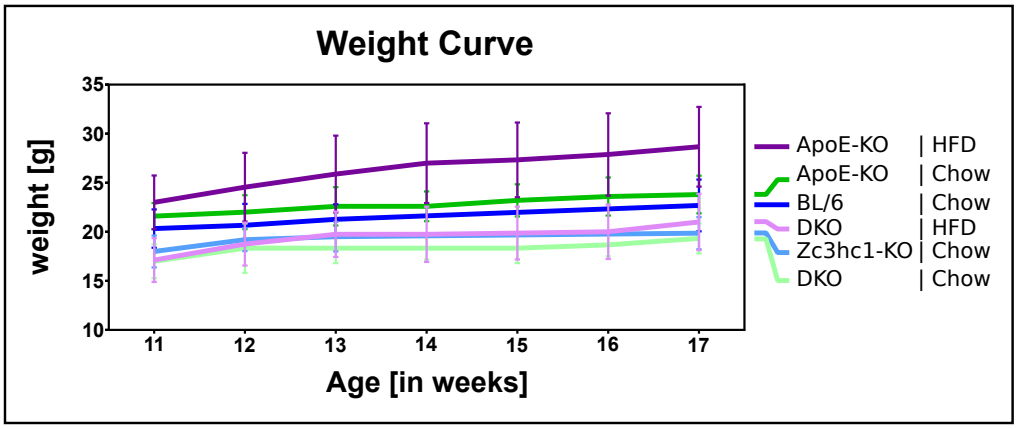

Figure 3.21.: Comparison of weight gain of mice with different genotypes and diets. All mice with *Zc3hc1*-deficiency have a similar weight (*Zc3hc1*-KO: $n = 7$; DKO-Chow: $n = 3$; DKO-HFD: $n = 8$), regardless of the diet or additional knockout of the ApoE-gene (double-KO, DKO). All corresponding controls have higher weights: ApoE-KO mice on normal, or Chow diet ($n = 5$) have slightly higher weight compared to wildtype mice (BL/6 on Chow, $n = 16$), and this difference is increased even further with the high-fat Western type diet (ApoE-KO on HFD, $n = 9$). Values shown are mean, bars represent SD.

Table 3.3.: Comparison of Plasma Lipids in *Zc3hc1*-KO ApoE-KO mice and ApoE-KO controls. Lipids were measured in Plasma isolated from fasting blood samples at the end of the feeding period. TC: Total Cholesterol; HDL-C: High Density Lipoprotein-Cholesterol; nonHDL-C: Total minus HDL-Cholesterol; TG: Triglycerides; PL: Phospholipids.

	ApoE-KO		*Zc3hc1*-KO ApoE-KO	
	average ± std [mM]	n	average ± std [mM]	n
TC	26.53 ± 7.04	10	25.25 ± 6.55	12
HDL-C	0.38 ± 0.16	8	0.55 ± 0.28	10
nonHDL-C	25.37 ± 6.95	9	24.51 ± 6.54	10
TG	1.38 ± 0.51	10	1.50 ± 0.70	12
PL	5.21 ± 1.50	10	6.16 ± 1.72	12

Plaque size

Plaque size was assessed in 10 sections of the aortic root, which were 40µm apart, and stained with ORO (see section 2.13). Plaque area was normalised to aorta area (see figure 3.22). No differences in relative plaque size were observed between double-KO mice ($n = 8$) and ApoE-KO controls ($n = 8$).

Plaque coverage in the thoracic aorta

Another method, aortic *en-face* preparation, was used to quantify plaque development in the whole aorta. Thoracic aorta segments were opened longitudinally, and plaques were then visualised with ORO. To determine the Plaque Coverage (in %), the plaque area was normalised to the aorta area.
The *en-face* analysis revealed no difference in plaque coverage between double-KO and ApoE-KO animals ($n = 12$ vs. 14, respectively; see figure 3.23).

Collagen content

Collagen content was analysed in 5 sections of the aortic root, which were stained with Masson's Trichrome to visualise collagen fibers. Collagen content was calculated as % of plaque area (see figure 3.24). Double-KO mice had significantly reduced collagen content compared to ApoE-KO controls (29.18% vs. 38.38%, $p = 0,0385$).

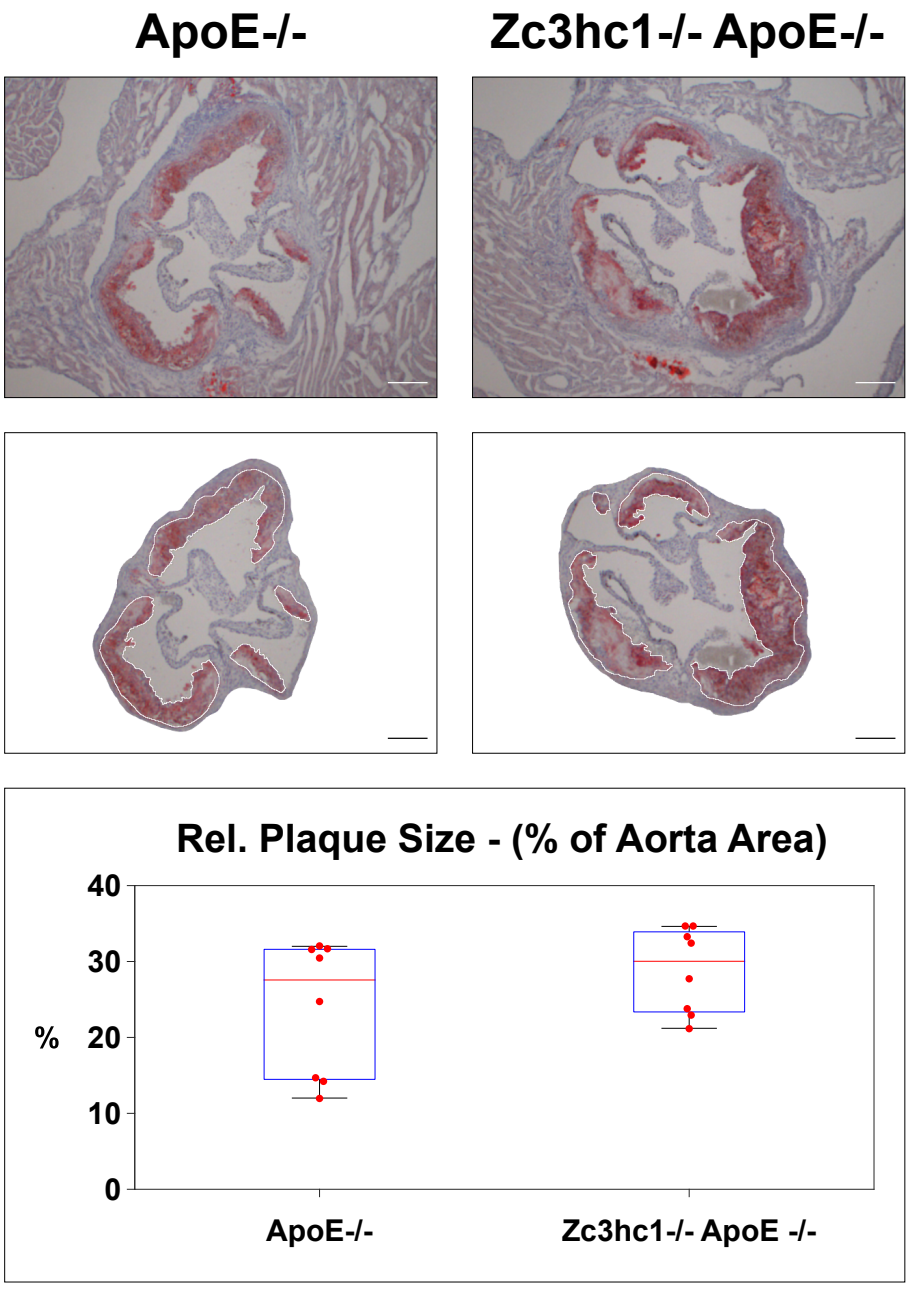

Figure 3.22.: Plaque Size. Top: ORO stained heart sections. Middle: Image processing (with the software GIMP) for the analysis; aorta area was selected, including lumen and valves. The plaque area was then selected (white outlines) and calculated as percent of the aorta area. Bottom: box plot showing the distribution of relative plaque size in both groups. No difference was seen. Whiskers: smallest/ largest value; Box: first and third quartile; Line: median; Dots: individual data points. Scale bar: 200µm.

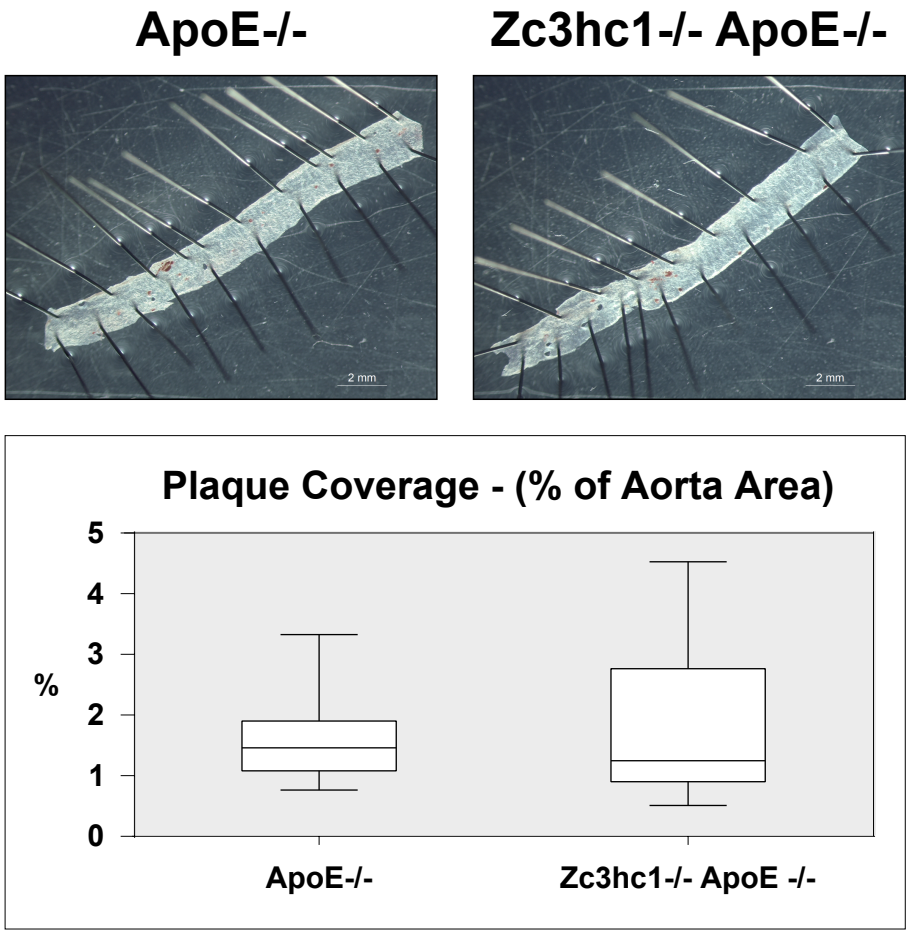

Figure 3.23.: Quantification of Plaque Coverage in thoracic aortas. Top: aortas were cleaned from fat and adventitia, opened longitudinally, stained with ORO for plaques and pinned on 2.5% agarose with minutien pins. Bottom: box plot showing the distribution of plaque coverage of the thoracic aorta (plaque area as percent of aorta area) in both groups. No difference was seen. Whiskers: smallest/ largest value; Box: first and third quartile; Line: median.

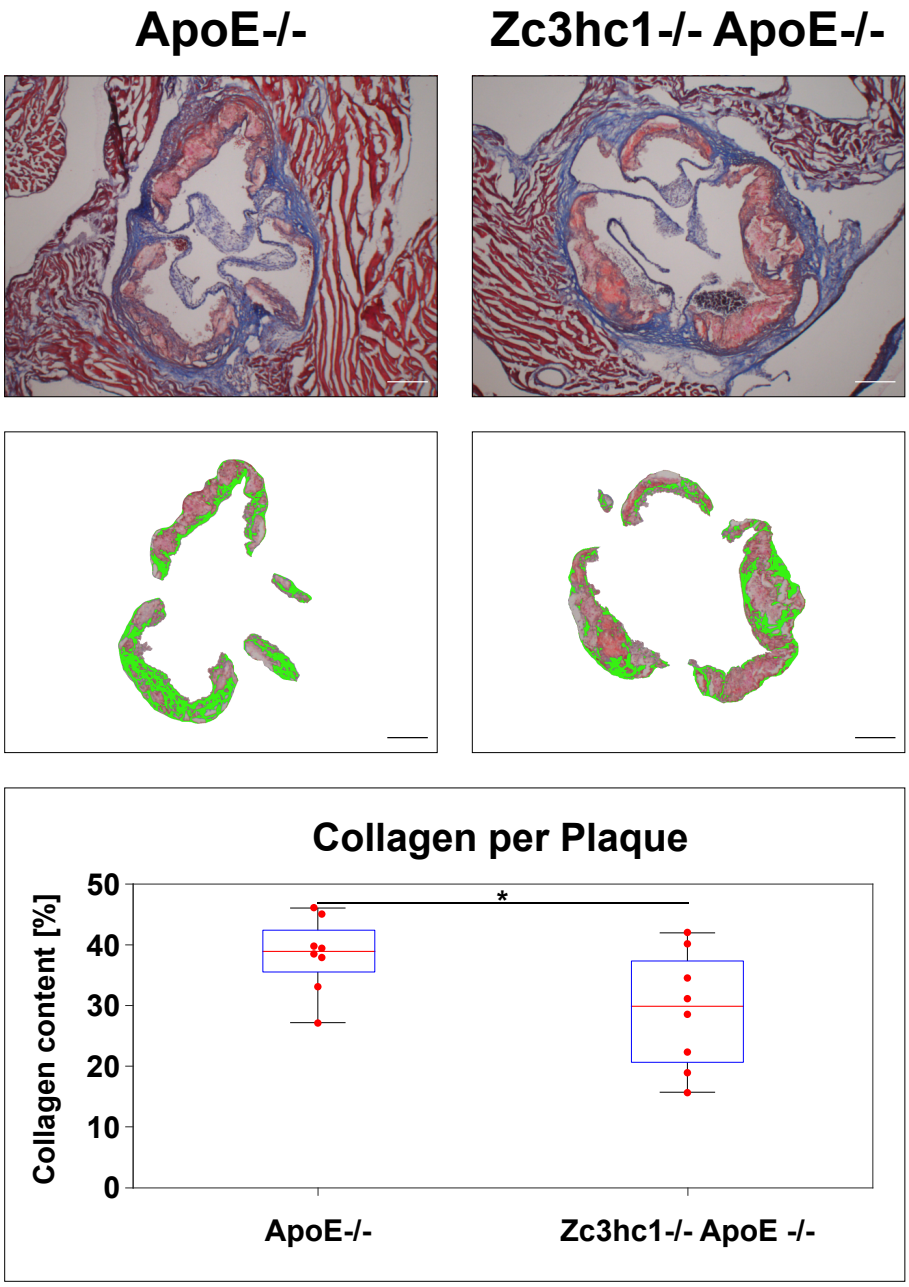

Figure 3.24.: Collagen Content. Top: Masson's Trichrome staining of heart sections. Middle: overlay of the plaque area and the collagen fibers (colored in green). Plaque area was selected with the software GIMP, supported with the ORO stained images, and cut out. The collagen fibers, appearing in blue in this staining, were then selected with an image processing algorithm written in Matlab. Collagen area was then normalised to the plaque area. Bottom: box plot showing the distribution of collagen content in both groups. Double-KO animals had less collagen than the ApoE-KO controls (29.18% vs. 38.38%, $p = 0,0385$). Whiskers: smallest/ largest value; Box: first and third quartile; Line: median; Dots: individual data points. Scale bar: 200µm.

MoMa content

Similarly to collagen content, the amount of inflammatory Monocytes and Macrophages was determined. In 5 sections, parallel to those used to quantify collagen, Monocytes and Macrophages were stained with the anti-Monocyte + Macrophage [MOMA-2] antibody, and the positive stained area was normalised to plaque area. There was no difference between the two groups ($n = 7$ vs. $n = 6$ in the controls; see figure 3.25).

SMC content

Similarly to collagen content, the amount of SMCs in the plaque was determined. In 5 sections, parallel to those used to quantify collagen and Monocytes and Macrophages, SMCs were stained with the anti-α-SMA antibody, and the positive stained area was normalised to plaque area. *Zc3hc1*-KO ApoE-KO animals had in average 0.53% SMCs per plaque, compared to 1.36% in the ApoE-KO controls ($n = 8$ in both groups); however, this difference was not significant (see figure 3.26).

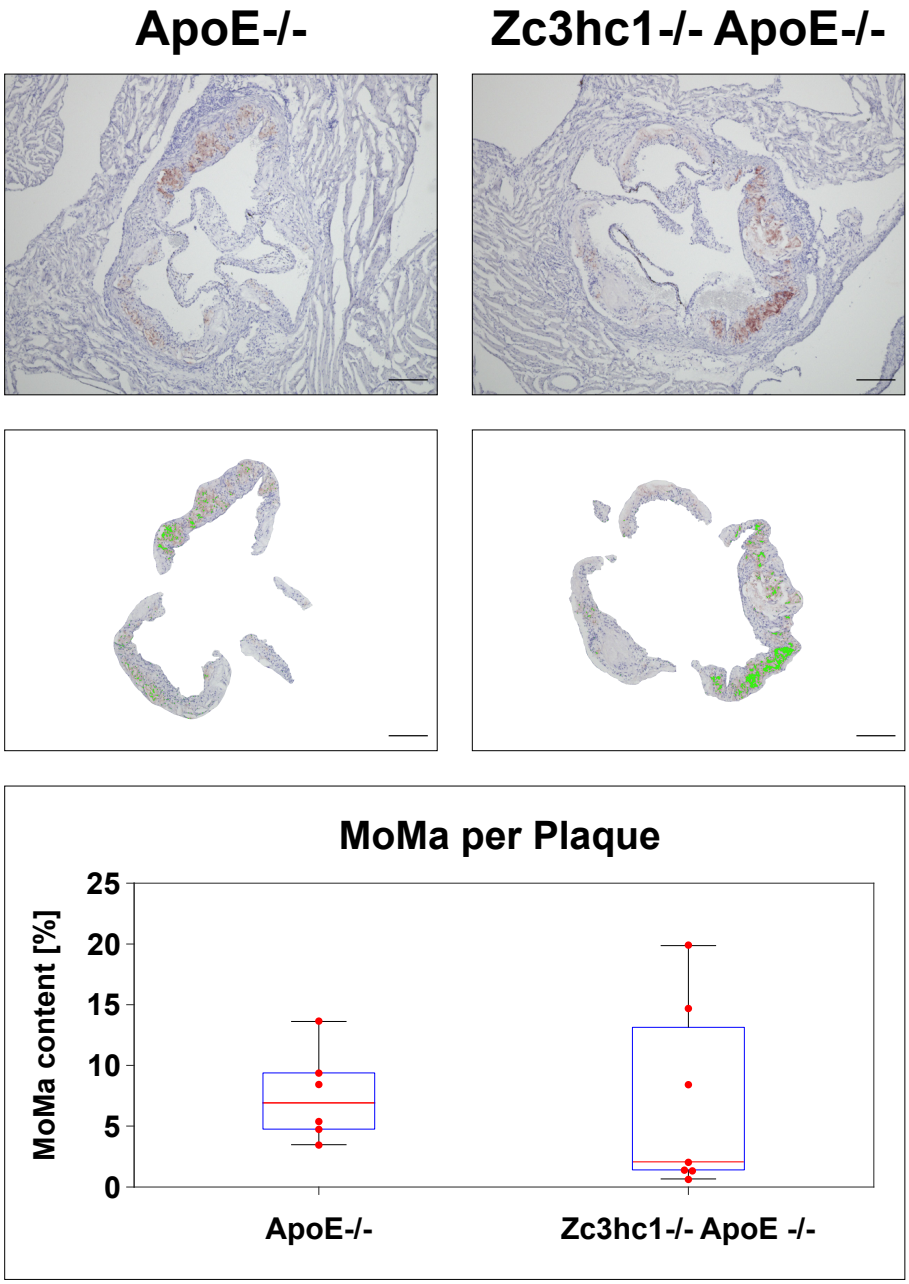

Figure 3.25.: Monocytes and Macrophages per plaque. Top: staining of heart sections with the anti-Monocyte + Macrophage [MOMA-2] antibody. Middle: overlay of the plaque area and the positive MoMa2-area (colored in green). For the analysis, plaque area was selected with the software GIMP, supported with the ORO stained images, and cut out. The brown area resembling the positive staining was then selected with an automated image analysis algorithm with Matlab (see section 2.13.3). Positive MoMa-stained area was then normalised to the plaque area. Bottom: box plot showing the distribution of MoMa content in both groups. Double-KO animals (6.93%, $n = 7$) showed no difference in MoMa-content compared with the ApoE-KO controls (7.51%, $n = 6$). Whiskers: smallest/ largest value; Box: first and third quartile; Line: median; Dots: individual data points. Scale bar: 200µm.

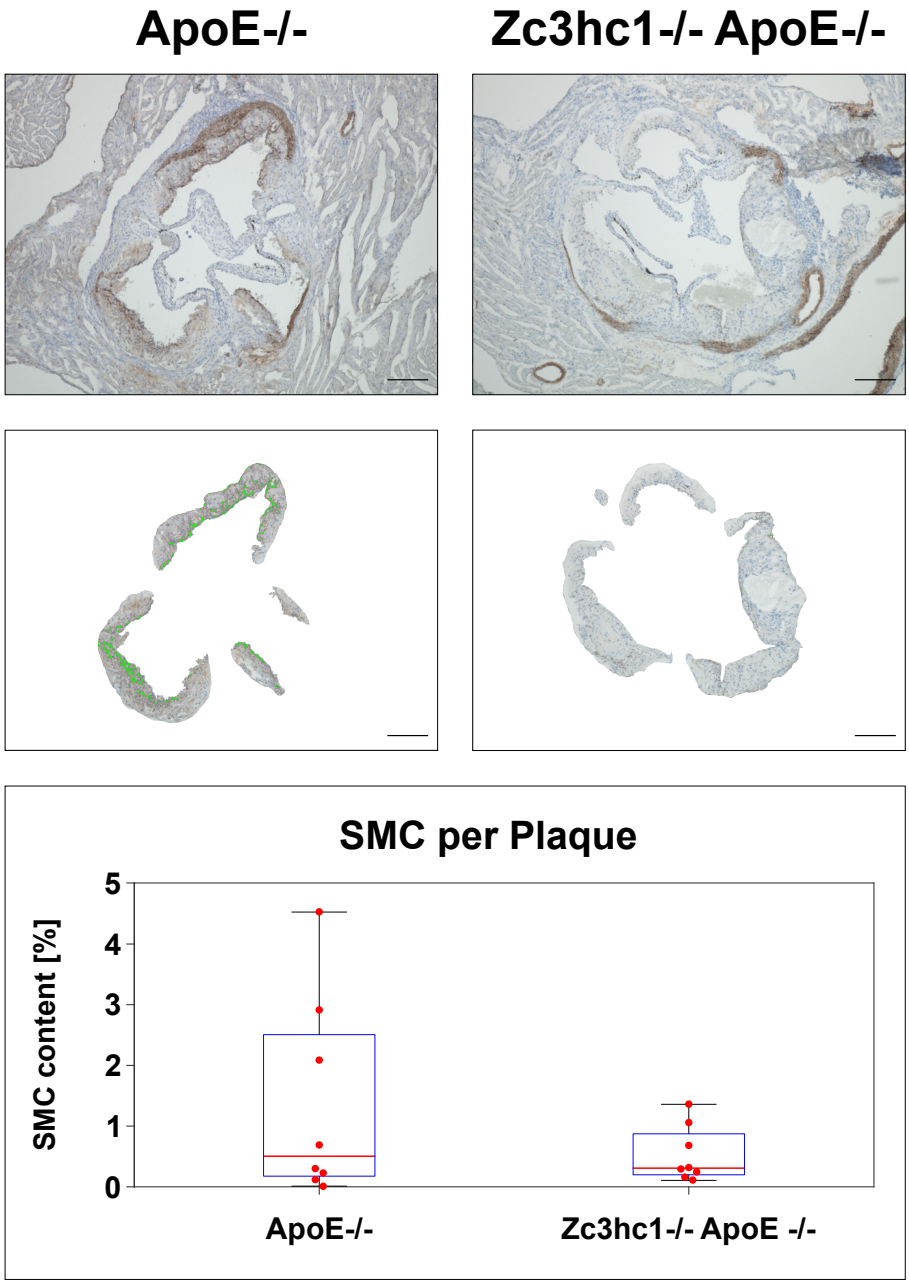

Figure 3.26.: Smooth Muscle Cell-content in the plaque. Top: staining of heart sections with the anti-α-SMA antibody. Middle: overlay of the plaque area and the positive SMC-area (colored in green). For the analysis, plaque area was selected with the software GIMP, supported with the ORO stained images, and cut out. The brown area resembling the positive staining was then selected with an automated image analysis algorithm with Matlab (see section 2.13.3). Positive SMC-stained area was then normalised to the plaque area. Bottom: box plot showing the distribution of SMC-content in both groups. Double-KO animals showed a trend towards lower SMC-content compared with the ApoE-KO controls (0.53% ($n = 8$) vs. 1.36% ($n = 8$)), but the difference was not significant. Whiskers: smallest/ largest value; Box: first and third quartile; Line: median; Dots: individual data points. Scale bar: 200µm.

3.4. Characterization of primary mouse aortic SMCs

Aortic SMCs were isolated from *Zc3hc1*-KO and BL/6 mice, characterised, and analysed in terms of proliferation and migration.

3.4.1. Quantification of the SMC marker alpha-Smooth Muscle Actin

To quantify the purity of the populations, the isolated cells were characterised using the SMC-specific FITC-labeled anti-α-SMA antibody. Cells in P9 were either stained with the antibody or an isotype control, and were then, together with unstained cells, analysed by Flow Cytometry (see figure 3.27). Unstained cells showed no fluorescence, while the antibody used as an isotype control showed only low binding. More than 95% of both WT and *Zc3hc1*-KO aortic SMCs showed expression of α-SMA (figure 3.27, bottom row).

The results from the Flow Cytometry analysis were validated in microscopic images of cells stained with the same antibody (see figure 3.28).

3.4.2. Proliferation assay

Proliferation was analysed by seeding a defined cell number and counting the cells at different time points. *Zc3hc1*-KO SMCs showed a lower proliferation rate than control cells (see figure 3.29, black). After 96h, they have about 40% less cells compared to controls (n_{end}/n_0: 3.074, vs. 5.236 in WT controls, $p = 0.0124$). A similar yet non-significant trend was seen in an automated analysis of DAPI-stained images (see figure 3.29, gray).

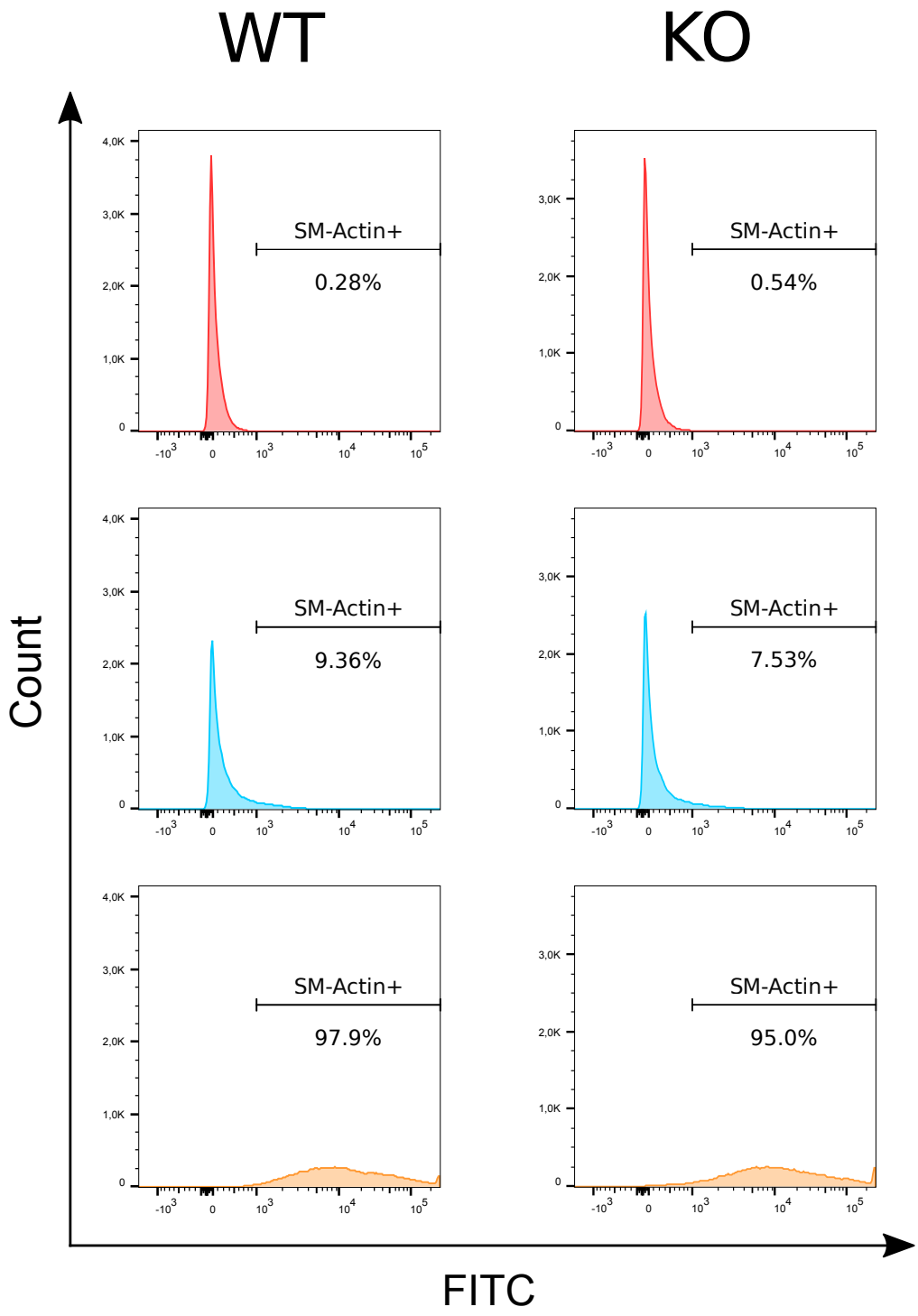

Figure 3.27.: Quantification of SMC marker α-SMA. Cells were analysed by Flow Cytometry. Top row: unstained; Middle row: Isotype Control; Bottom row: anti-α-SMA antibody.

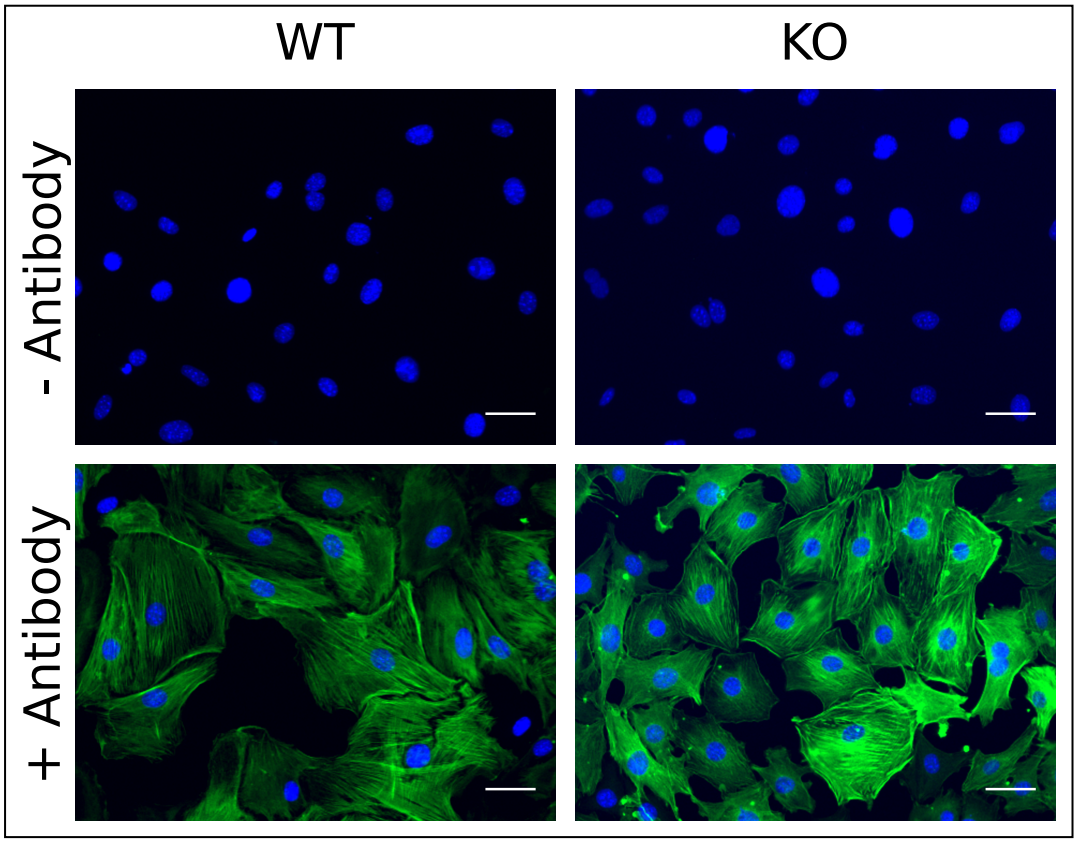

Figure 3.28.: Characterization of SMCs using the specific marker α-SMA. Shown are the overlay images of cells stained with the FITC-labeled anti-α-SMA antibody (green) and DAPI to visualise nuclei (blue). Top row: controls (without primary antibody). Bottom row: the typical actin pattern is visible in both WT and KO SMCs. Scale bar: 50µm.

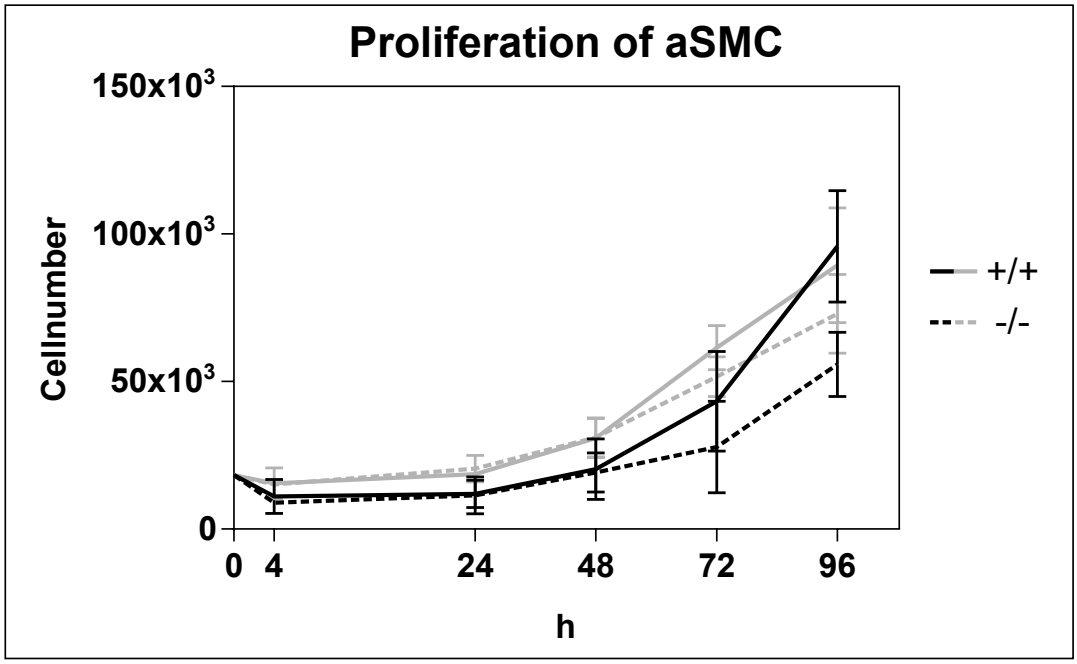

Figure 3.29.: Proliferation of female aortic SMCs. Shown here are the average values of three experiments. For each experiment, at each timepoint, three wells were counted with the Neubauer chamber (black curves), and three wells were photographed after DAPI-staining for automated analysis (gray curves, see also figure 3.30). Manual counting shows *Zc3hc1*-KO aortic SMCs to proliferate slower than WT cells, reaching about 60% after 96h ($p = 7.4 \times 10^{-5}$). In the automated analysis, aortic SMCs from *Zc3hc1*-KO mice also showed a lower proliferation rate compared to WT, yet the difference was not significant.

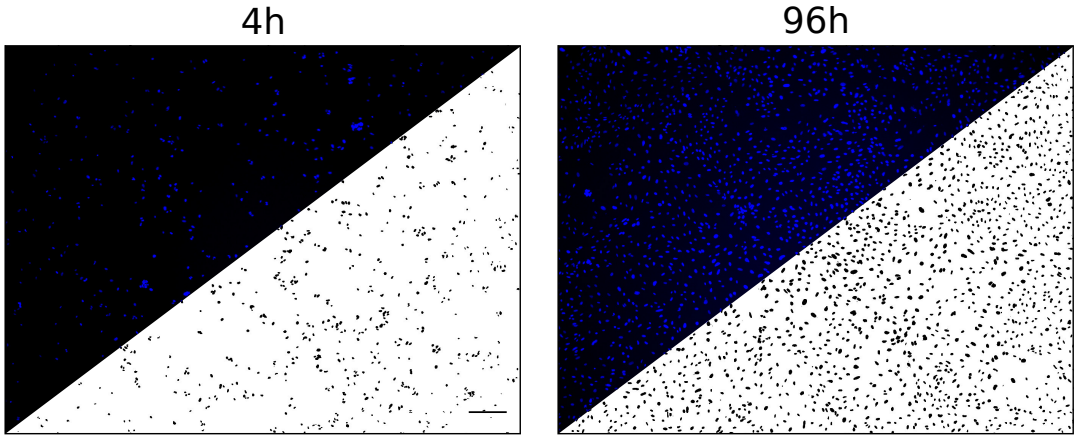

Figure 3.30.: Automated analysis of DAPI-stained images. Shown are the original fluorescence images from timepoints 4 and 96h, with the calculated segmentation as an overlay (see also section 2.16). Scale bar: 100µm.

3.4.3. Migration assay

Migration was analysed using a modified Boyden chamber assay (see section 2.17.1 and figure 2.12). The lower compartments were filled with culture medium containing serum as an attractant for the cells. For each group, the average of four wells was calculated and adjusted for baseline migration rate, which was derived from wells containing serum-free medium only.
Zc3hc1-KO aortic SMCs showed a significantly increased migration rate, reaching the plateau phase after 8 h (CI: 3.35 ± 0.39; average of 3 experiments). Wildtype SMCs do not reach the plateau within this time, and have a lower, but not significantly different CI at this very timepoint (2.65 ± 0.28, or 79% of KO SMCs).

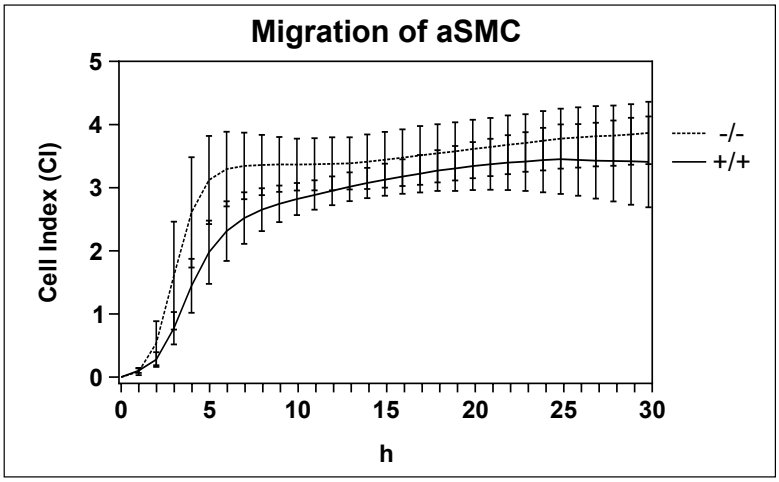

Figure 3.31.: Migration of female aortic SMCs. Cells were seeded in serum-free medium and migrated towards serum containing medium. Curves were corrected for baseline migration, which was measured using serum-free medium in both compartments. Shown here are average curves from three experiments. *Zc3hc1*-KO aortic SMCs have a slightly higher migration rate ($p < 0.0001$, paired t-test).

4. Discussion

CAD/ MI is a major risk of death in the western countries (GBD 2013 Mortality and Causes of Death Collaborators, 2015). Numerous studies have linked numerous chromosomal regions, so called loci, to the disease (CARDIoGRAMplusC4D Consortium et al., 2013; Erdmann et al., 2010; Lieb & Vasan, 2013; Samani et al., 2007; Schunkert et al., 2011; The IBC 50K CAD Consortium, 2011). Many regions contain genes of unknown function or no genes at all; the latter are considered to be either cis- or trans-regulators, for proximal or distant genes. Fine mapping of these loci can help to improve the assignment of the correct genes which are responsible for their respective locus to pop up in the analysis – hints as eQTL effects or even amino acid changes that might have a direct impact on protein function (Brænne et al., 2015) are robust indicators for good candidate genes, and these genes are considered worth being followed up in functional investigations.

Among those genes that were selected for further studies is *Zc3hc1*; it is marked by the SNP rs11556924, which causes an amino acid exchange at position 363 from Arginine to Histidine (R363H). *Zc3hc1* encodes the protein NIPA, which controls entry into mitosis by interaction with Cyclin B1 (Bassermann et al., 2005b), but also affects meiosis (Illert et al., 2012b). The function and structure of this gene are highly conserved between human and mouse (Ouyang et al., 2003). Thus, studying *Zc3hc1* in mouse provides a good model to investigate the functional role of this gene in atherosclerosis, a major risk factor of CAD, in order to elucidate the observed human GWAS-CAD association.

Two main goals were followed through in this thesis, assessing a) the influence of the SNP on the interaction between the protein NIPA and Cyclin B1 *in-vitro*, and b) the impact of the protein deficiency on the development of atherosclerosis in an ApoE-KO mouse model.

4.1. Influence of the SNP on the interaction between NIPA and Cyclin B1

The influence of the SNP rs11556924 on the interaction between the proteins NIPA and Cyclin B1 was investigated in a Mammalian Two-Hybrid assay (see section 3.1).

Protein-protein interactions can be analysed with different methods, such as cross-linking, co-immunoprecipitation (CoIP), fluorescence resonant energy transfer (FRET), or two-hybrid assays (Fields & Song, 1989; Markham et al., 2007; Berggård et al., 2007; Williamson & Sutcliffe, 2010; Arora et al., 2016). While the first two usually are used to detect unknown interaction partners for proteins, and also require antibodies with a good specificity, which are not always available for every target, FRET is based on the transfer of energy between fluorophores in close proximity. Two-hybrid assays are based on the overexpression of two proteins in eukaryotic or mammalian cells. The proteins of interest are fused to either a DNA-binding domain or a transcription-activating domain, which in case of interaction of the two tested proteins induce the expression of a reporter gene. The generated signal is quantifiable and correlates well with the interaction strength of the tested proteins (Estojak et al., 1995).

Here, the cDNA sequences of NIPA, NIPA-R363H and Cyclin B1 were cloned into fusion plasmids containing either a Gal4-binding domain (plasmid pCMV-BD) or the NFκB transcription activation domain (plasmid pCMV-AD). When interacting, they trigger the expression of the reporter gene luciferase, which can then be quantified in a luminometer.

The experiment was first carried out with NIPA-WT, using HeLa cells. The results showed a working assay, as the the controls showed expected luciferase activity levels (see figure 3.8). The internal control, Renilla luciferase, showed a similiar range of expression and activity in all samples. In cells transfected with the plasmids containing NIPA and Cyclin B1, however, the Firefly luciferase seemed to be not induced, as was seen by very low activity values in the range of the negative control. There was no difference between both combinations, NIPA-AD/ Cyclin B1-BD and NIPA-BD/ Cyclin B1-AD.

There could be many reasons leading to a lack of induction of the reporter gene Firefly luciferase. The most obvious reason would be no interaction between the target and

bait proteins, NIPA and Cyclin B1. This can be excluded as the two have already been shown to interact by Bassermann et al. (2007) in a GST pull-down assay with Cyclin B1 expressed in HeLa-cells, even with narrowing down the interaction domain in the protein NIPA to the amino acid residues 352 to 402 (including a proposed nuclear localization sequence, see figure 1.5). The observed lack of interaction might also be a false-negative result due to steric hindrance by the fusion proteins, which is a known problem in two-hybrid screens (Lievens et al., 2009), and can not be fully excluded.

Another reason could be a low transfection efficency. The experiment requires the simultaneous transfection of four plasmids: the AD- and BD- fusion plasmids, pFR-luc and pRL-TK. Although a highly sensitive setup, it seems to be working as can be seen in the controls, where interaction of the transfected control plasmids does indeed lead to formation of the working transcription activator and hence the expression of Firefly luciferase with measureable activity (see table A.1 for raw data). Also, the expression of the transfected fusion proteins was verified using a Western blot with an antibody against NIPA, showing a band at the expected height for the fusion proteins (see figure 3.9). Additionally, an immunoblot for Cyclin B1, or the activating/ binding domains could provide a more detailed insight into whether the fusion proteins are properly expressed or not. This could not be achieved due to an insufficient amount of time.

A more specific reason in this case could be the transfection itself – both proteins, NIPA and Cyclin B1, are involved in cell cycle control. Overexpression of either or the combination of both might lead to a disturbed cell cycle of the host cells; in fact, several publications reported problems with the overexpression of Cyclin B1 in yeast (Sarafan-Vasseur et al., 2002) or mammalian cells (Eichhorn et al., 2014), leading to cell death. This would, of course, impede the observation of interaction between the two proteins. A cell-free overexpression assay (*in-vitro* transcription-translation, IVTT) could be used to circumvent these difficulties.
A recently published study used a similar method as Bassermann et al. (2007), a GST pull-down on HEK-293T cell lysates which were previously transfected with Cyclin B1 (Linseman et al., 2017). They were able to successfully overexpress Cyclin B1 in the HEK-293T cell line. Both variants of NIPA, with or without the SNP, showed the ability to bind Cyclin B1, but there was no difference between the two. This might be attributed possibly to a too small effect of the SNP, or to an insufficient sensitivity of the GST pull-down assay to detect the difference. The mammalian two-hybrid assay, however, would have provided the necessary sensitivity (Berggård et al., 2007); however, no results were achieved with this experiment due to unresolved reasons.

4.2. Role of the Gene *Zc3hc1* in atherosclerosis

The main aim of this thesis was to determine which role the gene *Zc3hc1* plays in atherosclerosis. This question was addressed in a mouse model, which is a suitable model organism for the study of atherosclerosis (Knowles & Maeda, 2000; Fazio & Linton, 2001; Reardon & Getz, 2001; Daugherty, 2002; Allayee et al., 2003; Welch, 2012). Also, *Zc3hc1*-mRNA was found not only to be expressed in all analysed murine tissues (see figure 3.10), confirming and extending the expression profile found by Illert et al. (2012b), but especially the expression in atherosclerosis-relevant organs, such as aorta, heart, and liver, implies the possibility of an involvement in the disease.

Hence, the *Zc3hc1*-KO mouse line was generated, and the KO of the gene was confirmed. The KO-mice were also phenotyped, and then backcrossed to the proatherogenic ApoE-KO mouse line in order to analyse the influence of the gene *Zc3hc1* on the development of atherosclerosis. Together with a high-cholesterol diet, also called Western type diet, this genetic background provides a fast and reliable animal model for atherosclerosis (Zhang et al., 1992; Maeda, 2011).

The ApoE-background was chosen for several reasons. Firstly, the murine ApoE gene is located on chromosome 7, and hence not on the same chromosome as *Zc3hc1* which in the mouse is located on chromosome 6; this makes the intercrossing of the mouse lines possible. Intercrossing on the same chromosome would be mathematically nearly impossible to achieve.
Furthermore, the atherosclerosis development in the ApoE-KO mouse line closely resembles that seen in humans (see https://www.jax.org/news-and-insights/jax-blog/2013/november/which-jax-mouse-model-is-best-for-atherosclerosis-studies-apoe-or-ldlr-knoc, last retrieved 19.03.2017). Therefore, this mouse line is suited better for studying the onset of atherosclerotic lesions than other mouse models such as the Low-density lipoprotein receptor (LDLR)-KO line which is used more in dyslipidemia research. Additionally, the ApoE-model develops lesions faster and to a higher extent compared to LDLR (http://phenome.jax.org/db/q?rtn=projects/projdet&reqprojid=586, last retrieved 19.03.2017) or even without using the extra stimulus of a high-cholesterol diet (Getz & Reardon, 2016).

4.2.1. Confirmation of the *Zc3hc1*-KO mouse line

Zc3hc1-KO mice were viable, indicating that the gene *Zc3hc1* is not essential. The deficiency of *Zc3hc1* was confirmed on genomic, transcription, and on protein level, as well as by an assay detecting the activity of β-Gal, encoded by the introduced reporter gene lacZ.

For genotyping, a PCR with primers surrounding the loxP site between exons 5 and 6 was used. The loxP site is missing in the WT sequence, resulting in a shorter PCR product. Heterozygous mice have both versions, and thus also both PCR bands. knockout animals have the loxP site in both alleles, as can be seen in the PCR, where only the larger band is observable (see figure 3.11). This PCR was sufficient for a clear and unambiguous distinction between the genotypes. Further confirmation on genomic level was achieved by PCRs where one primer binds within the loxP site, or with both primers binding within the introduced lacZ-sequence. Both PCRs showed, as expected, bands only in transgene, but not in WT animals (see figures 2.4 and 3.11).

The transcription of the targeting cassette into *Zc3hc1* mRNA was verified by isolating mRNA, transcribing it into cDNA, and performing a PCR with a forward primer in exon 3 and a reverse primer in exon 9 (see figure 3.12). This PCR confirmed the expression of both the WT mRNA as well as the mRNA containing the targeting cassette.

The loss of the protein NIPA, which is encoded by the gene *Zc3hc1*, was also confirmed (see figure 3.14). The immunoblot shows additional bands; the one above 75kDa is already described by the manufacturer of the antibody to be a band of unknown identity. In liver, several bands were observed below the band for NIPA; they exist also in the protein sample from a KO animal, and hence seem to be unspecific.

The targeting cassette introduces, among other elements, the reporter gene lacZ, surrounded by two self-cleaving peptides. This results in the expression of the enzyme β-Gal which can be assayed using specific, dye-coupled substrates, such as X-Gal which releases a blue color when cleaved by β-Gal. As expected, the activity of β-Gal was found in heart cryosections from *Zc3hc1* HET and KO mice, but not in WT (see figure 3.15).

The results on all levels matched the expected outcomes for a successful targeting of

Zc3hc1 in order to disrupt the gene, and hence proved the production of a functional *Zc3hc1*-KO mouse line.

4.2.2. Phenotypical analysis of *Zc3hc1*-KO mice

After successfully generating *Zc3hc1*-KO mice, and confirming the deficiency, the impact of the loss of the protein NIPA on the overall phenotype of the mice was evaluated.

Although the gene *Zc3hc1* seemed to be not essential, as the KO mice were viable, there were changes in the phenotype. *Zc3hc1*-knockout mice were smaller (see figure 3.16) and had a lower bodyweight compared to wild types; the observed difference was about 15% less (see figure 3.17). A few animals had a shortened snout, and some were born with one or both eyes almost or fully closed; the numbers were too low, and thus not quantified. These findings were, in part, also reported by the International Mouse Phenotyping Consortium, IMPC (`http://www.mousephenotype.org/data/genes/MGI:1916023`, last retrieved 04.01.2017). Furthermore, the IMPC also found some cases of KO mice which had 12 instead of 13 rib pairs and thoracic vertebrae.

Offspring from matings of *Zc3hc1*-HET animals showed a non-mendelian distribution with a significantly different Chi square score (see table 3.1).
The average litter size, derived from all litters observed (> 300), was 5.2 animals per litter (see section 3.2.3). This number is within the range for the C57BL/6 mouse line (Flurkey, 2009).
The shifted genotype distribution could be caused by embryonic lethality due to the deficiency of *Zc3hc1* or its encoded protein NIPA, but since the average litter size is in the normal range, this might not be the case; the shift might rather take place prior to fertilization, i.e. during the oogenesis and spermatogenesis. And indeed, the meiotic prophase seems to be disrupted in KO animals, leading to a block of spermatogenesis, as reported by Illert et al. (2012b). Furthermore, in the same publication, the group reported fertility problems when mating KO males and females with WT partners; males and most of the females were infertile, while the few non-sterile female KO mice had only reduced fertility. Generating KO animals thus depends only on matings with HET male and females; mating HET with KO mice could be a step to increase the numbers of KO mice born; but, in case of *Zc3hc1*, male KO mice seem to be fully infertile, and the reduced fertility of the females might not be sufficient to increase the numbers.

Although *Zc3hc1*-KO mice have a lower birth rate, fertility problems, and showed phenotypical differences in terms of size and weight, their life span was not shorter or longer compared to WT animals. Mice left to die of age lived as long as the control group (see figure 3.18). Astonishingly, the first mice that died in both groups were actually litter mates, and also the other occurrences of death seemed to be rather synchronised.

4.2.3. Atherosclerosis study

The atherosclerosis study was carried out with female mice at the age of 10 weeks, which were put on a Western type diet for 8 weeks. Then, the development of atherosclerosis in *Zc3hc1*-KO ApoE-KO mice was analysed and compared to ApoE-KO animals as control.

Only female mice were included, although atherosclerosis studies with mice should always include both genders (Daugherty & Rateri, 2005). However, the birth rate for male double-KO mice was as low as 6% (see table 3.2), and hence the number of animals was not sufficient.

Weight, plasma lipids, plaque size

Weight gain was analysed during the feeding period; at the end, double-KO animals have a significantly lower bodyweight than ApoE-KO control mice (see figure 3.20). They also gained less, about one-third less compared to the control animals (3.9g vs. 5.7g). In fact, neither the ApoE-KO genetic background nor the Western type diet seem to affect the weight of *Zc3hc1*-deficient mice (see figure 3.21).

No influence on plasma lipid parameters such as Total Cholesterol, HDL-Cholesterol, LDL-Cholesterol and Triglycerides was found, all analysed plasma lipid parameters were in similar ranges (see table 3.3).
Atherosclerotic burden, both in the whole-aorta (*en-face*) as well as the aortic root (cross-section analysis), was also comparable between *Zc3hc1*-KO ApoE-KO mice and ApoE-KO animals as controls (see figures 3.22 and 3.23).
These findings, to some extent, can be considered as expected results, as NIPA, the protein encoded by *Zc3hc1*, plays a role in cell cycle control, and is unlikely involved

in lipid metabolism and inflammation – processes that drive the initial development of atherosclerotic plaques.

Additionally, the Western type diet pushes plaque development in a very short time (see section 4.2), especially in combination with the ApoE-KO-background, which might level out the possibly small effects of other genetic variants (Knowles & Maeda, 2000; Getz & Reardon, 2016). Hence, this experimental setup might arguably pose as a factor masking the effects of the studied gene *Zc3hc1*.

The results from *en-face* analysis, however, should be enjoyed with caution only, as the aortas lack the most important region, the aortic arch. These parts were lost during the preparation in most of the aortas due to technical difficulties while establishing the method, and the analysis was hence focussed on the thoracic parts only. While the arch, and particularly at the first branches, is the region most prone to lesion formation (Paigen et al., 1990; Mehrabian et al., 1991), the extent of plaque coverage in the descending aorta normally correlates well to that in the arch; as there is almost no observable plaque formation in the descending parts, this might indicate a very low overall plaque development in the aorta, and hence also the arch.

Plaque composition

As plaque burden showed no differences between the groups, plaque composition was analysed in more detail. Collagen is a structural component, and an indicator for plaque stability. It is mainly synthesised by SMCs. The amount and distribution of collagen in the plaque have a large influence on how vulnerable, i.e. prone to rupture a plaque is (Davies, 1996; Falk, 1992). Monocytes and Macrophages are indicators for the immunological state of a plaque (Moreno et al., 1994; Moore & Tabas, 2011). They are involved from the first occurrence of fat depositions within the vessel wall to the later stages of a plaque, including its rupture. SMCs are yet another main component of plaque architecture, migrating to build a capping structure over the plaque, synthesizing collagen to contribute to plaque stability, or even involved in clearing lipids within a plaque (Doran et al., 2008).

Double-KO mice showed significantly less collagen (see figure 3.24), but no difference in MoMa content (see figure 3.25), and a non-significant trend towards less SMC content

(see figure 3.26).
Low collagen and reduced number of SMCs fit very well together, as SMCs are the main contributors to collagen synthesis in a plaque. If their count is reduced, it might very well lead to a reduced collagen content in a plaque. To have a clearer conclusion about plaque stability, it might be necessary to analyse in more detail the distribution of collagen in a plaque; a thick fibrous cap, as well as a dense collagen network spanning the lesion, are indicators for more stability.

4.3. Studying primary mouse aortic SMCs *in-vitro*

As collagen was significantly decreased, and SMCs were also slightly reduced in double-KO mice, further investigation focused on the characterization of *Zc3hc1*-KO SMCs in terms proliferation and migration. Smooth Muscle Cells play an import role in the development of atherosclerotic plaques (see section 1.2). Proliferation (Ross & Glomset, 1973; O'Brien et al., 1993; M. R. Bennett et al., 1995; Lutgens et al., 1999; Dzau et al., 2002; M. R. Bennett et al., 2016) and migration (Ross, 1995; M. R. Bennett et al., 2016) are important characteristics to analyse.

4.3.1. Isolation and characterization of aortic SMCs

In order to characterise primary mouse aortic SMCs, first the isolation protocol was established (see section 2.14.2). As the isolated cells were derived from a primary culture, they were used for experiments only between passages P4 and P10.

They were first characterised by the expression of the SMC-specific marker α-SMA, which was quantified by Flow Cytometry, as well as by immunofluorescence staining of cells. And indeed, the populations showed high levels of purity, with more than 95% cells expressing varying amounts of α-SMA (see figure 3.27, flat and wide distributions), as analysed by Flow Cytometry, even at a relatively high passage number as P9, confirming the isolated cells to be SMCs.
They also showed the typical pattern of actin fibers in microscopical images of stainings with the same FITC-labeled α-SMA antibody (figure 3.28).

4.3.2. Proliferation of aortic SMCs

After the purity of the SMC populations was confirmed, WT and *Zc3hc1*-KO SMCs were used for experiments to determine the impact of the deficiency of *Zc3hc1* SMC-proliferation.
Proliferation of SMCs is an important process in atherosclerosis (Ross & Glomset, 1973; M. C. H. Clarke et al., 2008), and has long been assumed to be beneficial for more mature lesions (Newby & Zaltsman, 1999), but detrimental in early stages (O'Brien et al., 1993). It is becoming a target for therapeutic interventions (Dzau et al., 2002; M. R. Bennett et al., 2016).

Proliferation was tested in a very simple assay; cells were seeded, and trypsinised and counted manually at different timepoints.
A second, semi-automated quantification based on the analysis of images of DAPI-stained cells with ImageJ (Segura-Puimedon et al., 2016) was used to evaluate the results from manual counting.
Manual counting revealed *Zc3hc1*-KO cells to proliferate significantly slower than WT cells, reaching about 60% of the cell number after 96h.
Counting the DAPI-stained cells in images using an algorithm written in ImageJ confirmed the trend, although the difference was not significant in this assay.
Notably, in each counting method, both genotypes have comparable cell counts until 48h, and begin to diverge from then on (see figure 3.29).
The discrepancy in the results from the two counting methods may be attributed to the way of counting in each method. Counting with the Neubauer chamber relies on a very small sample size, with sometimes only few cells to count. This may result in a larger bias at low cell numbers. The analysis of microscopic images, though, provides a larger field of view, which means there is less bias through insufficient sample size and/ or cell count. On the other hand, there are other drawbacks in the automated analysis that might result in an observed higher or lower cell count. Computer-based cell detection is performed with a threshold-based operation, which can be inaccurate due to inhomogenous fluorescence levels. Also, the confluency might interfere with the detection of cells; either, cells, which in higher confluencies tend to become smaller, are 'lost' through a size-based cut-off, which normally is applied to reduce the counting of debris. Or individual cells are lost by being too close and visually melting together, which can lead to them being recognised as one object only. Similarly, such an algorithm can exaggerate cell numbers due to an over-recognition with a not properly chosen threshold and/ or

size-based cut-off.

In a recently published study, Jones et al. (2016) analysed the impact of the SNP rs11556924 on cell cycle dynamics and found the risk variant, which is the wildtype allele, to increase the activity of NIPA, thereby extending the length of mitosis. They did not find differences in the proliferation between the genotypes, which might be attributed to the cell line used in their study. The DLD-1 cell line originates from a human colon carcinoma, and hence might already have a perturbed cell cycle.
Nevertheless, the genome editing approach conducted by Jones et al. is an elegant way of analysing the effect of a SNP, and the results clearly show an implication of NIPA in cell cycle control.

4.3.3. Migration of aortic SMCs

Migration was tested with the Boyden chamber assay, a widely applied method (Gerthoffer, 2007), using a modified version with electronically integrated transwell migration plates (see sections 2.17.1 and 3.4.3).

The analysis showed that *Zc3hc1*-KO SMCs have a higher migration rate, reaching the plateau phase after about 8h. At this timepoint, the Cell Index of WT SMCs is lower, reaching only about 80% of the KO cells, and WT SMCs have not reached the plateau phase, either.

The observed results seem not to fit together, as deleting the gene *Zc3hc1* reduced the proliferation, but slightly increased migration of SMCs.
Most studies show that phenotyipcal changes of SMCs usually encompass proliferation and migration to be modified in similar directions – higher proliferation comes with higher migration and vice versa. This can be seen in SMCs undergoing a phenotypic switch (see section 1.2), which is a phenomenon occurring in atherosclerosis (G. R. Campbell & J. H. Campbell, 1985; Doran et al., 2008; Rensen et al., 2007; Jaeger et al., 1991; O'Callaghan & Williams, 2000; M. R. Bennett et al., 2016).
However, it can be speculated that a small perturbance of the cell cycle control, such as the reduction of proliferation by the deficiency of NIPA, may leave the cells' motility unharmed or even slightly favoured, as the NIPA-deficient cells seem not to prepare for division right after attaching.

And indeed, several publications indicate that a cell's ability to migrate is cell-cycle dependant (Boehm & Nabel, 2001; Louis & Zahradka, 2010), providing a possible functional link between the CAD-risk gene *Zc3hc1*, its gene product NIPA, which is involved in cell-cycle control, and atherosclerosis.

4.4. Outlook

Further experiments are needed for a better understanding of the association between the CAD-risk gene *Zc3hc1* and atherosclerosis.

To exclude methodological obstacles in the interaction study between the proteins NIPA and Cyclin B1, the overexpression of Cyclin B1 needs to be evaluated as well. In a next step, the experiment might need to be optimised in order to capture the already described interaction and, to take it even further, reveal possible differences between NIPA with or without the SNP.

The results from the *in-vivo* study suggest an impact of *Zc3hc1* on plaque stability. Hence, a detailed analysis of the plaque composition and architecture, with special focus on the distribution of collagen and SMCs within a plaque, might provide further insights.
Additionally, long term-experiments with mice with the ApoE-KO background on normal (Chow) diet, or even with an alternative genetic background, such as the less atherogenic LDLR-KO background, might provide a setup allowing for a spontaneous plaque development, and thus offer a more detailed insight into the role the gene *Zc3hc1* plays in this process.

The deficiency of *Zc3hc1* showed an effect on the proliferation and migration of primary mouse aortic SMCs, an atherosclerosis-relevant cell type. For a deeper understanding of the role the CAD-risk gene *Zc3hc1* plays in these processes, it might be useful to further characterise the ability of SMCs to switch phenotypes, or to analyse the impact of the SNP on the cell cycle in more detail.

Alltogether, these findings might then provide a mechanistic link for the association of the SNP rs11556924 with atherosclerosis.

Bibliography

Allayee, H.; Ghazalpour, A. & Lusis, A. J. (2003). Using mice to dissect genetic factors in atherosclerosis. *Arterioscler Thromb Vasc Biol* 23 (9), pp. 1501–1509.

Altshuler, D. & Daly, M. J. (2007). Guilt beyond a reasonable doubt. *Nat Genet* 39 (7), pp. 813–815.

Altshuler, D.; Daly, M. J. & Lander, E. S. (2008). Genetic mapping in human disease. *Science* 322 (5903), pp. 881–888.

Altshuler, D. et al. (2000). An SNP map of the human genome generated by reduced representation shotgun sequencing. *Nature* 407 (6803), pp. 513–516.

Andresdottir, M. B. et al. (2002). Fifteen percent of myocardial infarctions and coronary revascularizations explained by family history unrelated to conventional risk factors. The Reykjavik Cohort Study. *Eur Heart J* 23 (21), pp. 1655–1663.

Aqel, N. M. et al. (1984). Monocytic origin of foam cells in human atherosclerotic plaques. *Atherosclerosis* 53 (3), pp. 265–271.

Arora, B. et al. (2016). Chemical Crosslinking: Role In Protein And Peptide Science. *Curr Protein Pept Sci.*

Assmann, G.; Cullen, P. & Schulte, H. (2002). Simple scoring scheme for calculating the risk of acute coronary events based on the 10-year follow-up of the prospective cardiovascular Münster (PROCAM) study. *Circulation* 105 (3), pp. 310–315.

Assmann, G. et al. (2007). Assessing risk of myocardial infarction and stroke: new data from the Prospective Cardiovascular Münster (PROCAM) study. *Eur J Clin Invest* 37 (12), pp. 925–932.

Barrett, J. C. & Cardon, L. R. (2006). Evaluating coverage of genome-wide association studies. *Nat Genet* 38 (6), pp. 659–662.

Bassermann, F.; Peschel, C. & Duyster, J. (2005a). Mitotic entry: a matter of oscillating destruction. *Cell Cycle* 4 (11), pp. 1515–1517.

Bassermann, F. et al. (2005b). NIPA defines an SCF-type mammalian E3 ligase that regulates mitotic entry. *Cell* 122 (1), pp. 45–57.

Bassermann, F. et al. (2007). Multisite phosphorylation of nuclear interaction partner of ALK (NIPA) at G2/M involves cyclin B1/Cdk1. *Biol Chem* 282 (22), pp. 15965–15972.

Bennett, M. R.; Evan, G. I. & Schwartz, S. M. (1995). Apoptosis of human vascular smooth muscle cells derived from normal vessels and coronary atherosclerotic plaques. *J Clin Invest* 95 (5), pp. 2266–2274.

Bennett, M. R.; Sinha, S. & Owens, G. K. (2016). Vascular Smooth Muscle Cells in Atherosclerosis. *Circ Res* 118 (4), pp. 692–702.

Berggård, T.; Linse, S. & James, P. (2007). Methods for the detection and analysis of protein-protein interactions. *Proteomics* 7 (16), pp. 2833–2842.

Björkegren, J. L. M. et al. (2014). Plasma cholesterol-induced lesion networks activated before regression of early, mature, and advanced atherosclerosis. *PLos Genet* 10 (2), e1004201.

Björkegren, J. L. M. et al. (2015). Genome-wide significant loci: how important are they? Systems genetics to understand heritability of coronary artery disease and other common complex disorders. *J Am Coll Cardiol* 65 (8), pp. 830–845.

Boehm, M. & Nabel, E. G. (2001). Cell cycle and cell migration: new pieces to the puzzle. *Circulation* 103 (24), pp. 2879–2881.

Boer, J. M. et al. (1999). The joint impact of family history of myocardial infarction and other risk factors on 12-year coronary heart disease mortality. *Epidemiology* 10 (6), pp. 767–770.

Brænne et al. (2015). Prediction of Causal Candidate Genes in Coronary Artery Disease Loci. *Arterioscler Thromb Vasc Biol* 35 (10), pp. 2207–2217.

Broman, K. W. & Feingold, E. (2004). SNPs made routine. *Nat Methods* 1 (2), pp. 104–105.

Brookes, A. J. (1999). The essence of SNPs. *Gene* 234 (2), pp. 177–186.

Bruschke, A. V. et al. (1989). The dynamics of progression of coronary atherosclerosis studied in 168 medically treated patients who underwent coronary arteriography three times. *Am Heart J* 117 (2), pp. 296–305.

Burke, A. P. et al. (2001). Healed plaque ruptures and sudden coronary death: evidence that subclinical rupture has a role in plaque progression. *Circulation* 103 (7), pp. 934–940.

Campbell, G. R. & Campbell, J. H. (1985). Smooth muscle phenotypic changes in arterial wall homeostasis: implications for the pathogenesis of atherosclerosis. *Exp Mol Pathol* 42 (2), pp. 139–162.

CARDIoGRAMplusC4D Consortium (2015). A comprehensive 1,000 Genomes-based genome-wide association meta-analysis of coronary artery disease. *Nat Genet* 47 (10), pp. 1121–1130.

CARDIoGRAMplusC4D Consortium et al. (2013). Large-scale association analysis identifies new risk loci for coronary artery disease. *Nat Genet* 45 (1), pp. 25–33.

Cardozo, T. & Pagano, M. (2004). The SCF ubiquitin ligase: insights into a molecular machine. *Nat Rev Mol Cell Biol* 5 (9), pp. 739–751.

Chakravarti, A. (1999). Population genetics–making sense out of sequence. *Nat Genet* 21 (1 Suppl), pp. 56–60.

Chen, Q. et al. (2008). Cyclin B1 is localized to unattached kinetochores and contributes to efficient microtubule attachment and proper chromosome alignment during mitosis. *Cell Res* 18 (2), pp. 268–280.

Civelek, M. & Lusis, A. J. (2014). Systems genetics approaches to understand complex traits. *Nat Rev Genet* 15 (1), pp. 34–48.

Clarke, M. C. H. et al. (2008). Chronic apoptosis of vascular smooth muscle cells accelerates atherosclerosis and promotes calcification and medial degeneration. *Circ Res* 102 (12), pp. 1529–1538.

Clarke, R. et al. (2009). Genetic variants associated with Lp(a) lipoprotein level and coronary disease. *N Engl J Med* 361 (26), pp. 2518–2528.

Collins, A. (2009). Allelic association: linkage disequilibrium structure and gene mapping. *Mol Biotechnol* 41 (1), pp. 83–89.

Collins, F. S.; Brooks, L. D. & Chakravarti, A. (1998). A DNA polymorphism discovery resource for research on human genetic variation. *Genome Res* 8 (12), pp. 1229–1231.

Coronary Artery Disease (C4D) Genetics Consortium (2011). A genome-wide association study in Europeans and South Asians identifies five new loci for coronary artery disease. *Nat Genet* 43 (4), pp. 339–344.

Craig, K. L. & Tyers, M. (1999). The F-box: a new motif for ubiquitin dependent proteolysis in cell cycle regulation and signal transduction. *Prog Biophys Mol Biol* 72 (3), pp. 299–328.

D'Agostino, R. B. et al. (2008). General cardiovascular risk profile for use in primary care: the Framingham Heart Study. *Circulation* 117 (6), pp. 743–753.

Daugherty, A. (2002). Mouse models of atherosclerosis. *Am J Med Sci* 323 (1), pp. 3–10.

Daugherty, A. & Rateri, D. L. (2005). Development of experimental designs for atherosclerosis studies in mice. *Methods* 36 (2), pp. 129–138.

Davies, M. J. (1996). Stability and instability: two faces of coronary atherosclerosis. The Paul Dudley White Lecture 1995. *Circulation* 94 (8), pp. 2013–2020.

Demer, L. L.; Watson, K. E. & Boström, K. (1994). Mechanism of calcification in atherosclerosis. *Trends Cardiovasc Med* 4 (1), pp. 45–49.

Doherty, T. M. et al. (2003). Calcification in atherosclerosis: bone biology and chronic inflammation at the arterial crossroads. *Proc Natl Acad Sci USA* 100 (20), pp. 11201–11206.

Doran, A. C.; Meller, N. & McNamara, C. A. (2008). Role of smooth muscle cells in the initiation and early progression of atherosclerosis. *Arterioscler Thromb Vasc Biol* 28 (5), pp. 812–819.

Dzau, V. J.; Braun-Dullaeus, R. C. & Sedding, D. G. (2002). Vascular proliferation and atherosclerosis: new perspectives and therapeutic strategies. *Nat Med* 8 (11), pp. 1249–1256.

Eichhorn, J. M.; Kothari, A. & Chambers, T. C. (2014). Cyclin B1 overexpression induces cell death independent of mitotic arrest. *PLoS One* 9 (11), e113283.

Erbilgin, A. et al. (2013). Identification of CAD candidate genes in GWAS loci and their expression in vascular cells. *J Lipid Res* 54 (7), pp. 1894–1905.

Erdmann, J.; Linsel-Nitschke, P. & Schunkert, H. (2010). Genetic causes of myocardial infarction: new insights from genome-wide association studies. *Dtsch Arztebl Int* 107 (40), pp. 694–699.

Erdmann, J. et al. (2009). New susceptibility locus for coronary artery disease on chromosome 3q22.3. *Nat Genet* 41 (3), pp. 280–282.

Erdmann, J. et al. (2011). Genome-wide association study identifies a new locus for coronary artery disease on chromosome 10p11.23. *Eur Heart J* 32 (2), pp. 158–168.

Estojak, J.; Brent, R. & Golemis, E. A. (1995). Correlation of two-hybrid affinity data with in vitro measurements. *Mol Cell Biol* 15 (10), pp. 5820–5829.

Falk, E. (1983). Plaque rupture with severe pre-existing stenosis precipitating coronary thrombosis. Characteristics of coronary atherosclerotic plaques underlying fatal occlusive thrombi. *Br Heart J* 50 (2), pp. 127–134.

Falk, E. (1992). Why do plaques rupture? *Circulation* 86 (6 Suppl), pp. III30–III42.

Fazio, S. & Linton, M. F. (2001). Mouse models of hyperlipidemia and atherosclerosis. *Front Biosci* 6, pp. D515–D525.

Ferrell, J. E. (1998). How regulated protein translocation can produce switch-like responses. *Trends Biochem Sci* 23 (12), pp. 461–465.

Fields, S. & Song, O. (1989). A novel genetic system to detect protein-protein interactions. *Nature* 340 (6230), pp. 245–246.

Flurkey, K., ed. (2009). *The Jackson Laboratory Handbook on Genetically Standardized Mice*. 6. ed., 1. printing. Bar Harbor, Me: The Jackson Laboratory. 380 pp.

Fruchart, J.-C. et al. (2004). New risk factors for atherosclerosis and patient risk assessment. *Circulation* 109 (23 Suppl 1), pp. III15–III19.

Fuster, V. et al. (1988). Insights into the pathogenesis of acute ischemic syndromes. *Circulation* 77 (6), pp. 1213–1220.

Gabriel, S. B. et al. (2002). The structure of haplotype blocks in the human genome. *Science* 296 (5576), pp. 2225–2229.

Galis, Z. S. et al. (1994). Increased expression of matrix metalloproteinases and matrix degrading activity in vulnerable regions of human atherosclerotic plaques. *J Clin Invest* 94 (6), pp. 2493–2503.

GBD 2013 Mortality and Causes of Death Collaborators (2015). Global, regional, and national age–sex specific all-cause and cause-specific mortality for 240 causes of death, 1990–2013: a systematic analysis for the Global Burden of Disease Study 2013. *The Lancet* 385.9963, pp. 117–171.

Gerthoffer, W. T. (2007). Mechanisms of vascular smooth muscle cell migration. *Circulation research* 100 (5), pp. 607–621.

Getz, G. S. & Reardon, C. A. (2016). Do the Apoe-/- and Ldlr-/- Mice Yield the Same Insight on Atherogenesis? *Arterioscler Thromb Vasc Biol* 36 (9), pp. 1734–1741.

Guyton, J. R. & Klemp, K. F. (1994). Development of the atherosclerotic core region. Chemical and ultrastructural analysis of microdissected atherosclerotic lesions from human aorta. *Arterioscler Thromb Vasc Biol* 14 (8), pp. 1305–1314.

Ha, N.-T.; Freytag, S. & Bickeboeller, H. (2014). Coverage and efficiency in current SNP chips. *Eur J Hum Genet* 22 (9), pp. 1124–1130.

Hagting, A. et al. (1999). Translocation of cyclin B1 to the nucleus at prophase requires a phosphorylation-dependent nuclear import signal. *Curr Biol* 9 (13), pp. 680–689.

Hawe, E. et al. (2003). Family history is a coronary heart disease risk factor in the Second Northwick Park Heart Study. *Ann Hum Genet* 67 (Pt 2), pp. 97–106.

Helgadottir, A. et al. (2007). A common variant on chromosome 9p21 affects the risk of myocardial infarction. *Science* 316 (5830), pp. 1491–1493.

Hirschhorn, J. N. & Daly, M. J. (2005). Genome-wide association studies for common diseases and complex traits. *Nat Rev Genet* 6 (2), pp. 95–108.

Hwang, A. et al. (1995). Cell cycle-dependent regulation of the cyclin B1 promoter. *Biol Chem* 270 (47), pp. 28419–28424.

Illert, A. L. et al. (2012a). Extracellular signal-regulated kinase 2 (ERK2) mediates phosphorylation and inactivation of nuclear interaction partner of anaplastic lymphoma kinase (NIPA) at G2/M. *Biol Chem* 287 (45), pp. 37997–38005.

Illert, A. L. et al. (2012b). Targeted inactivation of nuclear interaction partner of ALK disrupts meiotic prophase. *Development* 139 (14), pp. 2523–2534.

International HapMap Consortium (2005). A haplotype map of the human genome. *Nature* 437 (7063), pp. 1299–1320.

Jaeger, E. et al. (1991). Joint occurrence of collagen mRNA containing cells and macrophages in human atherosclerotic vessels. *Atherosclerosis* 86 (1), pp. 55–68.

Jannot, A.-S.; Ehret, G. & Perneger, T. (2015). P $<$ 5 $\times$ 10(-8) has emerged as a standard of statistical significance for genome-wide association studies. *J Clin Epidemiol* 68 (4), pp. 460–465.

Jeffreys, A. J.; Kauppi, L. & Neumann, R. (2001). Intensely punctate meiotic recombination in the class II region of the major histocompatibility complex. *Nat Genet* 29 (2), pp. 217–222.

Johnson, G. C. et al. (2001). Haplotype tagging for the identification of common disease genes. *Nat Genet* 29 (2), pp. 233–237.

Jones, P. D. et al. (2016). The Coronary Artery Disease-associated Coding Variant in Zinc Finger C3HC-type Containing 1 (ZC3HC1) Affects Cell Cycle Regulation. *J Biol Chem* 291 (31), pp. 16318–16327.

Kimura, K. et al. (1998). Phosphorylation and activation of 13S condensin by Cdc2 in vitro. *Science* 282 (5388), pp. 487–490.

Klitzing, C. v. et al. (2011). APC/C(Cdh1)-mediated degradation of the F-box protein NIPA is regulated by its association with Skp1. *PLoS One* 6 (12), e28998.

Knowles, J. W. & Maeda, N. (2000). Genetic modifiers of atherosclerosis in mice. *Arterioscler Thromb Vasc Biol* 20 (11), pp. 2336–2345.

Koenig, W. & Khuseyinova, N. (2007). Biomarkers of atherosclerotic plaque instability and rupture. *Arterioscler Thromb Vasc Biol* 27 (1), pp. 15–26.

Krzywinski, M. et al. (2009). Circos: an information aesthetic for comparative genomics. *Genome Res* 19 (9), pp. 1639–1645.

Kunnas, T. & Nikkari, S. T. (2015). Association of Zinc Finger, C3HC-Type Containing 1 (ZC3HC1) rs11556924 Genetic Variant With Hypertension in a Finnish Population, the TAMRISK Study. *Medicine* 94 (32), e1221.

Laird, N. M. & Lange, C. (2006). Family-based designs in the age of large-scale gene-association studies. *Nat Rev Genet* 7 (5), pp. 385–394.

Lee, R. T. et al. (1991). Structure-dependent dynamic mechanical behavior of fibrous caps from human atherosclerotic plaques. *Circulation* 83 (5), pp. 1764–1770.

Libby, P. (2002). Inflammation in atherosclerosis. *Nature* 420 (6917), pp. 868–874.

Libby, P. & Theroux, P. (2005). Pathophysiology of coronary artery disease. *Circulation* 111 (25), pp. 3481–3488.

Lieb, W. & Vasan, R. S. (2013). Genetics of coronary artery disease. *Circulation* 128 (10), pp. 1131–1138.

Lieb, W. et al. (2013). Genetic predisposition to higher blood pressure increases coronary artery disease risk. *Hypertension* 61 (5), pp. 995–1001.

Lievens, S.; Lemmens, I. & Tavernier, J. (2009). Mammalian two-hybrids come of age. *Trends Biochem Sci* 34 (11), pp. 579–588.

Linseman, T. et al. (2017). Functional Validation of a Common Nonsynonymous Coding Variant in ZC3HC1 Associated With Protection From Coronary Artery Disease. *Circ Cardiovasc Genet* 10 (1).

López-Mejías, R. et al. (2013). The ZC3HC1 rs11556924 polymorphism is associated with increased carotid intima-media thickness in patients with rheumatoid arthritis. *Arthritis Res Ther* 15 (5), R152.

Loree, H. M. et al. (1992). Effects of fibrous cap thickness on peak circumferential stress in model atherosclerotic vessels. *Circ Res* 71 (4), pp. 850–858.

Louis, S. F. & Zahradka, P. (2010). Vascular smooth muscle cell motility: From migration to invasion. *Exp Clin Cardiol* 15 (4), e75–e85.

Lu, X. et al. (2012). Genome-wide association study in Han Chinese identifies four new susceptibility loci for coronary artery disease. *Nat Genet* 44 (8), pp. 890–894.

Lusis, A. J. (2000). Atherosclerosis. *Nature* 407 (6801), pp. 233–241.

Lutgens, E. et al. (1999). Biphasic pattern of cell turnover characterizes the progression from fatty streaks to ruptured human atherosclerotic plaques. *Cardiovasc Res* 41 (2), pp. 473–479.

Mackay, T. F. (2001). The genetic architecture of quantitative traits. *Annu Rev Genet* 35, pp. 303–339.

Maeda, N. (2011). Development of apolipoprotein E-deficient mice. *Arterioscler Thromb Vasc Biol* 31 (9), pp. 1957–1962.

Mall, M. et al. (2012). Mitotic lamin disassembly is triggered by lipid-mediated signaling. *J Cell Biol* 198 (6), pp. 981–990.

Maouche, S. & Schunkert, H. (2012). Strategies beyond genome-wide association studies for atherosclerosis. *Arterioscler Thromb Vasc Biol* 32 (2), pp. 170–181.

Marenberg, M. E. et al. (1994). Genetic susceptibility to death from coronary heart disease in a study of twins. *N Engl J Med* 330 (15), pp. 1041–1046.

Markham, K.; Bai, Y. & Schmitt-Ulms, G. (2007). Co-immunoprecipitations revisited: an update on experimental concepts and their implementation for sensitive interactome investigations of endogenous proteins. *Anal Bioanal Chem* 389 (2), pp. 461–473.

Mayer, B.; Erdmann, J. & Schunkert, H. (2007). Genetics and heritability of coronary artery disease and myocardial infarction. *Clin Res Cardiol* 96 (1), pp. 1–7.

McCarthy, M. I. & Hirschhorn, J. N. (2008). Genome-wide association studies: potential next steps on a genetic journey. *Hum Mol Genet* 17 (R2), R156–R165.

McGill, H. C.; McMahan, C. A. & Gidding, S. S. (2008). Preventing heart disease in the 21st century: implications of the Pathobiological Determinants of Atherosclerosis in Youth (PDAY) study. *Circulation* 117 (9), pp. 1216–1227.

McPherson, R. & Tybjaerg-Hansen, A. (2016). Genetics of Coronary Artery Disease. *Circ Res* 118 (4), pp. 564–578.

McPherson, R. et al. (2007). A common allele on chromosome 9 associated with coronary heart disease. *Science* 316 (5830), pp. 1488–1491.

Mehrabian, M.; Demer, L. L. & Lusis, A. J. (1991). Differential accumulation of intimal monocyte-macrophages relative to lipoproteins and lipofuscin corresponds to hemodynamic forces on cardiac valves in mice. *Arterioscler Thromb Vasc Biol* 11 (4), pp. 947–957.

Mendis, S.; Puska, P. & Norrving, B. (2011). *Global atlas on cardiovascular disease prevention and control*. Geneva: World Health Organization. 164 pp.

Moore, K. J. & Tabas, I. (2011). Macrophages in the pathogenesis of atherosclerosis. *Cell* 145 (3), pp. 341–355.

Moreno, P. R. et al. (1994). Macrophage infiltration in acute coronary syndromes. Implications for plaque rupture. *Circulation* 90 (2), pp. 775–778.

Morgan, D. (2007). *The Cell Cycle: Principles of Control*. Primers in biology. New Science Press.

Myocardial Infarction Genetics Consortium et al. (2009). Genome-wide association of early-onset myocardial infarction with single nucleotide polymorphisms and copy number variants. *Nat Genet* 41 (3), pp. 334–341.

Nemoto, T. et al. (2013). Regression of luminal stenosis at the site of silent plaque disruption in the era of optimal medical therapy. Low high-density lipoprotein cholesterol level isa potential risk of stenosis progression. *Circ J* 77 (10), pp. 2573–2577.

Newby, A. C. & Zaltsman, A. B. (1999). Fibrous cap formation or destruction–the critical importance of vascular smooth muscle cell proliferation, migration and matrix formation. *Cardiovasc Res* 41 (2), pp. 345–360.

Nurnberg, S. T. et al. (2016). From Loci to Biology: Functional Genomics of Genome-Wide Association for Coronary Disease. *Circ Res* 118 (4), pp. 586–606.

Nurse, P. (1990). Universal control mechanism regulating onset of M-phase. *Nature* 344 (6266), pp. 503–508.

O'Brien, E. R. et al. (1993). Proliferation in primary and restenotic coronary atherectomy tissue. Implications for antiproliferative therapy. *Circ Res* 73 (2), pp. 223–231.

O'Callaghan, C. J. & Williams, B. (2000). Mechanical strain-induced extracellular matrix production by human vascular smooth muscle cells: role of TGF-beta(1). *Hypertension* 36 (3), pp. 319–324.

Ouyang, T. et al. (2003). Identification and characterization of a nuclear interacting partner of anaplastic lymphoma kinase (NIPA). *Biol Chem* 278 (32), pp. 30028–30036.

Paigen, B. et al. (1990). Atherosclerosis susceptibility differences among progenitors of recombinant inbred strains of mice. *Arteriosclerosis* 10 (2), pp. 316–323.

Patil, N. et al. (2001). Blocks of limited haplotype diversity revealed by high-resolution scanning of human chromosome 21. *Science* 294 (5547), pp. 1719–1723.

Peter, M. et al. (1990). In vitro disassembly of the nuclear lamina and M phase-specific phosphorylation of lamins by cdc2 kinase. *Cell* 61 (4), pp. 591–602.

Reardon, C. A. & Getz, G. S. (2001). Mouse models of atherosclerosis. *Curr Opin Lipidol* 12 (2), pp. 167–173.

Reich, D. E. & Lander, E. S. (2001). On the allelic spectrum of human disease. *Trends Genet* 17 (9), pp. 502–510.

Reich, D. E. et al. (2001). Linkage disequilibrium in the human genome. *Nature* 411 (6834), pp. 199–204.

Rensen, S. S. M.; Doevendans, P. A. F. M. & Eys, G. J. J. M. van (2007). Regulation and characteristics of vascular smooth muscle cell phenotypic diversity. *Neth Heart J* 15 (3), pp. 100–108.

Reynolds, J. L. et al. (2004). Human vascular smooth muscle cells undergo vesicle-mediated calcification in response to changes in extracellular calcium and phosphate concentrations: a potential mechanism for accelerated vascular calcification in ESRD. *J Am Soc Nephrol* 15 (11), pp. 2857–2867.

Risch, N. & Merikangas, K. (1996). The future of genetic studies of complex human diseases. *Science* 273 (5281), pp. 1516–1517.

Ross, R. (1995). Cell biology of atherosclerosis. *Annu Rev Physiol* 57, pp. 791–804.

Ross, R. & Glomset, J. A. (1973). Atherosclerosis and the arterial smooth muscle cell: Proliferation of smooth muscle is a key event in the genesis of the lesions of atherosclerosis. *Science* 180 (4093), pp. 1332–1339.

Ross, R. et al. (1990). Localization of PDGF-B protein in macrophages in all phases of atherogenesis. *Science* 248 (4958), pp. 1009–1012.

Sachidanandam, R. et al. (2001). A map of human genome sequence variation containing 1.42 million single nucleotide polymorphisms. *Nature* 409 (6822), pp. 928–933.

Samani, N. J. et al. (2007). Genomewide association analysis of coronary artery disease. *N Engl J Med* 357 (5), pp. 443–453.

Sarafan-Vasseur, N. et al. (2002). Overexpression of B-type cyclins alters chromosomal segregation. *Oncogene* 21 (13), pp. 2051–2057.

Schadt, E. E. & Björkegren, J. L. M. (2012). NEW: network-enabled wisdom in biology, medicine, and health care. *Sci Transl Med* 4 (115), 115rv1.

Schoenhagen, P. et al. (2000). Extent and direction of arterial remodeling in stable versus unstable coronary syndromes : an intravascular ultrasound study. *Circulation* 101 (6), pp. 598–603.

Schunkert, H. et al. (2011). Large-scale association analysis identifies 13 new susceptibility loci for coronary artery disease. *Nat Genet* 43 (4), pp. 333–338.

Segura-Puimedon, M. et al. (2016). Proatherosclerotic Effect of the α1-Subunit of Soluble Guanylyl Cyclase by Promoting Smooth Muscle Phenotypic Switching. *Am J Pathol* 186 (8), pp. 2220–2231.

Sherry, S. T. et al. (2001). dbSNP: the NCBI database of genetic variation. *Nucleic Acids Res* 29 (1), pp. 308–311.

Soranzo, N. et al. (2009). A genome-wide meta-analysis identifies 22 loci associated with eight hematological parameters in the HaemGen consortium. *Nat Genet* 41 (11), pp. 1182–1190.

Stary, H. C. et al. (1994). A definition of initial, fatty streak, and intermediate lesions of atherosclerosis. A report from the Committee on Vascular Lesions of the Council on Arteriosclerosis, American Heart Association. *Arterioscler Thromb Vasc Biol* 14 (5), pp. 840–856.

Syvänen, A. C. (2001). Accessing genetic variation: genotyping single nucleotide polymorphisms. *Nat Rev Genet* 2 (12), pp. 930–942.

The IBC 50K CAD Consortium (2011). Large-scale gene-centric analysis identifies novel variants for coronary artery disease. *PLos Genet* 7 (9), e1002260.

Trégouët, D.-A. et al. (2009). Genome-wide haplotype association study identifies the SLC22A3-LPAL2-LPA gene cluster as a risk locus for coronary artery disease. *Nat Genet* 41 (3), pp. 283–285.

Tuzcu, E. M. et al. (2001). High prevalence of coronary atherosclerosis in asymptomatic teenagers and young adults: evidence from intravascular ultrasound. *Circulation* 103 (22), pp. 2705–2710.

Venter, J. C. et al. (2001). The sequence of the human genome. *Science* 291 (5507), pp. 1304–1351.

Wang, A. et al. (1997). Overexpression of cyclin B1 in human colorectal cancers. *J Cancer Res Clin Oncol* 123 (2), pp. 124–127.

Wang, D. G. et al. (1998). Large-scale identification, mapping, and genotyping of single-nucleotide polymorphisms in the human genome. *Science* 280 (5366), pp. 1077–1082.

Wang, F. et al. (2011). Genome-wide association identifies a susceptibility locus for coronary artery disease in the Chinese Han population. *Nat Genet* 43 (4), pp. 345–349.

Wang, J. C. & Bennett, M. (2012). Aging and atherosclerosis: mechanisms, functional consequences, and potential therapeutics for cellular senescence. *Circ Res* 111 (2), pp. 245–259.

Wang, W. Y. S. et al. (2005). Genome-wide association studies: theoretical and practical concerns. *Nat Rev Genet* 6 (2), pp. 109–118.

Watson, K. E. et al. (1994). TGF-beta 1 and 25-hydroxycholesterol stimulate osteoblast-like vascular cells to calcify. *J Clin Invest* 93 (5), pp. 2106–2113.

Webb, T. R. et al. (2017). Systematic Evaluation of Pleiotropy Identifies 6 Further Loci Associated With Coronary Artery Disease. *J Am Coll Cardiol* 69 (7), pp. 823–836.

Welch, C. L. (2012). Beyond genome-wide association studies: the usefulness of mouse genetics in understanding the complex etiology of atherosclerosis. *Arterioscler Thromb Vasc Biol* 32 (2), pp. 207–215.

Wellcome Trust Case Control Consortium (2007). Genome-wide association study of 14,000 cases of seven common diseases and 3,000 shared controls. *Nature* 447 (7145), pp. 661–678.

Wexler, L. et al. (1996). Coronary artery calcification: pathophysiology, epidemiology, imaging methods, and clinical implications. A statement for health professionals from the American Heart Association. Writing Group. *Circulation* 94 (5), pp. 1175–1192.

Wilcox, J. N. et al. (1989). Localization of tissue factor in the normal vessel wall and in the atherosclerotic plaque. *Proc Natl Acad Sci USA* 86 (8), pp. 2839–2843.

Williamson, M. P. & Sutcliffe, M. J. (2010). Protein-protein interactions. *Biochem Soc Trans* 38 (4), pp. 875–878.

Witztum, J. L. (1994). The oxidation hypothesis of atherosclerosis. *Lancet* 344 (8925), pp. 793–795.

Yang, X. (2012). Use of functional genomics to identify candidate genes underlying human genetic association studies of vascular diseases. *Arterioscler Thromb Vasc Biol* 32 (2), pp. 216–222.

Yuan, J. et al. (2006). Stable gene silencing of cyclin B1 in tumor cells increases susceptibility to taxol and leads to growth arrest in vivo. *Oncogene* 25 (12), pp. 1753–1762.

Zhang, S. H. et al. (1992). Spontaneous hypercholesterolemia and arterial lesions in mice lacking apolipoprotein E. *Science* 258 (5081), pp. 468–471.

A. Appendix

A.1. Abbreviations

APS	Ammonium persulfate
ApoE	Apolipoprotein E
β-Gal	β-Galactosidase
BSA	Bovine Serum Albumin
CAD	Coronary Artery Disease
CI	Cell Index
CoIP	co-immunoprecipitation
CVD	Cardiovascular Disease
DAPI	4',6-Diamidino-2-phenylindole
dNTP	Deoxyribose Nucleoside Triphosphate
DMEM	Dulbecco's Modified Eagle Medium
DMF	Dimethylformamide
DMSO	Dimethyl Sulfoxide
DTT	Dithiothreitol
EDTA	Ethylenediaminetetraacetic Acid
eQTL	expression Quantitative Trait Locus
FBS	Fetal Bovine Serum
FITC	Fluorescein Isothiocyanate
FRET	fluorescence resonant energy transfer
GAPDH	Glyceraldehyde 3-Phosphate Dehydrogenase
GWAS	Genomewide Association Study

HCl	Hydrogen Chloride
HET	Heterozygous
HRP	Horseradish Peroxidase
IgG	Immunoglobulin G
KOMP	Knockout Mouse Project
KO	knockout
LB	Lysogeny Broth
LD	Linkage Disequilibrium
LDLR	Low-density lipoprotein receptor
MCS	Multiple Cloning Site
MI	Myocardial Infarction
MoMa	Monocytes and Macrophages
NIPA	Nuclear Interaction Partner of ALK
NaOH	Sodium Hydroxide
ORO	Oil Red O
P/S	Penicillin/ Streptomycin
PBS	Phosphate-Buffered Saline
PFA	Paraformaldehyde
PMSF	Phenylmethanesulfonylfluoride
PVDF	Polyvinylidene Fluoride
SDS	Sodium Dodecyl Sulfate
SDS-PAGE	Sodium Dodecyl Sulfate Polyacrylamide Gel Electrophoresis
SMC	Smooth Muscle Cell
α-SMA	α-Smooth Muscle Actin
SNP	Single Nucleotide Polymorphism
TBE	Tris/Borate/EDTA-Buffer
TBS	Tris-Buffered Saline
TEMED	Tetramethylethylenediamine
Tris	Tris(hydroxymethyl)aminomethane
WT	Wildtype

A.2. Sequencing Results

A.2.1. Alignments for Cyclin B1

```
                                10        20        30
ref_Cyclin  ------ATGGCGCTCCGAGTCACCAGGAACTCGAAAATTAATGCT
Cyclin_3    ggatcc....................................
Cyclin_4    ggatcc....................................

            40        50        60        70        80
ref_Cyclin  GAAAATAAGGCGAAGATCAACATGGCAGGCGCAAAGCGCGTTCCT
Cyclin_3    .............................................
Cyclin_4    .............................................

                    90        100       110       120
ref_Cyclin  ACGGCCCCTGCTGCAACCTCCAAGCCCGGACTGAGGCCAAGAACA
Cyclin_3    .............................................
Cyclin_4    .............................................

           130       140       150       160       170
ref_Cyclin  GCTCTTGGGGACATTGGTAACAAAGTCAGTGAACAACTGCAGGCC
Cyclin_3    .............................................
Cyclin_4    .............................................

                   180       190       200       210
ref_Cyclin  AAAATGCCTATGAAGAAGGAAGCAAAACCTTCAGCTACTGGAAAA
Cyclin_3    .............................................
Cyclin_4    .............................................

           220       230       240       250       260
ref_Cyclin  GTCATTGATAAAAAACTACCAAAACCTCTTGAAAAGGTACCTATG
Cyclin_3    .............................................
Cyclin_4    .............................................

                   270       280       290       300
ref_Cyclin  CTGGTGCCAGTGCCAGTGTCTGAGCCAGTGCCAGAGCCAGAACCT
Cyclin_3    .............................................
Cyclin_4    .............................................

           310       320       330       340       350
ref_Cyclin  GAGCCAGAACCTGAGCCTGTTAAAGAAGAAAAACTTTCGCCTGAG
Cyclin_3    .............................................
Cyclin_4    .............................................
```

```
                360               370               380               390
ref_Cyclin  CCTATTTTGGTTGATACTGCCTCTCCAAGCCCAATGGAAACATCT
Cyclin_3    ..................................................
Cyclin_4    ..................................................

           400               410               420               430               440
ref_Cyclin  GGATGTGCCCCTGCAGAAGAAGACCTGTGTCAGGCTTTCTCTGAT
Cyclin_3    ..................................................
Cyclin_4    ..................................................

                450               460               470               480
ref_Cyclin  GTAATTCTTGCAGTAAATGATGTGGATGCAGAAGATGGAGCTGAT
Cyclin_3    ..................................................
Cyclin_4    ..................................................

           490               500               510               520               530
ref_Cyclin  CCAAACCTTTGTAGTGAATATGTGAAAGATATTTATGCTTATCTG
Cyclin_3    ..................................................
Cyclin_4    ..................................................

                540               550               560               570
ref_Cyclin  AGACAACTTGAGGAAGAGCAAGCAGTCAGACCAAAATACCTACTG
Cyclin_3    ..................................................
Cyclin_4    ..................................................

           580               590               600               610               620
ref_Cyclin  GGTCGGGAAGTCACTGGAAACATGAGAGCCATCCTAATTGACTGG
Cyclin_3    ..................................................
Cyclin_4    ..................................................

                630               640               650               660
ref_Cyclin  CTAGTACAGGTTCAAATGAAATTCAGGTTGTTGCAGGAGACCATG
Cyclin_3    ..................................................
Cyclin_4    ..................................................

           670               680               690               700               710
ref_Cyclin  TACATGACTGTCTCCATTATTGATCGGTTCATGCAGAATAATTGT
Cyclin_3    ..................................................
Cyclin_4    ..................................................

                720               730               740               750
ref_Cyclin  GTGCCCAAGAAGATGCTGCAGCTGGTTGGTGTCACTGCCATGTTT
Cyclin_3    ..................................................
Cyclin_4    ..................................................
```

```
            760        770        780        790        800
ref_Cyclin  ATTGCAAGCAAATATGAAGAAATGTACCCTCCAGAAATTGGTGAC
Cyclin_3    ..................................................
Cyclin_4    ..................................................

                  810        820        830        840
ref_Cyclin  TTTGCTTTTGTGACTGACAACACTTATACTAAGCACCAAATCAGA
Cyclin_3    ..................................................
Cyclin_4    ..................................................

            850        860        870        880        890
ref_Cyclin  CAGATGGAAATGAAGATTCTAAGAGCTTTAAACTTTGGTCTGGGT
Cyclin_3    ..................................................
Cyclin_4    ..................................................

                  900        910        920        930
ref_Cyclin  CGGCCTCTACCTTTGCACTTCCTTCGGAGAGCATCTAAGATTGGA
Cyclin_3    ..................................................
Cyclin_4    ..................................................

            940        950        960        970        980
ref_Cyclin  GAGGTTGATGTCGAGCAACATACTTTGGCCAAATACCTGATGGAA
Cyclin_3    ..................................................
Cyclin_4    ..................................................

                  990        1000       1010       1020
ref_Cyclin  CTAACTATGTTGGACTATGACATGGTGCACTTTCCTCCTTCTCAA
Cyclin_3    ..................................................
Cyclin_4    ..................................................

           1030       1040       1050       1060       1070
ref_Cyclin  ATTGCAGCAGGAGCTTTTTGCTTAGCACTGAAAATTCTGGATAAT
Cyclin_3    ..................................................
Cyclin_4    ..................................................

                  1080       1090       1100       1110
ref_Cyclin  GGTGAATGGACACCAACTCTACAACATTACCTGTCATATACTGAA
Cyclin_3    ..................................................
Cyclin_4    ..................................................

           1120       1130       1140       1150       1160
ref_Cyclin  GAATCTCTTCTTCCAGTTATGCAGCACCTGGCTAAGAATGTAGTC
Cyclin_3    ..................................................
Cyclin_4    ..................................................
```

```
                    1170              1180              1190              1200
ref_Cyclin  ATGGTAAATCAAGGACTTACAAAGCACATGACTGTCAAGAACAAG
Cyclin_3    ...................................................
Cyclin_4    ...................................................

            1210              1220              1230              1240              1250
ref_Cyclin  TATGCCACATCGAAGCATGCTAAGATCAGCACTCTACCACAGCTG
Cyclin_3    ...................................................
Cyclin_4    ...................................................

                    1260              1270              1280              1290
ref_Cyclin  AATTCTGCACTAGTTCAAGATTTAGCCAAGGCTGTGGCAAAGGTG
Cyclin_3    ...................................................
Cyclin_4    ...................................................

            1300
ref_Cyclin  TAA------
Cyclin_3    ...gtcgac
Cyclin_4    ...gtcgac
```

Figure A.1.: Sequencing results for Cyclin B1 clones 3 and 4, in comparison to the reference sequence. Both clones have the correct sequences, and contain the amended restriction enzyme sites, at the beginning for BamHI, and at the end for SalI (denoted by small letters).

A.2.2. Alignments for NIPA-R363H after mutagenesis

```
                          800               810               820
ref_NIPA            TGCAGCTCTCCCTGATAACATGTTCGCAATG
NIPA_full_R363H_pre ..................gg..............
NIPA_R363H_1        ...................................
NIPA_R363H_2        ...................................
NIPA_R363H_3        ...................................
NIPA_R363H_4        ...................................
NIPA_R363H_5        ...................................
NIPA_R363H_6        ...................................
NIPA_R363H_7        ...................................
NIPA_R363H_8        ...................................
                          corrected from G to A by mutagenesis
```

Figure A.2.: Sequencing results for NIPA-R363H after mutagenesis to correct one mutated base. All tested clones show a successful mutagenesis.

A.2.3. Alignments for NIPA-WT after mutagenesis

```
                                  10                  20                  30
ref_NIPA_wt  ------ATGGCGGCGCCCTGTGAGGGACAAGCGTTTGCCGTAGGG
NIPA_wt_1    ggatcc.....................................
NIPA_wt_2    ggatcc.....................................
NIPA_wt_3    ggatcc.....................................
NIPA_wt_4    ggatcc.....................................
NIPA_wt_5    ggatcc.....................................
NIPA_wt_6    ggatcc.....................................

             40                  50                  60                  70                  80
ref_NIPA_wt  GTTGAAAAGAATTGGGGTGCAGTAGTTCGCTCCCCAGAAGGGACC
NIPA_wt_1    ..............................................
NIPA_wt_2    ..............................................
NIPA_wt_3    ..............................................
NIPA_wt_4    ..............................................
NIPA_wt_5    ..............................................
NIPA_wt_6    ..............................................

                     90                  100                 110                 120
ref_NIPA_wt  CCCCAGAAAATCCGGCAGCTGATAGATGAGGGGATTGCCCCGGAA
NIPA_wt_1    ..............................................
NIPA_wt_2    ..............................................
NIPA_wt_3    ..............................................
NIPA_wt_4    ..............................................
NIPA_wt_5    ..............................................
NIPA_wt_6    ..............................................

             130                 140                 150                 160                 170
ref_NIPA_wt  GAGGGAGGCGTGGACGCGAAGGACACGTCTGCCACATCCCAGTCA
NIPA_wt_1    ..............................................
NIPA_wt_2    ..............................................
NIPA_wt_3    ..............................................
NIPA_wt_4    ..............................................
NIPA_wt_5    ..............................................
NIPA_wt_6    ..............................................

                     180                 190                 200                 210
ref_NIPA_wt  GTTAATGGATCACCCCAAGCGGAACAACCTTCATTGGAATCTACA
NIPA_wt_1    ..............................................
NIPA_wt_2    ..............................................
NIPA_wt_3    ..............................................
NIPA_wt_4    ..............................................
NIPA_wt_5    ..............................................
NIPA_wt_6    ..............................................
```

```
                220               230               240               250               260
ref_NIPA_wt  AGCAAAGAAGCCTTCTTTAGCAGAGTGGAAACATTTTCTTCTTTG
NIPA_wt_1    .................................................
NIPA_wt_2    .................................................
NIPA_wt_3    .................................................
NIPA_wt_4    .................................................
NIPA_wt_5    .................................................
NIPA_wt_6    .................................................


                      270               280               290               300
ref_NIPA_wt  AAATGGGCAGGTAAGCCCTTTGAGCTGTCTCCACTCGTCTGTGCA
NIPA_wt_1    .................................................
NIPA_wt_2    .................................................
NIPA_wt_3    .................................................
NIPA_wt_4    .................................................
NIPA_wt_5    .................................................
NIPA_wt_6    .................................................


                310               320               330               340               350
ref_NIPA_wt  AAATATGGCTGGGTCACAGTGGAATGTGATATGCTCAAGTGCTCT
NIPA_wt_1    .................................................
NIPA_wt_2    .................................................
NIPA_wt_3    .................................................
NIPA_wt_4    .................................................
NIPA_wt_5    .................................................
NIPA_wt_6    .................................................


                      360               370               380               390
ref_NIPA_wt  AGCTGTCAAGCTTTTCTCTGTGCCAGTTTACAACCAGCTTTTGAC
NIPA_wt_1    .................................................
NIPA_wt_2    .................................................
NIPA_wt_3    .................................................
NIPA_wt_4    .................................................
NIPA_wt_5    .................................................
NIPA_wt_6    .................................................


                400               410               420               430               440
ref_NIPA_wt  TTTGACAGATATAAGCAACGATGTGCTGAGCTGAAGAAAGCCTTG
NIPA_wt_1    .................................................
NIPA_wt_2    .................................................
NIPA_wt_3    .................................................
NIPA_wt_4    .................................................
NIPA_wt_5    .................................................
NIPA_wt_6    .................................................
```

```
                  450                 460                 470                 480
ref_NIPA_wt  TGTACTGCCCATGAGAAGTTCTGTTTCTGGCCAGACAGCCCATCC
NIPA_wt_1    .............................................
NIPA_wt_2    .............................................
NIPA_wt_3    .............................................
NIPA_wt_4    .............................................
NIPA_wt_5    .............................................
NIPA_wt_6    .............................................

                  490                 500                 510                 520                 530
ref_NIPA_wt  CCAGACCGATTTGGGATGTTGCCCCTGGATGAGCCTGCTATTCTT
NIPA_wt_1    .............................................
NIPA_wt_2    .............................................
NIPA_wt_3    .............................................
NIPA_wt_4    .............................................
NIPA_wt_5    .............................................
NIPA_wt_6    .............................................

                  540                 550                 560                 570
ref_NIPA_wt  GTTAGTGAATTCCTAGATCGTTTTCAAAGCCTTTGTCACTTGGAC
NIPA_wt_1    .............................................
NIPA_wt_2    .............................................
NIPA_wt_3    .............................................
NIPA_wt_4    .............................................
NIPA_wt_5    .............................................
NIPA_wt_6    .............................................

                  580                 590                 600                 610                 620
ref_NIPA_wt  CTCCAGCTTCCTTCCCTAAGGCCGGAGGACTTGAAAACTATGTGC
NIPA_wt_1    .............................................
NIPA_wt_2    .............................................
NIPA_wt_3    .............................................
NIPA_wt_4    .............................................
NIPA_wt_5    .............................................
NIPA_wt_6    .............................................

                  630                 640                 650                 660
ref_NIPA_wt  TTGACAGAAGACAAGATCAGTCTTCTCCTACACTTGCTTGAAGAT
NIPA_wt_1    .............................................
NIPA_wt_2    .............................................
NIPA_wt_3    .............................................
NIPA_wt_4    .............................................
NIPA_wt_5    .............................................
NIPA_wt_6    .............................................
```

```
                670                680                690                700                710
ref_NIPA_wt  GAACTTGATCACCGAACTGATGAGAGAAAAACTACAATCAAATTA
NIPA_wt_1    ..................................................
NIPA_wt_2    ..................................................
NIPA_wt_3    ..................................................
NIPA_wt_4    ..................................................
NIPA_wt_5    ..................................................
NIPA_wt_6    ..................................................

                       720                730                740                750
ref_NIPA_wt  GGCTCAGACATCCAAGTCCACGTCACTGCCTGTATTCTCTCTGTG
NIPA_wt_1    ..................................................
NIPA_wt_2    ..................................................
NIPA_wt_3    ..................................................
NIPA_wt_4    ..................................................
NIPA_wt_5    ..................................................
NIPA_wt_6    ..................................................

                760                770                780                790                800
ref_NIPA_wt  TGTGGCTGGGCGTGTAGTTCCTCTTTGGAATCCATGCAGCTCTCC
NIPA_wt_1    ..................................................
NIPA_wt_2    ..................................................
NIPA_wt_3    ..................................................
NIPA_wt_4    ..................................................
NIPA_wt_5    ..................................................
NIPA_wt_6    ..................................................

                       810                820                830                840
ref_NIPA_wt  CTGATAACATGTTCGCAATGTATGAGGAAGGTGGGGCTCTGGGGC
NIPA_wt_1    ..................................................
NIPA_wt_2    ..................................................
NIPA_wt_3    ..................................................
NIPA_wt_4    ..................................................
NIPA_wt_5    ..................................................
NIPA_wt_6    ..................................................

                850                860                870                880                890
ref_NIPA_wt  TTCCAGCAGATTGAATCGTCCATGACTGACCTGGATGCATCCTTT
NIPA_wt_1    ..................................................
NIPA_wt_2    ..................................................
NIPA_wt_3    ..................................................
NIPA_wt_4    ..................................................
NIPA_wt_5    ..................................................
NIPA_wt_6    ..................................................
```

```
                  900        910        920        930
ref_NIPA_wt  GGCCTGACCAGCTCCCCAATCCCAGGCCTTGAGGGGCGACCAGAG
NIPA_wt_1    ....................................................
NIPA_wt_2    ....................................................
NIPA_wt_3    ....................................................
NIPA_wt_4    ....................................................
NIPA_wt_5    ....................................................
NIPA_wt_6    ....................................................

                  940        950        960        970        980
ref_NIPA_wt  CGCTTACCTCTGGTGCCTGAATCTCCTCGGAGGATGATGACCCGG
NIPA_wt_1    ....................................................
NIPA_wt_2    ....................................................
NIPA_wt_3    ....................................................
NIPA_wt_4    ....................................................
NIPA_wt_5    ....................................................
NIPA_wt_6    ....................................................

                  990        1000       1010       1020
ref_NIPA_wt  AGCCAGGATGCCACTTTCTCCCCAGGCTCAGAGCAGGCTGAAAAG
NIPA_wt_1    ....................................................
NIPA_wt_2    ....................................................
NIPA_wt_3    ....................................................
NIPA_wt_4    ....................................................
NIPA_wt_5    ....................................................
NIPA_wt_6    ....................................................

                  1030       1040       1050       1060       1070
ref_NIPA_wt  AGCCCTGGTCCCATTGTCTCTCGAACTCGGAGCTGGGACTCTTCC
NIPA_wt_1    ....................................................
NIPA_wt_2    ....................................................
NIPA_wt_3    ....................................................
NIPA_wt_4    ....................................................
NIPA_wt_5    ....................................................
NIPA_wt_6    ....................................................

                  1080       1090       1100       1110
ref_NIPA_wt  AGTCCTGTTGACCGTCCTGAGCCAGAGGCTGCTAGCCCCACCACC
NIPA_wt_1    ..............:.....................................
NIPA_wt_2    ..............a.....................................
NIPA_wt_3    ..............:.....................................
NIPA_wt_4    ..............:.....................................
NIPA_wt_5    ..............:.....................................
NIPA_wt_6    ..............:.....................................
```

```
                1120          1130          1140          1150          1160
ref_NIPA_wt     AGAACTCGCCCAGTGACCCGAAGCATGGGAACAGGAGACACCCCT
NIPA_wt_1       .............................................
NIPA_wt_2       .............................................
NIPA_wt_3       .............................................
NIPA_wt_4       .............................................
NIPA_wt_5       .............................................
NIPA_wt_6       .............................................

                     1170          1180          1190          1200
ref_NIPA_wt     GGCCTGGAGGTACCATCTAGCCCTCTGCGGAAAGCCAAGCGAGCT
NIPA_wt_1       .............................................
NIPA_wt_2       .............................................
NIPA_wt_3       .............................................
NIPA_wt_4       .............................................
NIPA_wt_5       .............................................
NIPA_wt_6       .............................................

                1210          1220          1230          1240          1250
ref_NIPA_wt     CGCCTCTGCTCCTCCAGCAGTTCGGACACATCTTCCCGAAGCTTC
NIPA_wt_1       .............................................
NIPA_wt_2       .............................................
NIPA_wt_3       .............................................
NIPA_wt_4       .............................................
NIPA_wt_5       .............................................
NIPA_wt_6       .............................................

                     1260          1270          1280          1290
ref_NIPA_wt     TTTGATCCCACCTCTCAGCATAGAGACTGGTGCCCTTGGGTGAAT
NIPA_wt_1       .............................................
NIPA_wt_2       .............................................
NIPA_wt_3       .............................................
NIPA_wt_4       .............................................
NIPA_wt_5       .............................................
NIPA_wt_6       .............................................

                1300          1310          1320          1330          1340
ref_NIPA_wt     ATCACACTTGGCAAAGAAAGCAGGGAGAATGGTGGAACTGAACCA
NIPA_wt_1       .............................................
NIPA_wt_2       .............................................
NIPA_wt_3       .............................................
NIPA_wt_4       .............................................
NIPA_wt_5       .............................................
NIPA_wt_6       .............................................
```

```
                    1350              1360              1370              1380
ref_NIPA_wt  GATGCCAGCGCCCCAGCAGAGCCAGGCTGGAAAGCAGTGCTGACC
NIPA_wt_1    ..............................................
NIPA_wt_2    ..............................................
NIPA_wt_3    ..............................................
NIPA_wt_4    ..............................................
NIPA_wt_5    ..............................................
NIPA_wt_6    ..............................................

                1390              1400              1410              1420              1430
ref_NIPA_wt  ATCCTCTTGGCGCACAAACAGTCTAGCCAGCCAGCTGAAACGGAC
NIPA_wt_1    ..............................................
NIPA_wt_2    ..............................................
NIPA_wt_3    ..............................................
NIPA_wt_4    ..............................................
NIPA_wt_5    ..............................................
NIPA_wt_6    ..............................................

                    1440              1450              1460              1470
ref_NIPA_wt  TCCATGAGTCTCTCTGAGAAATCAAGGAAAGTATTCCGAATATTT
NIPA_wt_1    ..............................................
NIPA_wt_2    ..............................................
NIPA_wt_3    ..............................................
NIPA_wt_4    ..............................................
NIPA_wt_5    ..............................................
NIPA_wt_6    ..............................................

                1480              1490              1500
ref_NIPA_wt  CGGCAGTGGGAATCTCTGTGCTCATGCTGA------
NIPA_wt_1    ..............................gtcgac
NIPA_wt_2    ..............................gtcgac
NIPA_wt_3    ..............................gtcgac
NIPA_wt_4    ..............................gtcgac
NIPA_wt_5    ..............................gtcgac
NIPA_wt_6    ..............................gtcgac
```

Figure A.3.: Sequencing results for NIPA-WT after mutagenesis from NIPA-R363H to change the SNP back to wildtype. All but one tested clones show a successful mutagenesis.

A.3. Raw Data of Luciferase activity measurement

Table A.1.: Luminescence measurement for the mammalian two-hybrid assay with NIPA-WT and Cyclin B1. The other combinations serve as controls; p53 & SV40 as positive, p53 & TRAF as negative, NFκB as strong positive and NIP1-300 & Mau2 as functional control, respectively. $L_{Firefly}$: luminescence of firefly luciferase; $L_{Renilla}$: luminescence of Renilla luciferase; RLU: relative light unit, calculated as $L_{Firefly}/L_{Renilla}$.

BD-Fusion	AD-Fusion	$L_{Firefly}$	$L_{Renilla}$	RLU (mean ± std)
p53	SV40	218 258	170 317	1.29 ± 0.06
		239 341	173 301	
		224 249	184 395	
p53	TRAF	16 485	187 780	0.10 ± 0.01
		20 554	190 744	
		16 991	171 962	
NFκB		10 917 799	186 283	53.64 ± 3.63
		9 636 226	192 568	
		9 694 376	185 460	
Nip1-300	Mau2	3 719 512	373 092	9.87 ± 0.30
		2 990 120	316 164	
		3 817 977	374 949	
Cyclin B1	NIPA-WT	12 638	358 480	0.04 ± 0.00
		10 751	297 249	
		11 078	249 794	
NIPA-WT	Cyclin B1	10 720	188 982	0.06 ± 0.00
		16 369	259 392	
		11 141	173 344	

A.4. Matlab Scripts for Plaque size analysis

Oil red O-Analysis, Main file

```
% Ask user for the folder to analyse
 ExpPath = uigetdir();

% Check if a folder was selected, otherwise an exception is thrown
if ~isdir
    fprintf('%s is not a folder!!\nn',ExpPath);
else
    % search for all the pics in the Folder; change if other format used
    imList = dir([ExpPath,filesep,'*.png']);
    %imList = dir([ExpPath,filesep,'*.jpg']);
    %imList = dir([ExpPath,filesep,'*.tif']);

    % initializing result matrices
    normalizedPlaques = [];
    plaqueAreas = [];
    aortaAreas = [];

    % loop over all pics in the list
    for i=1:length(imList)

        % some informative output for the user
        fprintf('Handing over Image: %s\n', imList(i).name);

        % calling the analysis for the given image
        imagePath = sprintf('%s',ExpPath,filesep,imList(i).name);
        [PlaqueArea, AortaArea, NormalizedPlaque] = OilredAnalysis(
           imagePath);

        % saving results in the result matrices
        normalizedPlaques(i) = NormalizedPlaque;
        plaqueAreas(i) = PlaqueArea;
        aortaAreas(i) = AortaArea;
    end
```

```
    %% saving the ouput after analysing all images
    % converting the Filenames into saveable format
    newlist=struct2cell(imList);

    % writing data to be saved into a 'dataset'
    exportData = dataset({newlist(1,:)','Image'},{plaqueAreas','Plaque'
       },{aortaAreas','Aorta'},{normalizedPlaques', 'NormalizedPlaque'})
       ;

    % setting the location to save the file
    exportName=sprintf('%s',ExpPath, filesep, 'Plaque_Scores.csv');

    % exporting it...
    export(exportData,'file', exportName, 'Delimiter', ',')

    % some more informative output for the user
    fprintf('Scores saved, Analysis complete!\n\n\n');
end
```

Oil red O-Analysis

```
function [PlaqueArea, AortaArea, NormalizedPlaque] = OilredAnalysis(
   imagePath)
%% Description
% This function can be used to evaluate Oilred-Stainings.
% Image data has to be preprocessed - you need to cut out the area of
% interest (e.g. aorta from a heart aortic-root-cross section...), and
% make the background white.
% This function returns 3 values: Plaque area, Aorta area, and normalized
    Plaque.
%
% Plaque color has to be adjusted according to used color (e.g. RGB
   [244,20,131]).
%
%
% Input:    Full Path to the Image as a string variable
%           (e.g. 'C:\Users\Username\Desktop\Image1.png').
```

```
% Output:   PlaqueArea (value in px)
%           Aorta area (value in px)
%           NormalizedPlaque (value)

%% Loading the Picture
image = imread(imagePath);

% Some useful output for the user...
fprintf('Calculating Scores... ');

% Important color values, need to be adjusted!
Plaque = image(:,:,1) == 244& image(:,:,2) == 20 & image(:,:,3) ==131;
% save the plaque image as black/white-mask
imwrite(Plaque,sprintf('%s%s',imagePath(1:end-4),'_Plaque.tif'))

% selecting aorta as everything non-white (white: background)
Aorta = image(:,:,1)~=255 & image(:,:,2)~=255 & image(:,:,3)~=255;
% save the aorta image as black/white-mask
imwrite(Aorta,sprintf('%s%s',imagePath(1:end-4),'_Aorta.tif'))

%% Calculating the Scores (by adding up all pixels)
AortaArea = sum(sum(Aorta~=0));
PlaqueArea = sum(sum(Plaque~=0));

% normalizing plaque area to aorta area
NormalizedPlaque = PlaqueArea/AortaArea;

% Some useful output for the user...
fprintf('done!\n\n');
```

A.5. Matlab Scripts for Collagen analysis

Collagen-Analysis, Main file

```
% Ask user for the folder to analyse
```

```
 ExpPath = uigetdir();

% Check if a folder was selected, otherwise an exception is thrown
if ~isdir
    fprintf('%s is not a folder!!\nn',ExpPath);
else
    % search for all the pics in the Folder; change if other format used
    imList = dir([ExpPath,filesep,'*.png']);
    %imList = dir([ExpPath,filesep,'*.jpg']);
    %imList = dir([ExpPath,filesep,'*.tif']);

    % initializing result matrices
    normalizedCollagens = [];
    plaqueAreas = [];
    collagenAreas = [];

        % setting thresholds for collagen (blue)-selection in rgb/ycbcr
            channels
    rgbThresh = 140;
    ycbcrThresh = 112;

    % loop over all pics in the list
    for i=1:length(imList)

        % some informative output for the user
        fprintf('Handing over Image: %s\n', imList(i).name);

        % calling the analysis for the given image
        imagePath = sprintf('%s',ExpPath,filesep,imList(i).name);
        [PlaqueArea, CollagenArea, NormalizedCollagen] = CollagenAnalysis
            (imagePath, rgbThresh, ycbcrThresh);

        % saving results in the result matrices
        normalizedCollagens(i) = NormalizedCollagen;
        plaqueAreas(i) = PlaqueArea;
        collagenAreas(i) = CollagenArea;
    end
```

```
    %% saving the ouput after analysing all images
    % converting the Filenames into saveable format
    newlist=struct2cell(imList);

    % writing data to be saved into a 'dataset'
    exportData = dataset({newlist(1,:)','Image'},{plaqueAreas', '
        Plaque_Area'},{collagenAreas', 'Collagen_Area'},{
        normalizedCollagens', 'normalizedCollagens'});

    % setting the location to save the file
    exportName=sprintf('%s%s%s%i%s%i%s',ExpPath, filesep, '
        Collagen_Scores_',rgbThresh,'_',ycbcrThresh,'.csv');

    % exporting it...
    export(exportData,'file', exportName, 'Delimiter', ',')

     % some more informative output for the user
    fprintf('Scores saved, Analysis complete!\n\n\n');
end
```

Collagen-Analysis

```
function [PlaqueArea, CollagenArea, NormalizedCollagen] =
    CollagenAnalysis(imagePath, rgbThresh, ycbcrThresh)
%% Description
% This function can be used to evaluate Collagen-Stainings (Masson's
    Trichrome)
% Image data has to be preprocessed - you need to cut out the area of
% interest (e.g. plaque from a heart aortic-root-cross section...), and
% make the background white.
% This function returns 3 values: Plaque area, Collagen area, and
    normalized Collagen.
%
% Thresholds have to be adjusted for individual image properties.
%
%
```

```
% Input:    Full Path to the Image as a string variable
%           (e.g. 'C:\Users\Username\Desktop\Image1.png'),
%                       Thresholds for color selection: ycbcrThresh,
    rgbThresh
% Output:   PlaqueArea (value in px)
%           CollagenArea (value in px)
%           NormalizedCollagen (value)

%% Loading the Picture
image = imread(imagePath);

% Some useful output for the user...
fprintf('Calculating Scores... ');

% transforming the image into ycbcr-color map
ycbcrImage=rgb2ycbcr(image);

% selecting Collagen by using the thresholds ycbcrThresh in the luminance
    -channel of the ycbcr-image, and the rgbThresh in the red-channel of
    the RGB-image
collagenImage = ycbcrImage(:,:,1) < ycbcrThresh & image(:,:,1) <
    rgbThresh;
% save the collagen image as black/white-mask
imwrite(collagenImage, sprintf('%s%s',imagePath(1:end-4), '_Collagen.tif'
     ));

%% Calculating the Scores (by adding up all pixels)
% selecting plaque as everything non-white (white: background)
PlaqueArea=sum(sum(image(:,:,1)~=255 & image(:,:,2)~=255 & image(:,:,3)
    ~=255));
CollagenArea = sum(sum(collagenImage~=0));

% normalizing collagen area to plaque area
NormalizedCollagen=CollagenArea/PlaqueArea;

% Some useful output for the user...
fprintf('done!\n\n');
```

A.6. Matlab Scripts for MoMa analysis

MoMa-Analysis, Main file

```
% Ask user for the folder to analyse
 ExpPath = uigetdir();

% Check if a folder was selected, otherwise an exception is thrown
if ~isdir
    fprintf('%s is not a folder!!\nn',ExpPath);
else
    % search for all the pics in the Folder; change if other format used
    imList = dir([ExpPath,filesep,'*.png']);
    %imList = dir([ExpPath,filesep,'*.jpg']);
    %imList = dir([ExpPath,filesep,'*.tif']);

    % initializing result matrices
    totalMOMAs = [];
    strongMOMAs = [];
    plaqueAreas = [];

    % loop over all pics in the list
    for i=1:length(imList)

        % some informative output for the user
        fprintf('Handing over Image: %s\n', imList(i).name);

        % calling the analysis for the given image
        imagePath = sprintf('%s',ExpPath,filesep,imList(i).name);
        [PlaqueArea, StrongMOMA, TotalMOMA] = MOMAAnalysis(imagePath);

        % saving results as fractions of 1 (compared to total plaque area
           )
```

```
        totalMOMAs(i) = TotalMOMA;
        strongMOMAs(i) = StrongMOMA;
        plaqueAreas(i) = PlaqueArea;
end
```

```
    %% saving the ouput after analysing all images
    % converting the Filenames into saveable format
    newlist=struct2cell(imList);

    % writing data to be saved into a 'dataset'
    exportData = dataset({newlist(1,:)','Image'},{plaqueAreas', 'Plaque'
       },{totalMOMAs', 'TotalMoMa'},{strongMOMAs', 'StrongMoMa'});

    % setting the location to save the file
    exportName=sprintf('%s',ExpPath, filesep, 'MoMa_Scores.csv');

    % exporting it...
    export(exportData,'file', exportName, 'Delimiter', ',')

    % some more informative output for the user
    fprintf('Scores saved, Analysis complete!\n\n\n');
end
```

MoMa-Analysis

```
function [PlaqueArea, StrongMOMA, TotalMOMA] = MOMAAnalysis(imagePath)
%% Description
% This function can be used to evaluate MoMa-Stainings performed with
% NOVA-RED or HRP-Staining.
% Image data has to be preprocessed - you need to cut out the area of
% interest (e.g. plaque from a heart aortic-root-cross section...), and
% make the background white.
% This function returns 3 values. Plaque Area, Total MoMa, Strong MoMa
%
% Thresholds have to be adjusted for individual image properties.
%
%
```

```
% Input:    Full Path to the Image as a string variable
%           (e.g. 'C:\Users\Username\Desktop\Image1.png').
% Output:   PlaqueArea (value in px)
%           StrongMOMA (value)
%           TotalMOMA (value)

%% Loading the Picture
image = imread(imagePath);

% Some useful output for the user...
fprintf('Calculating Scores... ');

% transforming the image into ycbcr-color map
ycbcrImage=rgb2ycbcr(image);

% Calculating the strong MoMa signal, using thresholds on the RGB-image
strongMOMAImage=image(:,:,3)<=145 & image(:,:,2)<=140 &  100<image(:,:,1)
    <=200;
% StrongMOMA=image(:,:,3)<=125 & image(:,:,2)<=130 &  100<image(:,:,1)
    <=200;

% save the strong MoMa image as black/white-mask
imwrite(strongMOMAImage, sprintf('%s%s',imagePath(1:end-4), '_StrongMOMA.
    tif' ));

% Calculating the total MoMa signal, as a sum of the "strong" MoMa signal
     and by selecting most of MoMa staining by using this threshold in
    the Blue-Yellow Chrominance-channel of the ycbcr-image
normalMOMA= ycbcrImage(:,:,2) < 126;
totalMOMAImage=normalMOMA+StrongMOMAImage;

% save the total MoMa image as black/white-mask
imwrite(totalMOMAImage, sprintf('%s%s',imagePath(1:end-4), '_TotalMOMA.
    tif' ));

%% Calculating the Scores
% selecting plaque area as everything non-white (white: background)
```

```
PlaqueArea=sum(sum(image(:,:,1)~=255 & image(:,:,2)~=255 & image(:,:,3)
    ~=255));

% normalizing strong MoMa to plaque area
StrongMOMA=sum(sum(StrongMOMAImage~=0)/PlaqueArea);

% normalizing total MoMa to plaque area
TotalMOMA=sum(sum(totalMOMAImage~=0)/PlaqueArea);

% Some useful output for the user...
fprintf('done!\n\n');
```

A.7. Matlab Scripts for SMC analysis

SMC-Analysis, Main file

```
% Ask user for the folder to analyse
 ExpPath = uigetdir();

% Check if a folder was selected, otherwise an exception is thrown
if ~isdir
    fprintf('%s is not a folder!!\nn',ExpPath);
else
    % search for all the pics in the Folder; change if other format used
    imList = dir([ExpPath,filesep,'*.png']);
    %imList = dir([ExpPath,filesep,'*.jpg']);
    %imList = dir([ExpPath,filesep,'*.tif']);

    % initializing result matrices
    totalSMCs = [];
    strongSMCs = [];
    totalPlaques = [];

    % loop over all pics in the list
    for i=1:length(imList)
```

```
        % some informative output for the user
        fprintf('Handing over Image: %s\n', imList(i).name);

        % calling the analysis for the given image
        imagePath = sprintf('%s',ExpPath,filesep,imList(i).name);
        [TotalPlaque, StrongSMC, TotalSMC] = SMCAnalysis(imagePath);

        % saving results as fractions of 1 (compared to total plaque area
            )
        totalSMCs(i) = TotalSMC;
        strongSMCs(i) = StrongSMC;
        totalPlaques(i) = TotalPlaque;
    end

    %% saving the ouput after analysing all images
    % converting the Filenames into saveable format
    newlist=struct2cell(imList);

    % writing data to be saved into a 'dataset'
    exportData = dataset({newlist(1,:)','Image'},{totalPlaques', 'Plaque'
        },{totalSMCs', 'TotalSMC'},{strongSMCs', 'StrongSMC'});

    % setting the location to save the file
    exportName=sprintf('%s',ExpPath, filesep, 'SMC_Scores.csv');

    % exporting it...
    export(exportData,'file', exportName, 'Delimiter', ',')

    % some more informative output for the user
    fprintf('Scores saved, Analysis complete!\n\n\n');
end
```

SMC-Analysis

```
function [PlaqueArea, StrongSMC, TotalSMC] = SMCAnalysis(imagePath)
%% Description
```

```
% This function can be used to evaluate SMC-Stainings performed with
% NOVA-RED or HRP-Staining.
% Image data has to be preprocessed - you need to cut out the area of
% interest (e.g. plaque from a heart aortic-root-cross section...), and
% make the background white.
% This function returns 3 values. Plaque Area, Total SMC, Strong SMC
%
% Thresholds have to be adjusted for individual image properties.
%
%
% Input:    Full Path to the Image as a string variable
%           (e.g. 'C:\Users\Username\Desktop\Image1.png').
% Output:   PlaqueArea (value in px)
%           StrongSMC (value)
%           TotalSMC (value)
```

```
%% Loading the Picture
image = imread(imagePath);

% Some output for the user...
fprintf('Calculating Scores... ');

% mapping original RGB-image on a different colormap (YCbCr)
ycbcrImage=rgb2ycbcr(image);

% Calculating the strong SMC signal, using thresholds on the RGB-image
strongSMCImage=image(:,:,3)<=125 & image(:,:,2)<=130 &  100<image(:,:,1)
   <=200;
% strongSMCImage=image(:,:,3)<=145 & image(:,:,2)<=140 &  100<image
   (:,:,1)<=200;

% save the strong SMC image as black/white-mask
imwrite(strongSMCImage, sprintf('%s%s',imagePath(1:end-4), '_StrongSMC.
   tif' ));

% Calculating the total SMC signal, as a sum of the "strong" SMC signal
   and by selecting most of SMC staining by using this threshold in the
```

```
   Blue-Yellow Chrominance-channel of the ycbcr-image
normalSMC= ycbcrImage(:,:,2) < 126;
totalSMCImage=normalSMC+strongSMCImage;

% save the total SMC image as black/white-mask
imwrite(totalSMCImage, sprintf('%s%s',imagePath(1:end-4), '_TotalSMC.tif'
    ));

%% Calculating the Scores
% selecting plaque area as everything non-white (white: background)
PlaqueArea=sum(sum(image(:,:,1)~=255 & image(:,:,2)~=255 & image(:,:,3)
   ~=255));

% normalizing strong SMC to plaque area
StrongSMC=sum(sum(strongSMCImage~=0)/PlaqueArea);

% normalizing total SMC to plaque area
TotalSMC=sum(sum(totalSMCImage~=0)/PlaqueArea);

% Some useful output for the user...
fprintf('done!\n\n');
```

A.8. ImageJ macro for automated counting of DAPI-stained cells

ImageJ macro for automated counting DAPI-stained cells

```
// User is prompted to select a folder
dir = getDirectory("Choose a Directory");
     // selecting all png-images from this folder
     list = getFileList(dir);
     for (i=0; i<list.length; i++) {
       if( endsWith(list[i],"png") && !startsWith(list[i],"mask") ){
       }
```

```
    else{
     list[i] = 0;
    }
  }
  // Threshold for cell detection is set here
  thresh = 28;
  setBatchMode(true);
  // loop over all images starts
  for (i=0; i<list.length; i++) {
    if( list[i] != 0 ){
      // update a result window, this will be saved as xls-file later
      showProgress(i, list.length);
      open(dir+list[i]);
      // converted to 8-bit
      run("8-bit");
      setAutoThreshold("Default dark");
      // applying the threshold
      setThreshold(thresh, 255);
      setOption("BlackBackground", false);
      // converting image to black and white
      run("Convert to Mask");
      // smoothing edges of detected cells
      run("Watershed");
      // counting them
      run("Analyse Particles...", "show=Masks summarise");
      // save the image
      saveAs("Jpeg", dir+"mask_"+thresh+"_"+list[i]);
      close;
      //selectWindow("Results");
      //saveAs("Results", dir+"Results"+list[i]+".xls");
     }
  }
  // save the summary table
  selectWindow("Summary");
  saveAs("Results", dir+"Summary_"+thresh+".xls");
  print("Summary saved! Done!!");
```

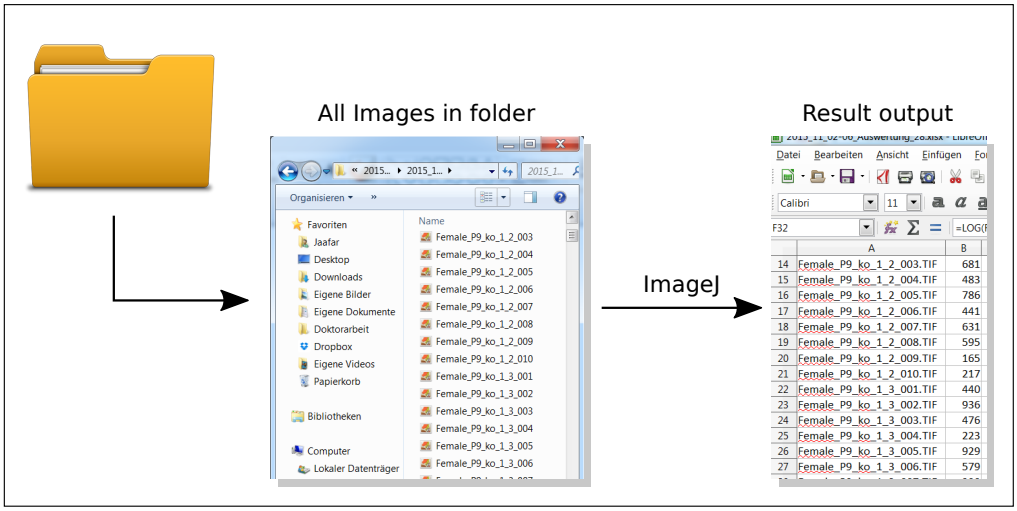

Figure A.4.: Exemplary result output from ImageJ. Images from the whole experiment, with unique names, are stored in one folder, and analysed in one sweep by the macro in ImageJ. The results are saved in tabular format (xls-file), given as the number of counted cells per image, and can be easily used for further analyses.